

Drivers of plant nutrient acquisition and allocation strategies and their influence  
on plant responses to environmental change

by

Evan A. Perkowski, B.S.

A Dissertation

In

Biological Sciences

Submitted to the Graduate Faculty  
of Texas Tech University in  
Partial Fulfillment of  
the Requirements for  
the Degree of

Doctor of Philosophy

Approved

Nicholas G. Smith, Ph.D.  
Chair of Committee

Aimée T. Classen, Ph.D.

Natasja van Gestel, Ph.D.

Lindsey C. Slaughter, Ph.D.

Dylan W. Schwilk, Ph.D.

Mark Sheridan, Ph.D.  
Dean of the Graduate School

May 2023

Copyright 2023, Evan A. Perkowski

## Acknowledgements

Placeholder for text

## Table of Contents

<b>Acknowledgements . . . . .</b>	ii
<b>Abstract . . . . .</b>	vii
<b>List of Tables . . . . .</b>	viii
<b>List of Figures . . . . .</b>	x
<b>1. Introduction . . . . .</b>	1
<b>2. Structural carbon costs to acquire nitrogen are determined by nitrogen and light availability in two species with different nitrogen acquisition strategies . . . . .</b>	4
2.1    Introduction . . . . .	4
2.2    Methods . . . . .	8
2.2.1 <i>Experiment setup</i> . . . . .	8
2.2.2 <i>Plant measurements and calculations</i> . . . . .	9
2.2.3 <i>Statistical analyses</i> . . . . .	10
2.3    Results . . . . .	12
2.3.1 <i>Carbon costs to acquire nitrogen</i> . . . . .	12
2.3.2 <i>Whole plant nitrogen biomass</i> . . . . .	15
2.3.3 <i>Root carbon biomass</i> . . . . .	17
2.3.4 <i>Root nodule biomass</i> . . . . .	19
2.4    Discussion . . . . .	23
<b>3. Soil nitrogen availability modifies leaf nitrogen economies in mature temperate deciduous forests: a direct test of photosynthetic least-cost theory . . . . .</b>	31
3.1    Introduction . . . . .	31
3.2    Methods . . . . .	35
3.2.1 <i>Study site description</i> . . . . .	35
3.2.2 <i>Experimental design</i> . . . . .	36
3.2.3 <i>Leaf gas exchange and trait measurements</i> . . . . .	36
3.2.4 <i><math>A_{net}/C_i</math> curve-fitting and parameter estimation</i> . . . . .	39

3.2.5	<i>Proportion of leaf nitrogen allocated to photosynthesis and structure</i>	41
3.2.6	<i>Tradeoffs between nitrogen and water use</i>	42
3.2.7	<i>Soil nitrogen availability and pH</i>	43
3.2.8	<i>Statistical analyses</i>	45
3.3	Results	47
3.3.1	<i>Leaf N content</i>	47
3.3.2	<i>Net photosynthesis and leaf biochemistry</i>	50
3.3.3	<i>Leaf N allocation</i>	53
3.3.4	<i>Tradeoffs between nitrogen and water use</i>	56
3.4	Discussion	59
3.4.1	<i>Soil nitrogen availability modifies tradeoffs between nitrogen and water use</i>	60
3.4.2	<i>Soil pH did not modify tradeoffs between nitrogen and water usage</i>	62
3.4.3	<i>Species identity explains a large amount of variation in leaf and whole plant traits</i>	63
3.4.4	<i>Implications for photosynthetic least-cost theory model development</i>	64
3.4.5	<i>Conclusions</i>	66
4.	<b>The relative cost of resource use for photosynthesis drives variance in leaf nitrogen content across climate and soil resource availability gradients</b>	67
4.1	Introduction	67
4.2	Methods	69
4.2.1	<i>Site descriptions and sampling methodology</i>	69
4.2.2	<i>Leaf trait measurements</i>	69
4.2.3	<i>Site climate data</i>	75
4.2.4	<i>Site edaphic characteristics</i>	75
4.2.5	<i>Plant functional group assignments</i>	77
4.2.6	<i>Data analysis</i>	78

4.3 Results . . . . .	80
4.3.1 Cost to acquire nitrogen relative to water ( $\beta$ ) . . . . .	80
4.3.2 Leaf $C_i:C_a$ . . . . .	84
4.3.3 Leaf nitrogen content . . . . .	87
4.3.4 Structural equation model . . . . .	91
4.4 Discussion . . . . .	94
<b>5. Optimal resource investment to photosynthetic capacity maximizes nutrient allocation to whole plant growth under elevated CO<sub>2</sub> . . . . .</b>	<b>95</b>
5.1 Introduction . . . . .	95
5.2 Methods . . . . .	100
5.2.1 Seed treatments and experimental design . . . . .	100
5.2.2 Growth chamber conditions . . . . .	101
5.2.3 Leaf gas exchange measurements . . . . .	103
5.2.4 Leaf trait measurements . . . . .	104
5.2.5 $A/C_i$ curve fitting and parameter estimation . . . . .	106
5.2.6 Stomatal limitation . . . . .	106
5.2.7 Proportion of leaf nitrogen allocated to photosynthesis and structure . . . . .	107
5.2.8 Whole plant traits . . . . .	109
5.2.9 Statistical analyses . . . . .	111
5.3 Results . . . . .	113
5.3.1 Leaf nitrogen content, chlorophyll content, and mass per area . . . . .	113
5.3.2 Leaf biochemistry and stomatal conductance . . . . .	117
5.3.3 Leaf nitrogen allocation . . . . .	121
5.3.4 Whole plant growth and total leaf area . . . . .	125
5.3.5 Carbon costs to acquire nitrogen . . . . .	125
5.3.6 Nitrogen fixation . . . . .	129
5.4 Discussion . . . . .	133

5.4.1	<i>Soil nitrogen fertilization has divergent effects on leaf and whole plant acclimation responses to CO<sub>2</sub></i>	134
5.4.2	<i>Implications for future model development</i>	138
5.4.3	<i>Study limitations and future directions</i>	139
5.4.4	<i>Conclusions</i>	141
6.	<b>Conclusions</b>	143
	<b>References</b>	145

**Abstract**

## List of Tables

2.1 Analysis of variance results exploring species-specific effects of light availability, nitrogen fertilization, and their interactions on carbon costs to acquire nitrogen, whole-plant nitrogen biomass, and root carbon biomass . . . . .	13
2.2 Analysis of variance results exploring effects of light availability, nitrogen fertilization, and their interactions on <i>G. max</i> root nodule biomass and the ratio of root nodule biomass to root biomass* . . . . .	20
2.3 Slopes of the regression line describing the relationship between each dependent variable and nitrogen fertilization at each light level* . . . . .	21
3.1 Effects of soil N availability, soil pH, and species on leaf N content per unit leaf area ( $N_{\text{area}}$ ), leaf N content per unit leaf mass ( $N_{\text{mass}}$ ), and leaf mass per unit leaf area ( $M_{\text{area}}$ ) . . . . .	48
3.2 Effects of soil N availability, soil pH, species, and $N_{\text{area}}$ on leaf biochemistry . . . . .	51
3.3 Effects of soil N availability, soil pH, and species on the proportion of leaf nitrogen content allocated to photosynthesis, Rubisco, bioenergetics, and structure . . . . .	54
3.4 Effects of soil N availability, soil pH, species, and $N_{\text{area}}$ on tradeoffs between nitrogen and water use . . . . .	57

5.1 Effects of soil nitrogen fertilization, inoculation, and CO <sub>2</sub> treatments on $N_{\text{area}}$ , $N_{\text{mass}}$ , $M_{\text{area}}$ , and $Chl_{\text{area}}$ . . . . .	115
5.2 Effects of soil nitrogen fertilization, inoculation, and CO <sub>2</sub> on leaf biochemistry . . . . .	119
5.3 Effects of soil N availability, soil pH, species, and $N_{\text{area}}$ on leaf nitrogen allocation . . . . .	123
5.4 Effects of soil N availability, soil pH, species, and $N_{\text{area}}$ on total leaf area, whole plant biomass, and costs of nitrogen acquisition . . . .	127
5.5 Effects of soil N availability, soil pH, species, and $N_{\text{area}}$ on leaf biochemistry . . . . .	131

## List of Figures

2.1 Relationships between soil nitrogen fertilization and light availability on carbon costs to acquire nitrogen in <i>G. hirsutum</i> and <i>G. max</i> . . . . .	14
2.2 Relationships between soil nitrogen fertilization and light availability on whole-plant nitrogen biomass in <i>G. hirsutum</i> and <i>G. max</i> . . . . .	16
2.3 Relationships between soil nitrogen fertilization and light availability on root carbon biomass in <i>G. hirsutum</i> and <i>G. max</i> . . . . .	18
2.4 Effects of shade cover and nitrogen fertilization on root nodule biomass and the ratio of root nodule biomass to root biomass in <i>G. max</i> . . . . .	22
3.1 Effects of soil N availability and species on leaf N content per unit leaf area, leaf nitrogen content per unit leaf biomass, and leaf mass per leaf area . . . . .	49
3.2 Effects of soil N availability, species, and leaf N content leaf biochemistry . . . . .	52
3.3 Effects of soil N availability, species, and leaf N content on the fraction of leaf nitrogen allocated to photosynthesis and structure . . . . .	55
3.4 Effects of soil N availability, species, and leaf N content on tradeoffs between nitrogen and water use . . . . .	58

4.1	Maps that detail site locations along 2006-2020 mean annual precipitation (panel A) and mean annual temperature (panel B) gradients in Texas, USA. . . . .	74
4.2	Effects of soil nitrogen availability and soil moisture on the unit cost ratio $\beta$ . . . . .	83
4.3	Effects of 4-day mean vapor pressure deficit, 2-day soil moisture (per water holding capacity), and soil nitrogen availability on $\chi$ . . . . .	86
4.4	Effects of $\chi$ , soil nitrogen availability, and soil moisture on leaf nitrogen content per unit leaf area, leaf nitrogen content per unit leaf biomass, and leaf mass per area. . . . .	90
4.5	Structural equation model results exploring direct and indirect drivers of $N_{\text{area}}$ . . . . .	93
5.1	Effects of $\text{CO}_2$ , fertilization, and inoculation on leaf nitrogen per unit leaf area, leaf nitrogen content, leaf mass per unit leaf area, and chlorophyll content per unit leaf area. . . . .	116
5.2	Effects of $\text{CO}_2$ , fertilization, and inoculation on maximum rate of Rubisco carboxylation, the maximum rate of RuBP regeneration, and the ratio of the maximum rate of RuBP regeneration to the maximum rate of Rubisco carboxylation leaf mass per unit leaf area, dark respiration, stomatal conductance, and stomatal limitation. . . . .	120
5.3	Effects of $\text{CO}_2$ , fertilization, and inoculation on the relative fraction of leaf nitrogen allocated to photosynthesis and the fraction of leaf nitrogen allocated to structure. . . . .	124

5.4 Effects of CO <sub>2</sub> , fertilization, and inoculation on total leaf area, total biomass, and structural carbon costs to acquire nitrogen. . . . .	128
5.5 Effects of CO <sub>2</sub> , fertilization, and inoculation on nodule biomass, nodule: root biomass, and percent nitrogen fixed from the atmosphere. . . . .	132

1                           **Chapter 1**  
2                           **Introduction**

3         Photosynthesis represents the largest carbon flux between the atmosphere  
4     and biosphere, and is regulated by complex ecosystem carbon and nutrient cycles  
5     (Hungate et al. 2003; IPCC 2021). As a result, the inclusion of robust, empirically  
6     tested representations of photosynthetic processes is critical in order for terrestrial  
7     biosphere models to accurately and reliably simulate carbon and nutrient fluxes  
8     between the atmosphere and terrestrial biosphere (Wieder et al. 2015; Smith and  
9     Dukes 2013; Prentice et al. 2015; Oreskes et al. 1994). Despite evidence that  
10   the inclusion of coupled carbon and nutrient cycles can improve model uncer-  
11   tainty (Arora et al. 2020; Braghieri et al. 2022; Shi et al. 2016), widespread  
12   divergence in predicted carbon and nutrient fluxes is still apparent across model  
13   products (Friedlingstein et al. 2014; Davies-Barnard et al. 2020). This divergence  
14   could be due to an incomplete understanding of how plants acclimate to chang-  
15   ing environments, particularly in response to shifts in soil resource availability or  
16   aboveground climate (Smith and Dukes 2013; Davies-Barnard et al. 2020).

17         Photosynthetic least-cost theory (Prentice et al. 2014; Wang et al. 2017;  
18     Smith et al. 2019; Scott and Smith 2022) provides a contemporary framework  
19     for incorporating plant acclimation responses to changing environments in ter-  
20     restrial biosphere models by unifying photosynthetic optimal coordination (Chen  
21     et al. 1993; Maire et al. 2012) and least-cost (Wright et al. 2003) theories.  
22     First principles of the theory predict that plants acclimate to a given environment  
23     by minimizing the summed costs of nutrient and water use in such a way that

24 maximizes the use of available light and allows photosynthesis to be optimized  
25 by equal colimitation of Ribulose-1,5-bisphosphate carboxylase-oxygenase ("Ru-  
26 bisco") carboxylation and Ribulose-1,5-bisphosphate ("RuBP") regeneration rates.  
27 Optimality models leveraging patterns expected from photosynthetic least-cost  
28 theory have been developed (Wang et al. 2017; Smith et al. 2019; Stocker et al.  
29 2020; Scott and Smith 2022), though empirical tests of the theory are sparse.

30 In the time since designing experiments for this dissertation, environmen-  
31 tal gradient studies have shown broad support for patterns expected from theory  
32 (Paillassa et al. 2020; Querejeta et al. 2022; Westerband et al. 2023), and  
33 the theory has been shown to be capable of predicting leaf across environmental  
34 changes such as atmospheric CO<sub>2</sub>, temperature, growing season irradiance, and  
35 vapor pressure deficit (Peng et al. 2021; Dong et al. 2017; Dong et al. 2020;  
36 Dong et al. 2022; Dong et al. 2022; Luo et al. 2021; Smith and Keenan 2020).  
37 Specifically, the theory is capable of simulating the reduction in leaf nitrogen  
38 content and photosynthetic capacity with increasing CO<sub>2</sub>, strong nitrogen-water  
39 use tradeoffs in response to changing temperature and vapor pressure deficit, and  
40 strong nitrogen-water use tradeoffs in response to shifts in soil nutrient availability  
41 and soil moisture. However, targetted experiments that test underlying mecha-  
42 nisms of the theory, particularly in response to changing soil resource availability  
43 and interactions between soil resource availability and aboveground climatic fac-  
44 tors, are needed to evaluate the generality of patterns expected from theory and  
45 determine whether the theory is suitable for implementation in future generations  
46 of terrestrial biosphere models.

47 In this dissertation, I conduct a nitrogen-by-light manipulative greenhouse

**48** experiment, a nitrogen-by-sulfur manipulative field experiment, a soil resource  
**49** availability and climate environmental gradient field experiment, and a CO<sub>2</sub>-by-  
**50** inoculation-by-nitrogen manipulative growth chamber experiment to test under-  
**51** lying assumptions of photosynthetic least-cost theory.

52

## Chapter 2

53       **Structural carbon costs to acquire nitrogen are determined by**  
54       **nitrogen and light availability in two species with different nitrogen**  
55       **acquisition strategies**

56   2.1 Introduction

57           Carbon and nitrogen cycles are tightly coupled in terrestrial ecosystems.  
58       This tight coupling influences photosynthesis (Walker et al. 2014; Rogers et al.  
59       2017), net primary productivity (LeBauer and Treseder 2008; Thomas et al. 2013),  
60       decomposition (Cornwell et al. 2008; Bonan et al. 2013; Sulman et al. 2019), and  
61       plant resource competition (Gill and Finzi 2016; Xu-Ri and Prentice 2017). Ter-  
62       restrial biosphere models are beginning to include connected carbon and nitrogen  
63       cycles to improve the realism of their simulations (Fisher et al. 2010; Brzostek  
64       et al. 2014; Wieder et al. 2015; Shi et al. 2016; Zhu et al. 2019). Simula-  
65       tions from these models indicate that coupling carbon and nitrogen cycles can  
66       drastically influence future biosphere-atmosphere feedbacks under global change,  
67       such as elevated carbon dioxide or nitrogen deposition (Thornton et al. 2007;  
68       Goll et al. 2012; Wieder et al. 2015; Wieder et al. 2019). Nonetheless, there  
69       are still limitations in our quantitative understanding of connected carbon and  
70       nitrogen dynamics (Thomas et al. 2015; Meyerholt et al. 2016; Rogers et al.  
71       2017; Exbrayat et al. 2018; Shi et al. 2019), forcing models to make potentially  
72       unreliable assumptions.

73           Plant nitrogen acquisition is a process in terrestrial ecosystems by which  
74       carbon and nitrogen are tightly coupled (Vitousek and Howarth 1991; Delaire  
75       et al. 2005; Brzostek et al. 2014). Plants must allocate photosynthetically de-

76 rived carbon belowground to produce and maintain root systems or exchange with  
77 symbiotic soil microbes in order to acquire nitrogen (Högberg et al. 2008; Hög-  
78 berg et al. 2010). Thus, plants have an inherent carbon cost associated with  
79 acquiring nitrogen, which can include both direct energetic costs associated with  
80 nitrogen acquisition and indirect costs associated with building structures that  
81 support nitrogen acquisition (Gutschick 1981; Rastetter et al. 2001; Vitousek  
82 et al. 2002; Menge et al. 2008). Model simulations (Fisher et al. 2010; Brzostek  
83 et al. 2014; Shi et al. 2016; Allen et al. 2020) and meta-analyses (Terrer et al.  
84 2018) suggest that these carbon costs vary between species, particularly those  
85 with different nitrogen acquisition strategies. For example, simulations using iter-  
86 ations of the Fixation and Uptake of Nitrogen (FUN) model indicate that species  
87 that acquire nitrogen from non-symbiotic active uptake pathways (e.g. mass flow)  
88 generally have larger carbon costs to acquire nitrogen than species that acquire  
89 nitrogen through symbiotic associations with nitrogen-fixing bacteria (Brzostek  
90 et al. 2014; Allen et al. 2020).

91 Carbon costs to acquire nitrogen likely vary in response to changes in soil  
92 nitrogen availability. For example, if the primary mode of nitrogen acquisition  
93 is through non-symbiotic active uptake, then nitrogen availability could decrease  
94 carbon costs to acquire nitrogen as a result of increased per-root nitrogen up-  
95 take (Franklin et al. 2009; Wang et al. 2018). However, if the primary mode of  
96 nitrogen acquisition is through symbiotic active uptake, then nitrogen availabil-  
97 ity may incur additional carbon costs to acquire nitrogen if it causes microbial  
98 symbionts to shift toward parasitism along the parasitism–mutualism continuum  
99 (Johnson et al. 1997; Hoek et al. 2016; Friel and Friesen 2019) or if it reduces

100 the nitrogen acquisition capacity of a microbial symbiont (van Diepen et al. 2007;  
101 Soudzilovskaia et al. 2015; Muñoz et al. 2016). Species may respond to shifts in  
102 soil nitrogen availability by switching their primary mode of nitrogen acquisition  
103 to a strategy with lower carbon costs to acquire nitrogen in order to maximize  
104 the magnitude of nitrogen acquired from a belowground carbon investment and  
105 outcompete other individuals for soil resources (Rastetter et al. 2001; Menge et al.  
106 2008).

107 Environmental conditions that affect demand to acquire nitrogen to sup-  
108 port new and existing tissues could also be a source of variance in plant carbon  
109 costs to acquire nitrogen. For example, an increase in plant nitrogen demand could  
110 increase carbon costs to acquire nitrogen if this increases the carbon that must be  
111 allocated belowground to acquire a proportional amount of nitrogen (Kulmatiski  
112 et al. 2017; Noyce et al. 2019). This could be driven by a temporary state of  
113 diminishing return associated with investing carbon toward building and main-  
114 taining structures that are necessary to support enhanced nitrogen uptake, such  
115 as fine roots (Matamala and Schlesinger 2000; Norby et al. 2004; Arndal et al.  
116 2018), mycorrhizal hyphae (Saleh et al. 2020), or root nodules (Parvin et al. 2020).  
117 Alternatively, if the environmental factor that increases plant nitrogen demand  
118 causes nitrogen to become more limiting in the system (e.g. atmospheric CO<sub>2</sub>;  
119 Luo et al. (2004), LeBauer and Treseder (2008), Vitousek et al. (2010), Liang  
120 et al. (2016)), species might switch their primary mode of nitrogen acquisition to  
121 a strategy with lower relative carbon costs to acquire nitrogen in order to gain a  
122 competitive advantage over species with either different or more limited modes of  
123 nitrogen acquisition (Ainsworth and Long 2005; Taylor and Menge 2018).

124        Using a plant economics approach, we examined the influence of plant  
125    nitrogen demand and soil nitrogen availability on plant carbon costs to acquire  
126    nitrogen. This was done by growing a species capable of forming associations  
127    with nitrogen-fixing bacteria (*Glycine max* L. (Merr)) and a species not capable  
128    of forming these associations (*Gossypium hirsutum* L.) under four levels of light  
129    availability (plant nitrogen demand proxy) and four levels of soil nitrogen fertil-  
130    ization (soil nitrogen availability proxy) in a full-factorial, controlled greenhouse  
131    experiment. We used this experimental set-up to test the following hypotheses:

- 132        1. An increase in plant nitrogen demand due to increasing light availability will  
133        increase carbon costs to acquire nitrogen through a proportionally larger  
134        increase in belowground carbon than whole-plant nitrogen acquisition. This  
135        will be the result of an increased investment of carbon toward belowground  
136        structures that support enhanced nitrogen uptake, but at a lower nitrogen  
137        return.
- 138        2. An increase in soil nitrogen availability will decrease carbon costs to acquire  
139        nitrogen as a result of increased per root nitrogen uptake in *G. hirsutum*.  
140        However, soil nitrogen availability will not affect carbon costs to acquire  
141        nitrogen in *G. max* because of the already high return of nitrogen supplied  
142        through nitrogen fixation.

**143** 2.2 Methods

**144** 2.2.1 *Experiment setup*

**145** *Gossypium hirsutum* and *G. max* were planted in individual 3 liter pots  
**146** (NS-300; Nursery Supplies, Orange, CA, USA) containing a 3:1 mix of unfertil-  
**147** ized potting mix (Sungro Sunshine Mix #2, Agawam, MA, USA) to native soil  
**148** extracted from an agricultural field most recently planted with *G. max* at the  
**149** USDA-ARS Laboratory in Lubbock, TX, USA (33.59°N, -101.90°W). The field  
**150** soil was classified as Amarillo fine sandy loam (75% sand, 10% silt, 15% clay).  
**151** Upon planting, all *G. max* pots were inoculated with *Bradyrhizobium japonicum*  
**152** (Verdesian N-Dure™ Soybean, Cary, NC, USA) to stimulate root nodulation. In-  
**153** dividuals of both species were grown under similar, unshaded, ambient greenhouse  
**154** conditions for 2 weeks to germinate and begin vegetative growth. Three blocks  
**155** were set up in the greenhouse, each containing four light treatments created us-  
**156** ing shade cloth that reduced incoming radiation by either 0 (full sun), 30, 50,  
**157** or 80%. Two weeks post-germination, individuals were randomly placed in the  
**158** four light treatments in each block. Individuals received one of four nitrogen fer-  
**159** tilization doses as 100ml of a modified Hoagland solution (Hoagland and Arnon  
**160** 1950) equivalent to either 0, 70, 210, or 630 ppm N twice per week within each  
**161** light treatment. Nitrogen fertilization doses were received as topical agents to  
**162** the soil surface. Each Hoagland solution was modified to keep concentrations of  
**163** other macro- and micronutrients equivalent (Supplementary Table S1). Plants  
**164** were routinely well watered to eliminate water stress.

165 2.2.2 *Plant measurements and calculations*

166 Each individual was harvested after 5 weeks of treatment, and biomass  
167 was separated by organ type (leaves, stems, and roots). Nodules on *G. max*  
168 roots were also harvested. With the exception of the 0% shade cover and 630  
169 ppm N treatment combination, all treatment combinations in both species had  
170 lower average dry biomass:pot volume ratios than the 1:1 ratio recommended by  
171 Poorter et al. (2012) to minimize the likelihood of pot volume-induced growth  
172 limitation (Supplementary Tables S2, S3; Supplementary Fig. S1). All harvested  
173 material was dried, weighed, and ground by organ type. Carbon and nitrogen  
174 content ( $\text{g g}^{-1}$ ) was determined by subsampling from ground and homogenized  
175 biomass of each organ type using an elemental analyzer (Costech 4010; Costech,  
176 Inc., Valencia, CA, USA). We scaled these values to total leaf, stem, and root  
177 carbon and nitrogen biomass (g) by multiplying dry biomass of each organ type  
178 by carbon or nitrogen content of each corresponding organ type. Whole-plant  
179 nitrogen biomass (g) was calculated as the sum of total leaf (g), stem (g), and  
180 root (g) nitrogen biomass. Root nodule carbon biomass was not included in the  
181 calculation of root carbon biomass; however, relative plant investment toward root  
182 or root nodule standing stock was estimated as the ratio of root biomass to root  
183 nodule biomass ( $\text{g g}^{-1}$ ), following similar metrics to those adopted by Dovrat et al.  
184 (2018) and Dovrat et al. (2020).

185 Carbon costs to acquire nitrogen ( $\text{gC gN}^{-1}$ ) were estimated as the ratio of  
186 total root carbon biomass (gC) to whole-plant nitrogen biomass (gN). This cal-  
187 culation quantifies the relationship between carbon spent on nitrogen acquisition  
188 and whole-plant nitrogen acquisition by using root carbon biomass as a proxy for

189 estimating the magnitude of carbon allocated toward nitrogen acquisition. This  
190 calculation therefore assumes that the magnitude of root carbon standing stock is  
191 proportional to carbon transferred to root nodules or mycorrhizae, or lost through  
192 root exudation or turnover. This assumption has been supported in species that  
193 associate with ectomycorrhizal fungi (Hobbie 2006; Hobbie and Hobbie 2008), but  
194 is less clear in species that acquire nitrogen through non-symbiotic active uptake  
195 or symbiotic nitrogen fixation. It is also unclear whether relationships between  
196 root carbon standing stock and carbon transfer to root nodules are similar in mag-  
197 nitude to carbon lost through exudation or when allocated toward other active  
198 uptake pathways. Thus, because of the way we performed our measurements, our  
199 proximal values of carbon costs to acquire nitrogen are underestimates.

200 2.2.3 *Statistical analyses*

201 We explored the effects of light and nitrogen availability on carbon costs to  
202 acquire nitrogen using separate linear mixed-effects models for each species. Mod-  
203 els included shade cover, nitrogen fertilization, and interactions between shade  
204 cover and nitrogen fertilization as continuous fixed effects, and also included block  
205 as a random intercept term. Three separate models for each species were built  
206 with this independent variable structure for three different dependent variables: (i)  
207 carbon costs to acquire nitrogen ( $\text{gC gN}^{-1}$ ); (ii) whole-plant nitrogen biomass (de-  
208 nominator of carbon cost to acquire nitrogen;  $\text{gN}$ ); and (iii) root carbon biomass  
209 (numerator of carbon cost to acquire nitrogen;  $\text{gC}$ ). We constructed two additional  
210 models for *G. max* with the same model structure described above to investigate  
211 the effects of light availability and nitrogen fertilization on root nodule biomass

212 (g) and the ratio of root nodule biomass to root biomass (unitless).

213 We used Shapiro–Wilk tests of normality to determine whether species-  
214 specifc linear mixed-effects model residuals followed a normal distribution. None  
215 of our models satisfied residual normality assumptions when models were fit using  
216 untransformed data (Shapiro–Wilk:  $P < 0.05$  in all cases). We attempted to satisfy  
217 residual normality assumptions by first fitting models using dependent variables  
218 that were natural-log transformed. If residual normality assumptions were still  
219 not met (Shapiro–Wilk:  $P < 0.05$ ), then models were fit using dependent variables  
220 that were square root transformed. All residual normality assumptions were satis-  
221 fied when models were fit with either a natural-log or square root transformation  
222 (Shapiro–Wilk:  $P > 0.05$  in all cases). Specifically, we natural-log transformed *G.*  
223 *hirsutum* carbon costs to acquire nitrogen and *G. hirsutum* whole-plant nitrogen  
224 biomass. We also square root transformed *G. max* carbon costs to acquire nitro-  
225 gen, *G. max* whole-plant nitrogen biomass, root carbon biomass in both species,  
226 *G. max* root nodule biomass, and the *G. max* ratio of root nodule biomass to root  
227 biomass. We used the ‘lmer’ function in the ‘lme4’ R package (Bates et al. 2015)  
228 to fit each model and the ‘Anova’ function in the ‘car’ R package (Fox and Weis-  
229 berg 2019) to calculate Wald’s  $\chi^2$  to determine the significance ( $\alpha = 0.05$ ) of each  
230 fixed effect coefficient. Finally, we used the ‘emmeans’ R package (Lenth 2019)  
231 to conduct post-hoc comparisons of our treatment combinations using Tukey’s  
232 tests. Degrees of freedom for all Tukey’s tests were approximated using the Ken-  
233 ward–Roger approach (Kenward and Roger 1997). All analyses and plots were  
234 conducted in R version 4.0.1 (R Core Team 2021).

**235** 2.3 Results

**236** 2.3.1 *Carbon costs to acquire nitrogen*

**237** Carbon costs to acquire nitrogen in *G. hirsutum* increased with increasing  
**238** light availability ( $p < 0.001$ ; Table 2.1; Fig. 2.1) and decreased with increasing  
**239** nitrogen fertilization ( $p < 0.001$ ; Table 2.1; Fig. 2.1). There was no interaction  
**240** between light availability and nitrogen fertilization ( $p = 0.486$ , Table 2.1; Fig.  
**241** 2.1).

**242** Carbon costs to acquire nitrogen in *G. max* also increased with increasing  
**243** light availability ( $p < 0.001$ , Table 2.1; Fig. 2.1) and decreased with increasing  
**244** nitrogen fertilization ( $p < 0.001$ ; Table 2.1; Fig. 2.1). There was no interaction  
**245** between light availability and nitrogen fertilization ( $p = 0.261$ , Table 2.1; Fig.  
**246** 2.1).

**Table 2.1.** Analysis of variance results exploring species-specific effects of light availability, nitrogen fertilization, and their interactions on carbon costs to acquire nitrogen, whole-plant nitrogen biomass, and root carbon biomass

	df	Carbon costs to acquire nitrogen			Whole-plant nitrogen biomass			Root carbon biomass		
		Coefficient	$\chi^2$	p	Coefficient	$\chi^2$	p	Coefficient	$\chi^2$	p
<i>G. hirsutum</i>										
Intercept		1.594	-	-	-3.232	-	-	0.432	-	-
Light (L)	1	-1.09E-02	56.494	<0.001	-6.41E-03	91.275	<0.001	-2.62E-03	169.608	<0.001
Nitrogen (N)	1	-1.34E-03	54.925	<0.001	1.83E-03	118.784	<0.001	1.15E-04	2.901	0.089
L*N	1	3.88E-06	0.485	0.486	-1.34E-05	10.721	0.001	-1.67E-06	3.140	0.076
<i>G. max</i>										
Intercept		1.877	-	-	0.239	-	-	0.438	-	-
Light (L)	1	-7.67E-03	174.156	<0.001	-6.72E-04	39.799	<0.001	-2.55E-03	194.548	<0.001
Nitrogen (N)	1	-2.35E-04	21.948	<0.001	1.55E-04	70.771	<0.001	2.52E-04	19.458	<0.001
L*N	1	-2.89E-06	1.262	0.261	-6.32E-07	1.435	0.231	-3.16E-06	10.803	0.001

\*Significance determined using Wald's  $\chi^2$  tests ( $P=0.05$ ).  $P$ -values<0.05 are in bold and  $p$ -values between 0.05 and 0.1 are italicized. Negative coefficients for light treatments indicate a positive effect of increasing light availability on all response variables, as light availability is treated as percent shade cover in all linear mixed-effects models.

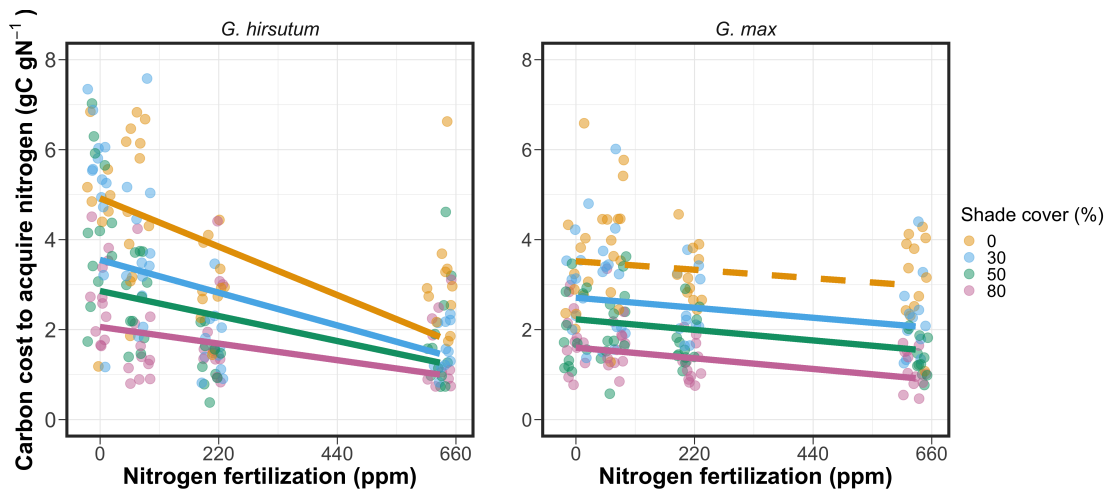


**Figure 2.1.** Relationships between soil nutrient fertilization and light availability on carbon costs to acquire nitrogen in *G. hirsutum* and *G. max*. Nitrogen fertilization treatments are represented on the x-axis. Shade cover treatments are represented through colored points and trendlines. Trendlines were created by back-transforming marginal mean slopes and intercepts from species-specific linear mixed-effects models. These values were calculated using the ‘emtrends’ and ‘emmmeans’ functions in the ‘emmeans’ R package (Lenth, 2019). Points are jittered for visibility. Yellow points and trendlines represent the 0% shade cover treatment, blue points and trendlines represent the 30% shade cover treatment, green points and trendlines represent the 50% shade cover treatment, and purple points and trendlines represent the 80% shade cover treatment. Solid trendlines indicate slopes that are significantly different from zero (Tukey:  $p < 0.05$ ), while dashed trendlines indicate slopes that are not statistically different from zero.

**247** 2.3.2 *Whole plant nitrogen biomass*

**248** Whole-plant nitrogen biomass in *G. hirsutum* was driven by an interaction  
**249** between light availability and nitrogen fertilization ( $p = 0.001$ ; Table 2.1; Fig.  
**250** 2.2). This interaction indicated a greater stimulation of whole-plant nitrogen  
**251** biomass by nitrogen fertilization as light levels increased (Table 2.1; Fig. 2.2).

**252** Whole-plant nitrogen biomass in *G. max* increased with increasing light  
**253** availability ( $p < 0.001$ ) and nitrogen fertilization ( $p < 0.001$ ), with no interaction  
**254** between light availability and nitrogen fertilization ( $p = 0.231$ ; Table 2.1; Fig.  
**255** 2.2).

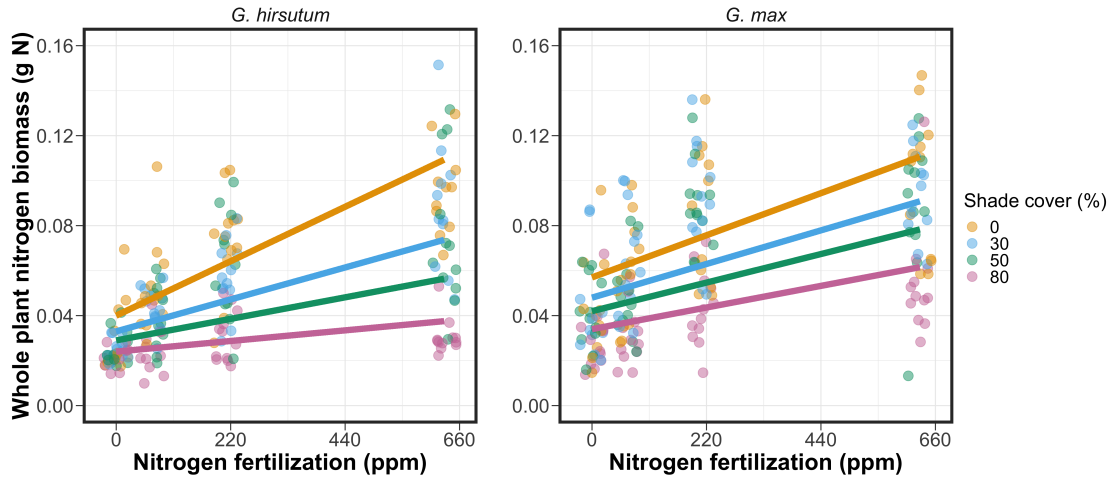


**Figure 2.2.** Relationships between soil nutrient fertilization and light availability on whole-plant nitrogen biomass in *G. hirsutum* and *G. max*. Whole-plant nitrogen biomass is the denominator of the carbon cost to acquire nitrogen calculation. Nitrogen fertilization treatments are represented on the x-axis. Shade cover treatments are represented through colored points and trendlines. Trendlines were created by back-transforming marginal mean slopes and intercepts from species-specific linear mixed-effects models. These values were calculated using the ‘emtrends’ and ‘emmmeans’ functions in the ‘emmeans’ R package (Lenth 2019). Points are jittered for visibility. Yellow points and trendlines represent the 0% shade cover treatment, blue points and trendlines represent the 30% shade cover treatment, green points and trendlines represent the 50% shade cover treatment, and purple points and trendlines represent the 80% shade cover treatment. Solid trendlines indicate slopes that are significantly different from zero (Tukey:  $P < 0.05$ ), while dashed trendlines indicate slopes that are not statistically different from zero.

**256** 2.3.3 *Root carbon biomass*

**257** Root carbon biomass in *G. hirsutum* significantly increased with increasing  
**258** light availability ( $p < 0.001$ ; Table 2.1; Fig. 2.3) and marginally increased with  
**259** nitrogen fertilization ( $p = 0.089$ ; Table 2.1; Fig. 2.3). There was also a marginal  
**260** interaction between light availability and nitrogen fertilization ( $p = 0.076$ ; Table  
**261** 2.1), driven by an increase in the positive response of root carbon biomass to  
**262** increasing nitrogen fertilization as light availability increased. This resulted in  
**263** significantly positive trends between root carbon biomass and nitrogen fertilization  
**264** in the two highest light treatments (Tukey:  $p < 0.05$  in both cases; Table 2.3;  
**265** Fig. 2.3) and no effect of nitrogen fertilization in the two lowest light treatments  
**266** (Tukey:  $p > 0.05$  in both cases; Table 2.3; Fig. 2.3).

**267** There was an interaction between light availability and nitrogen fertiliza-  
**268** tion on root carbon biomass in *G. max* ( $p = 0.001$ ; Table 2.1; Fig. 2.3). Post-hoc  
**269** analyses indicated that the positive effects of nitrogen fertilization on *G. max* root  
**270** carbon biomass increased with increasing light availability (Table 2.3; Fig. 2.3).  
**271** There were also positive individual effects of increasing nitrogen fertilization ( $p <$   
**272**  $0.001$ ) and light availability ( $p < 0.001$ ) on *G. max* root carbon biomass (Table  
**273** 2.1; Fig. 2.3).

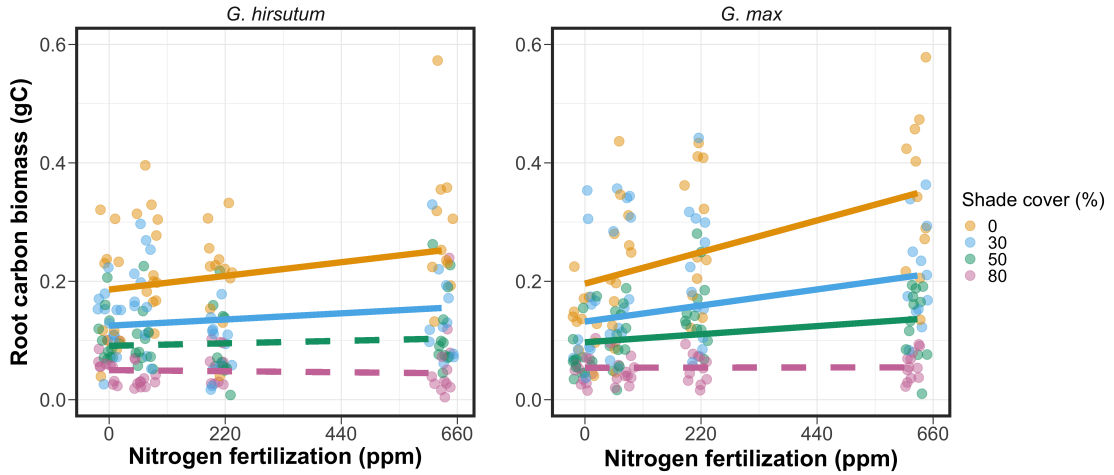


**Figure 2.3.** Relationships between soil nutrient fertilization and light availability on root carbon biomass in *G. hirsutum* and *G. max*. Root carbon biomass is the numerator of the carbon cost to acquire nitrogen calculation. Nitrogen fertilization treatments are represented on the x-axis. Shade cover treatments are represented through colored points and trendlines. Trendlines were created by back-transforming marginal mean slopes and intercepts from species-specific linear mixed-effects models. These values were calculated using the ‘emtrends’ and ‘emmmeans’ functions in the ‘emmeans’ R package (Lenth 2019). Points are jittered for visibility. Yellow points and trendlines represent the 0% shade cover treatment, blue points and trendlines represent the 30% shade cover treatment, green points and trendlines represent the 50% shade cover treatment, and purple points and trendlines represent the 80% shade cover treatment. Solid trendlines indicate slopes that are significantly different from zero (Tukey:  $p < 0.05$ ), while dashed trendlines indicate slopes that are not statistically different from zero.

**274** 2.3.4 *Root nodule biomass*

**275** Root nodule biomass in *G. max* increased with increasing light availability  
**276** ( $p < 0.001$ ; Table 2.2; Fig. 2.4A) and decreased with increasing nitrogen fertiliza-  
**277** tion ( $p < 0.001$ ; Table 2.2; Fig. 2.4A). There was no interaction between nitrogen  
**278** fertilization and light availability ( $p = 0.133$ ; Table 2.2; Fig. 2.4A). The ratio of  
**279** root nodule biomass to root biomass did not change in response to light avail-  
**280** ability ( $p = 0.481$ ; Table 2.2; Fig. 2.4B) but decreased with increasing nitrogen  
**281** fertilization ( $p < 0.001$ ; Table 2.2; Fig. 2.4B). There was no interaction between  
**282** nitrogen fertilization and light availability on the ratio of root nodule biomass to  
**283** root biomass ( $p = 0.621$ ; Table 2.2; Fig. 2.4B).

**Table 2.2.** Analysis of variance results exploring effects of light availability, nitrogen fertilization, and their interactions on *G. max* root nodule biomass and the ratio of root nodule biomass to root biomass\*

	Nodule biomass			Nodule biomass: root biomass			
	df	Coefficient	$\chi^2$	p	coefficient	$\chi^2$	p
(Intercept)		0.302	-	-	0.448	-	-
Light (L)	1	-1.81E-03	72.964	<b>&lt;0.001</b>	-8.76E-05	0.496	0.481
Nitrogen (N)	1	-2.83E-04	115.377	<b>&lt;0.001</b>	-5.09E-04	156.476	<b>&lt;0.001</b>
L*N	1	1.14E-06	2.226	0.133	-7.30E-07	0.244	0.621

\*Significance determined using Wald's  $\chi^2$  tests ( $\alpha = 0.05$ ). *p*-values less than 0.05 are in bold. Negative coefficients for light treatments indicate a positive effect of increasing light availability on all response variables, as light availability is treated as percent shade cover in all linear mixed-effects models. Root nodule biomass and nodule biomass: root biomass models were only constructed for *G. max* because *G. hirsutum* was not inoculated with *B. japonicum* and is not capable of forming root nodules.

**Table 2.3.** Slopes of the regression line describing the relationship between each dependent variable and nitrogen fertilization at each light level\*

Shade cover	Carbon cost to acquire nitrogen	Whole-plant nitrogen biomass	Root carbon biomass	Root nodule biomass	Nodule biomass root biomass
<i>G. hirsutum</i>					
0%	<b>-1.34E-03<sup>a</sup></b>	<b>1.83E-03<sup>a</sup></b>	<b>1.15E-04<sup>b</sup></b>	-	-
30%	<b>-1.22E-03<sup>a</sup></b>	<b>1.43E-03<sup>a</sup></b>	<b>1.17E-04<sup>b</sup></b>	-	-
50%	<b>-1.14E-03<sup>a</sup></b>	<b>1.17E-03<sup>a</sup></b>	3.12E-05 <sup>b</sup>	-	-
80%	<b>-1.02E-03<sup>a</sup></b>	<b>7.66E-04<sup>a</sup></b>	-1.89E-06 <sup>b</sup>	-	-
<i>G. max</i>					
0%	-2.35E-04 <sup>b</sup>	<b>1.55E-05<sup>b</sup></b>	<b>2.51E-04<sup>b</sup></b>	<b>-2.83E-04<sup>b</sup></b>	<b>-5.09E-04<sup>b</sup></b>
30%	<b>-3.22E-04<sup>b</sup></b>	<b>1.35E-05<sup>b</sup></b>	<b>1.57E-04<sup>b</sup></b>	<b>-2.49E-04<sup>b</sup></b>	<b>-5.31E-04<sup>b</sup></b>
50%	<b>-3.80E-04<sup>b</sup></b>	<b>1.23E-05<sup>b</sup></b>	<b>9.37E-05<sup>b</sup></b>	<b>-2.26E-04<sup>b</sup></b>	<b>-5.45E-04<sup>b</sup></b>
80%	<b>-4.66E-04<sup>b</sup></b>	<b>1.04E-05<sup>b</sup></b>	-9.95E-07 <sup>b</sup>	<b>-1.92E-04<sup>b</sup></b>	<b>-5.67E-04<sup>b</sup></b>

\*Slopes represent estimated marginal mean slopes from linear mixed-effects models described in the Methods. Slopes were calculated using the ‘emmeans’ R package (Lenth 2019). Superscripts indicate slopes fit to natural-log (<sup>a</sup>) or square root (<sup>b</sup>) transformed data. Slopes statistically different from zero (Tukey:  $p < 0.05$ ) are indicated in bold. Marginally significant slopes (Tukey:  $0.05 < p < 0.1$ ) are italicized.

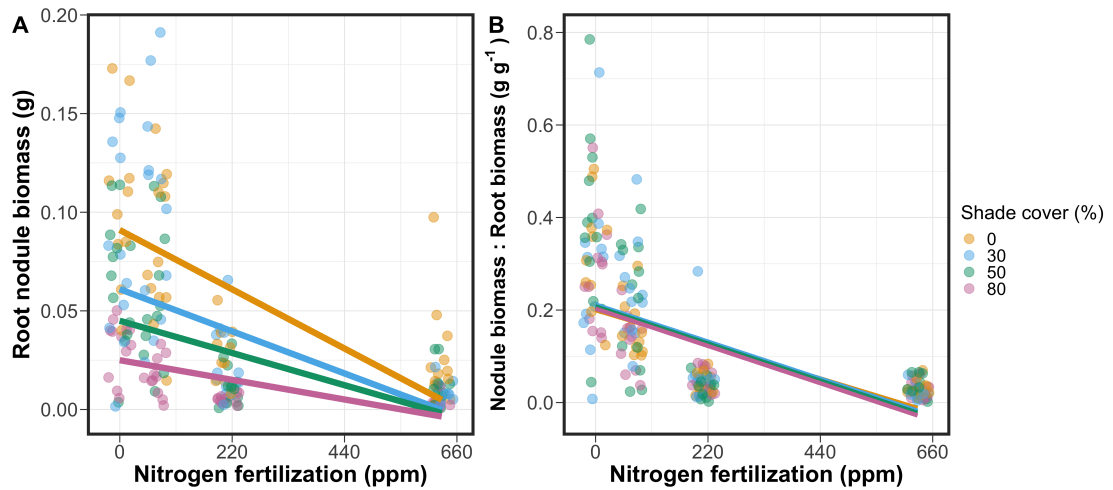


**Figure 2.4.** Effects of shade cover and nitrogen fertilization on root nodule biomass (A) and the ratio of root nodule biomass to root biomass (B) in *G. max*. Nitrogen fertilization treatments are represented on the x-axis. Shade cover treatments are represented through colored points and trendlines. Trendlines were created by back-transforming marginal mean slopes and intercepts from species-specific linear mixed-effects models. These values were calculated using the ‘emtrends’ and ‘emmeans’ functions in the ‘emmeans’ R package (Lenth 2019). Points are jittered for visibility. Yellow points and trendlines represent the 0% shade cover treatment, blue points and trendlines represent the 30% shade cover treatment, green points and trendlines represent the 50% shade cover treatment, and purple points and trendlines represent the 80% shade cover treatment. Solid trendlines indicate slopes that are significantly different from zero (Tukey:  $p < 0.05$ ), while dashed trendlines indicate slopes that are not statistically different from zero.

**284** 2.4 Discussion

**285** In this chapter, we determined the effects of light availability and soil ni-  
**286** trogen fertilization on root mass carbon costs to acquire nitrogen in *G. hirsutum*  
**287** and *G. max*. In support of our hypotheses, we found that carbon costs to acquire  
**288** nitrogen generally increased with increasing light availability and decreased with  
**289** increasing soil nitrogen fertilization in both species. These findings suggest that  
**290** carbon costs to acquire nitrogen are determined by factors that influence plant  
**291** nitrogen demand and soil nitrogen availability. In contrast to our second hypothe-  
**292** sis, root nodulation data suggested that *G. max* and *G. hirsutum* achieved similar  
**293** directional carbon cost responses to nitrogen fertilization despite a likely shift in  
**294** *G. max* allocation from nodulation to root biomass along the nitrogen fertilization  
**295** gradient (Fig. 2.4B).

**296** Both *G. max* and *G. hirsutum* experienced an increase in carbon costs to  
**297** acquire nitrogen due to increasing light availability. These patterns were driven by  
**298** a larger increase in root carbon biomass than whole-plant nitrogen biomass. In-  
**299** creases in root carbon biomass due to factors that increase plant nitrogen demand  
**300** are a commonly observed pattern, as carbon allocated belowground provides sub-  
**301** strate needed to produce and maintain structures that satisfy aboveground plant  
**302** nitrogen demand (Nadelhoffer and Raich 1992; Giardina et al. 2005; Raich et al.  
**303** 2014). Our findings suggest that plants allocate relatively more carbon for acquir-  
**304** ing nitrogen when demand increases over short temporal scales, which may cause  
**305** a temporary state of diminishing return due to asynchrony between belowground  
**306** carbon and whole-plant nitrogen responses to plant nitrogen demand (Kulmatiski  
**307** et al. 2017; Noyce et al. 2019). These responses might be attributed to a temporal

308 lag associated with producing structures that enhance nitrogen acquisition. For  
309 example, fine roots (Matamala and Schlesinger 2000; Norby et al. 2004; Arndal  
310 et al. 2018) and root nodules (Parvin et al. 2020) take time to build and first  
311 require the construction of coarse roots. Thus, full nitrogen returns from these  
312 investments may not occur immediately (Kayler et al. 2010; Kayler et al. 2017),  
313 and may vary by species acquisition strategy. We speculate that increases in ni-  
314 trogen acquisition from a given carbon investment may occur beyond the 5 week  
315 scope of this experiment. A similar study conducted over a longer temporal scale  
316 would address this.

317 Increasing soil nitrogen fertilization generally decreased carbon costs to  
318 acquire nitrogen in both species. These patterns were driven by a larger increase  
319 in whole-plant nitrogen biomass than root carbon biomass. In *G. hirsutum*, re-  
320 ductions in carbon costs to acquire nitrogen may have been due to an increase in  
321 per-root nitrogen uptake, allowing individuals to maximize the amount of nitro-  
322 gen acquired from a belowground carbon investment. Interestingly, increased soil  
323 nitrogen fertilization increased whole-plant nitrogen biomass in *G. max* despite  
324 reductions in root nodule biomass that likely reduced the nitrogen-fixing capac-  
325 ity of *G. max* (Andersen et al. 2005; Muñoz et al. 2016). While reductions in  
326 root nodulation due to increased soil nitrogen availability are commonly observed  
327 (Gibson and Harper 1985; Fujikake et al. 2003), our responses were observed in  
328 tandem with increased root carbon biomass, implying that *G. max* shifted relative  
329 carbon allocation from nitrogen fixation to soil nitrogen acquisition (Markham and  
330 Zekveld 2007; Dovrat et al. 2020). This was likely because there was a reduction in  
331 the carbon cost advantage of acquiring fixed nitrogen relative to soil nitrogen, and

**332** suggests that species capable of associating with symbiotic nitrogen-fixing bacte-  
**333** ria shift their relative nitrogen acquisition pathway to optimize nitrogen uptake  
**334** (Rastetter et al. 2001). Future studies should further investigate these patterns  
**335** with a larger quantity of phylogenetically related species, or different varieties  
**336** of a single species that differ in their ability to form associations with symbiotic  
**337** nitrogen-fixing bacteria to more directly test the impact of nitrogen fixation on  
**338** the patterns observed in this study.

**339** Carbon costs to acquire nitrogen are subsumed in the general discussion of  
**340** economic analogies to plant resource uptake (Bloom et al. 1985; Rastetter et al.  
**341** 2001; Vitousek et al. 2002; Phillips et al. 2013; Terrer et al. 2018; Henneron et al.  
**342** 2020). Despite this, terrestrial biosphere models rarely include these carbon costs  
**343** within their framework for predicting plant nitrogen uptake. There is currently  
**344** one plant resource uptake model, FUN, that quantitatively predicts carbon costs  
**345** to acquire nitrogen within a framework for predicting plant nitrogen uptake for  
**346** different nitrogen acquisition strategies (Fisher et al. 2010; Brzostek et al. 2014)  
**347** (Fisher et al. 2010; Brzostek et al. 2014). Iterations of FUN are currently  
**348** coupled to two terrestrial biosphere models: the Community Land Model 5.0 and  
**349** the Joint UK Land Environment Simulator (Shi et al. 2016; Lawrence et al.  
**350** 2019; Clark et al. 2011). Recent work suggests that coupling FUN to CLM 5.0  
**351** caused a large overprediction of plant nitrogen uptake associated with nitrogen  
**352** fixation (Davies-Barnard et al. 2020). Thus, empirical data from manipulative  
**353** experiments that explicitly quantify carbon costs to acquire nitrogen in species  
**354** capable of associating with nitrogen-fixing bacteria across different environmental  
**355** contexts is an important step toward identifying potential biases in models such

**356** as FUN.

**357** Our findings broadly support the FUN formulation of carbon costs to ac-  
**358** quire nitrogen in response to soil nitrogen availability. FUN calculates carbon  
**359** costs to acquire nitrogen based on the sum of carbon costs to acquire nitrogen  
**360** via nitrogen fixation, mycorrhizal active uptake, non-mycorrhizal active uptake,  
**361** and retranslocation (Fisher et al. 2010; Brzostek et al. 2014). Carbon costs to  
**362** acquire nitrogen via mycorrhizal or non-mycorrhizal active uptake pathways are  
**363** derived as a function of nitrogen availability, root biomass, and two parameterized  
**364** values based on nitrogen acquisition strategy (Brzostek et al. 2014). Due to this,  
**365** FUN simulates a net decrease in carbon costs to acquire nitrogen with increasing  
**366** nitrogen availability for mycorrhizal and non-mycorrhizal active uptake pathways,  
**367** assuming constant root biomass. This was a pattern we observed in *G. hirsutum*  
**368** regardless of light availability. In contrast, FUN would not simulate a net change  
**369** in carbon costs to acquire nitrogen via nitrogen fixation due to nitrogen avail-  
**370** ability. This is because carbon costs to acquire nitrogen via nitrogen fixation are  
**371** derived from a well-established function of soil temperature, which is independent  
**372** of soil nitrogen availability (Houlton et al. 2008; Fisher et al. 2010). We observed  
**373** a net reduction in carbon costs to acquire nitrogen in *G. max*, except when in-  
**374** dividuals were grown under 0% shade cover (Fig. 2.1). While a net reduction of  
**375** carbon costs in response to nitrogen fertilization runs counter to nitrogen fixa-  
**376** tion carbon costs simulated by FUN, these patterns were likely because *G. max*  
**377** individuals switched their primary mode of nitrogen acquisition from symbiotic  
**378** nitrogen fixation to a non-symbiotic active uptake pathway (Fig. 2.4B).

**379** It should be noted that the metric used in this study to determine carbon

380 costs to acquire nitrogen has several limitations. Most notably, this metric uses  
381 root carbon biomass as a proxy for estimating the amount of carbon spent on  
382 nitrogen acquisition. While it is true that most carbon allocated belowground  
383 has at least an indirect structural role in acquiring soil resources, it remains un-  
384 clear whether this assumption holds true for species that acquire nitrogen via  
385 symbiotic nitrogen fixation. We also cannot quantify carbon lost through root  
386 exudates or root turnover, which may increase due to factors that increase plant  
387 nitrogen demand (Tingey et al. 2000; Phillips et al. 2011), and can increase the  
388 magnitude of available nitrogen from soil organic matter through priming effects  
389 on soil microbial communities (Uselman et al. 2000; Bengtson et al. 2012). It is  
390 also not clear whether these assumptions hold under all environmental conditions,  
391 such as those that shift belowground carbon allocation toward a different mode of  
392 nitrogen acquisition (Taylor and Menge 2018; Friel and Friesen 2019) or between  
393 species with different acquisition strategies. In this study, increasing soil nitrogen  
394 fertilization increased carbon investment to roots relative to carbon transferred  
395 to root nodules (Fig. 2.4B). By assuming that carbon allocated to root carbon  
396 was proportional to carbon allocated to root nodules across all treatment com-  
397 binations, these observed responses to soil nitrogen fertilization were likely to be  
398 overestimated in *G. max*. We encourage future research to quantify these carbon  
399 fates independently.

400 Researchers conducting pot experiments must carefully choose pot volume  
401 to minimize the likelihood of pot volume-induced growth limitation (Poorter et al.  
402 2012). Poorter et al. (2012) indicate that researchers are likely to avoid growth  
403 limitations associated with pot volume if measurements are collected when the

404 plant biomass:pot volume ratio is less than 1 g L<sup>-1</sup>. In this experiment, all treat-  
405 ment combinations in both species had biomass:pot volume ratios less than 1 g  
406 L<sup>-1</sup> except for *G. max* and *G. hirsutum* that were grown under 0% shade cover  
407 and had received 630 ppm N. Specifically, *G. max* and *G. hirsutum* had average  
408 respective biomass:pot volume ratios of 1.24±0.07 g L<sup>-1</sup> and 1.34±0.13 g L<sup>-1</sup>, when  
409 grown under 0% shade cover and received 630 ppm N (Supplementary Tables S2,  
410 S3; Supplementary Fig. S1). If growth in this treatment combination was limited  
411 by pot volume, then individuals may have had larger carbon costs to acquire ni-  
412 trogen than would be expected if they were grown in larger pots. This pot volume  
413 induced growth limitation could cause a reduction in per-root nitrogen uptake as-  
414 sociated with more densely packed roots, which could reduce the positive effect  
415 of nitrogen fertilization on whole-plant nitrogen biomass relative to root carbon  
416 biomass (Poorter et al. 2012).

417 Growth limitation associated with pot volume provides a possible explana-  
418 tion for the marginally insignificant effect of increasing nitrogen fertilization on *G.*  
419 *max* carbon costs to acquire nitrogen when grown under 0% shade cover (Table  
420 2.3; Fig. 2.1). This is because the regression line describing the relationship be-  
421 tween carbon costs to acquire nitrogen and nitrogen fertilization in *G. max* grown  
422 under 0% shade cover would have flattened if growth limitation had caused larger  
423 than expected carbon costs to acquire nitrogen in the 0% shade cover, 630 ppm  
424 N treatment combination. This may have been exacerbated by the fact that *G.*  
425 *max* likely shifted relative carbon allocation from nitrogen fixation to soil nitrogen  
426 acquisition, which could have increased the negative effect of more densely packed  
427 roots on nitrogen uptake. These patterns could have also occurred in *G. hirsutum*

428 grown under 0% shade cover; however, there was no change in the effect of nitro-  
429 gen fertilization on *G. hirsutum* carbon costs to acquire nitrogen grown under 0%  
430 shade cover relative to other shade cover treatments. Regardless, the possibility  
431 of growth limitation due to pot volume suggests that effects of increasing nitro-  
432 gen fertilization on carbon costs to acquire nitrogen in both species grown under  
433 0% shade cover could have been underestimated. Follow-up studies using a simi-  
434 lar experimental design with a larger pot volume would be necessary in order to  
435 determine whether these patterns were impacted by pot volume-induced growth  
436 limitation.

437 In conclusion, this study provides empirical evidence that carbon costs to  
438 acquire nitrogen are influenced by light availability and soil nitrogen fertilization  
439 in a species capable of acquiring nitrogen via symbiotic nitrogen fixation and a  
440 species not capable of forming such associations. We show that carbon costs to  
441 acquire nitrogen generally increase with increasing light availability and decrease  
442 with increasing nitrogen fertilization. This study provides important empirical  
443 data needed to evaluate the formulation of carbon costs to acquire nitrogen in  
444 terrestrial biosphere models, particularly carbon costs to acquire nitrogen that  
445 are associated with symbiotic nitrogen fixation. Our findings broadly support  
446 the general formulation of these carbon costs in the FUN biogeochemical model  
447 in response to shifts in nitrogen availability. However, there is a need for future  
448 studies to explicitly quantify carbon costs to acquire nitrogen under different en-  
449 vironmental contexts, over longer temporal scales, and using larger selections of  
450 phylogenetically related species. In addition, we suggest that future studies mini-  
451 mize the limitations associated with the metric used here by explicitly measuring

**452** belowground carbon fates independently.

453

## Chapter 3

454      Soil nitrogen availability modifies leaf nitrogen economies in mature  
455      temperate deciduous forests: a direct test of photosynthetic least-cost  
456      theory

457      3.1    Introduction

458              Photosynthesis represents the largest carbon flux between the atmosphere  
459          and land surface (IPCC 2021), and plays a central role in biogeochemical cycling  
460          at multiple spatial and temporal scales (Vitousek and Howarth 1991; LeBauer and  
461          Treseder 2008; Kaiser et al. 2015; Wieder et al. 2015). Therefore, carbon and  
462          energy fluxes simulated by terrestrial biosphere models are sensitive to the formu-  
463          lation of photosynthetic processes (Ziehn et al. 2011; Bonan et al. 2011; Booth  
464          et al. 2012; Smith et al. 2016; Smith et al. 2017) and must be represented using  
465          robust, empirically tested processes (Prentice et al. 2015; Wieder et al. 2019).  
466              Current formulations of photosynthesis vary across terrestrial biosphere models  
467          (Smith and Dukes 2013; Rogers et al. 2017), which causes variation in modeled  
468          ecosystem processes (Knorr 2000; Knorr and Heimann 2001; Bonan et al. 2011;  
469          Friedlingstein et al. 2014) and casts uncertainty on the ability of these models to  
470          accurately predict terrestrial ecosystem responses and feedbacks to global change  
471          (Zaehle et al. 2005; Schaefer et al. 2012; Davies-Barnard et al. 2020).

472              Terrestrial biosphere models commonly represent C<sub>3</sub> photosynthesis through  
473          variants of the Farquhar et al. (1980) biochemical model (Smith and Dukes 2013;  
474          Rogers 2014; Rogers et al. 2017). This well-tested photosynthesis model es-  
475          timates leaf-level carbon assimilation, or photosynthetic capacity, as a function  
476          of the maximum rate of Ribulose-1,5-bisphosphate carboxylase-oxygenase (Ru-

477 bisco) carboxylation ( $V_{cmax}$ ) and the maximum rate of Ribulose-1,5-bisphosphate  
478 (RuBP) regeneration ( $J_{max}$ ) (Farquhar et al. 1980). Many terrestrial biosphere  
479 models predict these model inputs based on plant functional group specific linear  
480 relationships between leaf nutrient content and  $V_{cmax}$  (Smith and Dukes 2013;  
481 Rogers 2014; Rogers et al. 2017) under the tenet that a large fraction of leaf  
482 nutrients, and nitrogen (N) in particular, are partitioned toward building and  
483 maintaining enzymes that support photosynthetic capacity, such as Rubisco (Brix  
484 1971; Gulmon and Chu 1981; Evans 1989; Kattge et al. 2009; Walker et al. 2014).  
485 Terrestrial biosphere models also predict leaf nutrient content from soil nutrient  
486 availability based on the assumption that increasing soil nutrients generally in-  
487 creases leaf nutrients (Firn et al. 2019; Li et al. 2020; Liang et al. 2020) which, in  
488 the case of N, generally corresponds with an increase in photosynthetic processes  
489 (Li et al. 2020; Liang et al. 2020).

490       Recent work calls the generality of relationships between soil nutrient avail-  
491 ability, leaf nutrient content, and photosynthetic capacity into question, suggest-  
492 ing instead that leaf nutrients and photosynthetic capacity are better predicted as  
493 an integrated product of aboveground climate, leaf traits, and soil nutrient avail-  
494 ability, rather than soil nutrient availability alone (Dong et al. 2017; Dong et al.  
495 2020; Dong et al. 2022; Firn et al. 2019; Smith et al. 2019; Peng et al. 2021).  
496 It has been reasoned that this result is because plants allocate added nutrients to  
497 growth and storage rather than alterations in leaf chemistry (Smith et al. 2019),  
498 perhaps as a result of nutrient limitation of primary productivity (LeBauer and  
499 Treseder 2008; Fay et al. 2015). Additionally, recent work suggests that relation-  
500 ships between leaf nutrient content and photosynthesis vary across environments,

501 and that the proportion of leaf nutrient content allocated to photosynthetic tis-  
502 sue varies over space and time with plant acclimation and adaptation responses  
503 to light availability, vapor pressure deficit, soil pH, soil nutrient availability, and  
504 environmental factors that influence leaf mass per area (Pons and Pearcy 1994;  
505 Niinemets and Tenhunen 1997; Evans and Poorter 2001; Hikosaka and Shigeno  
506 2009; Ghimire et al. 2017; Onoda et al. 2017; Luo et al. 2021). The use of linear  
507 relationships between leaf nutrient content and Vcmax to predict photosynthetic  
508 capacity, as commonly used in terrestrial biosphere models (Rogers 2014), is not  
509 capable of detecting such responses.

510 Photosynthetic least-cost theory provides an alternative framework for un-  
511 derstanding relationships between soil nutrient availability, leaf nutrient content,  
512 and photosynthetic capacity (Harrison et al. 2021). Leveraging a two-input mi-  
513 croeconomics approach (Wright et al. 2003), the theory posits that plants accli-  
514 mate to a given environment by optimizing leaf photosynthesis rates at the lowest  
515 summed cost of using nutrients and water (Prentice et al. 2014; Wang et al. 2017;  
516 Smith et al. 2019; Paillassa et al. 2020). Across resource availability gradients,  
517 the theory predicts that optimal photosynthetic rates can be achieved by trading  
518 less efficient use of a resource that is less costly to acquire (or more abundant)  
519 for more efficient use of a resource more costly to acquire (or less abundant). For  
520 example, an increase in soil nutrient availability should reduce the cost of acquir-  
521 ing and using nutrients (Bae et al. 2015; Eastman et al. 2021; Perkowski et al.  
522 2021), which could increase leaf nutrient investments in photosynthetic proteins to  
523 allow similar photosynthetic rates to be achieved with higher nutrient use (lower  
524 nutrient use efficiency) but lower water use (greater water use efficiency). The

525 theory suggests similar tradeoffs in response to increasing soil pH (Paillassa et al.  
526 2020), specifically, that increasing soil pH should reduce the cost of acquiring soil  
527 nutrients due to an increase in plant-available nutrient concentration (Paillassa  
528 et al. 2020; Dong et al. 2022). The theory is also capable of reconciling dynamic  
529 leaf nutrient-photosynthesis relationships at global scales (Luo et al. 2021).

530 Patterns expected from photosynthetic least-cost theory have recently re-  
531 ceived empirical support both in global environmental gradient (Smith et al.  
532 2019; Paillassa et al. 2020; Luo et al. 2021; Querejeta et al. 2022; Wester-  
533 band et al. 2023) and local manipulative invasion (Bialic-Murphy et al. 2021)  
534 studies. However, nutrient addition experiments that directly examine nutrient-  
535 water use tradeoffs expected from the theory are rare (Guerrieri et al. 2011), and  
536 only global gradient studies testing the theory have considered soil pH in their  
537 analyses. As a result, there is a need to use nutrient addition and soil pH manu-  
538 lation experiments to test mechanisms driving responses predicted by the theory.  
539 Such experiments would also be useful to detect whether patterns expected from  
540 theory translate to finer spatial scales.

541 In this study, we measured leaf responses to soil N availability in five decid-  
542 uous tree species growing in the upper canopy of mature closed canopy temperate  
543 forests in the northeastern United States. Soil N availability and pH were manip-  
544 ulated through a N-by-pH field manipulation experiment with treatments applied  
545 since 2011, eight years prior to measurement. Two different soil N treatments were  
546 applied to increase N availability with opposing effects on soil pH. An additional  
547 N-free acidifying treatment was expected to decrease soil pH. We hypothesized  
548 that increased soil N availability would enable plants to increase nutrient uptake

549 and create more photosynthetic enzymes per leaf, allowing similar photosynthetic  
550 rates achieved with lower leaf C<sub>i</sub>:C<sub>a</sub> and increased leaf N content allocated to  
551 photosynthetic leaf tissue. We expected that this response would be driven by a  
552 reduction in the cost of acquiring N, which would cause trees to sacrifice efficient  
553 N use to enable more efficient use of other limiting resources (i.e., water). We  
554 hypothesized similar leaf responses to increasing soil pH.

555 3.2 Methods

556 3.2.1 *Study site description*

557 We conducted this study in summer 2019 at three stands located within  
558 a 20-km radius of Ithaca, NY, USA (42.444 °N, 76.502 °W). All stands contain  
559 mature, closed-canopy forests dominated by deciduous tree species. Stands con-  
560 tained abundant sugar maple (*Acer saccharum* Marshall), American beech (*Fagus*  
561 *grandifolia* Ehrh.), and white ash (*Fraxinus americana* L.), accounting for 43%,  
562 15%, and 17% of the total aboveground biomass across the three stands, respec-  
563 tively, with less frequent red maple (*Acer rubrum* L.; 9% of total aboveground  
564 biomass) and red oak occurrences (*Quercus rubra* L.; 10% of total aboveground  
565 biomass). Soils at each site were broadly classified as a channery silt loam Incep-  
566 tisols using the USDA NRCS Web Soil Survey data product (Soil Survey Staff  
567 2022). Between 2006 and 2020, study sites averaged 972 mm of precipitation per  
568 year and had an average temperature of 7.9 °C per a weather station located near  
569 the Cornell University campus (42.449 °N, 76.449 °W) part of the NOAA NCEI  
570 Global Historical Climatology Network (Menne et al. 2012).

**571** 3.2.2 *Experimental design*

**572** Four 40 m x 40 m plots were set up at each site in 2009, each with an  
**573** additional 10 m buffer along plot perimeters (60 m x 60 m total). The plots  
**574** were set up as a nitrogen-by-pH field manipulation experiment, with one each of  
**575** four treatments at each site. Two nitrogen treatments were applied, both at 50  
**576** kg N ha<sup>-1</sup> yr<sup>-1</sup>, as either sodium nitrate (NaNO<sub>3</sub>) to raise soil pH, or ammonium  
**577** sulfate ((NH<sub>4</sub>)<sub>2</sub>SO<sub>4</sub>) to acidify; an elemental sulfur treatment was selected to acid-  
**578** ify without N, applied at the same rate of S addition (57 kg S ha<sup>-1</sup> yr<sup>-1</sup>); and  
**579** control plots received no additions. All amendments were added in pelletized form  
**580** using hand-held fertilizer spreaders to both the main plots and buffers. Amend-  
**581** ments were divided into three equal doses distributed across the growing season  
**582** from 2011-2017 and added as a single dose from 2018 onward. During 2019, plots  
**583** were fertilized during the week of May 20.

**584** 3.2.3 *Leaf gas exchange and trait measurements*

**585** We sampled one leaf each from 6 to 10 individuals per plot between June  
**586** 25 and July 12, 2019 for gas exchange measurements (Table S1). Leaves were  
**587** collected from deciduous broadleaf trees represented across all sites and plots and  
**588** were replicated in efforts to mimic the species abundance of each plot at each  
**589** site. We also attempted to collect leaves from the upper canopy to reduce differ-  
**590** ential shading effects on leaf physiology. Leaves were accessed by pulling down  
**591** small branches using an arborist's slingshot and weighted beanbag attached to a  
**592** throwline. Branches were immediately recut under deionized water and remained  
**593** submerged to reduce stomatal closure and avoid xylem embolism (as in Smith &

594 Dukes, 2018) until gas exchange data were collected.

595 Randomly selected leaves with little to no visible external damage were  
596 attached to a Li-COR LI-6800 (Li-COR Bioscience, Lincoln, Nebraska, USA)  
597 portable photosynthesis machine to measure net photosynthesis ( $A_{\text{net}}$ ;  $\mu\text{mol m}^{-2} \text{s}^{-1}$ ),  
598 stomatal conductance ( $g_{\text{sw}}$ ;  $\text{mol m}^{-2} \text{s}^{-1}$ ), and intercellular  $\text{CO}_2$  concentration  
599 ( $C_i$ ;  $\mu\text{mol mol}^{-1}$ ) at different reference  $\text{CO}_2$  concentrations ( $C_a$ ;  $\mu\text{mol mol}^{-1}$ )  
600 concentrations (i.e., an  $A_{\text{net}}/C_i$  curve) under saturating light conditions (2,000  
601  $\mu\text{mol m}^{-2} \text{s}^{-1}$ ). Reference  $\text{CO}_2$  concentrations followed the sequence: 400, 300,  
602 200, 100, 50, 400, 400, 600, 800, 1000, 1200, 1500, and 2000  $\mu\text{mol mol}^{-1} \text{CO}_2$ . Leaf  
603 temperatures were not controlled in the cuvette and ranged from 21.8 °C to 31.7  
604 °C (mean±SD:  $27.2 \pm 2.2$  °C). A linear and second order log-polynomial nonlinear  
605 regression suggested no effect of temperature on stomatal conductance measured  
606 at 400  $\mu\text{mol mol}^{-1} \text{CO}_2$  or net photosynthesis measured at  $\mu\text{mol mol}^{-1} \text{CO}_2$  (Ta-  
607 ble S2-3; Fig. S1). All  $A_{\text{net}}/C_i$  curves were generated within one hour of branch  
608 severance.

609 Leaf morphological and chemical traits were collected on the same leaf used  
610 to generate each  $A_{\text{net}}/C_i$  curve. Images of each leaf were taken using a flat-bed  
611 scanner to determine fresh leaf area using the ‘LeafArea’ R package (Katabuchi  
612 2015), which automates leaf area calculations using ImageJ software (Schneider  
613 et al. 2012). Each leaf was dried at 65°C for at least 48 hours, weighed, and  
614 ground using a Retsch MM200 ball mill grinder (Verder Scientific, Inc., Newtown,  
615 PA, USA) until homogenized. Leaf mass per area ( $M_{\text{area}}$ ,  $\text{g m}^{-2}$ ) was calculated  
616 as the ratio of dry leaf biomass to fresh leaf area. Using a subsample of ground and  
617 homogenized leaf biomass, leaf N content ( $N_{\text{mass}}$ ;  $\text{gN g}^{-1}$ ) and leaf  $\delta^{13}\text{C}$  (‰, rela-

618 tive to VPDB) were measured at the Cornell Stable Isotope Lab with an elemental  
 619 analyzer (NC 2500, CE Instruments, Wigan, UK) interfaced to an isotope ratio  
 620 mass spectrometer (Delta V Isotope Ratio Mass Spectrometer, ThermoFisher Sci-  
 621 entific, Waltham, MA, USA). Leaf N content per unit leaf area ( $N_{\text{area}}$ ; gN m<sup>-2</sup>)  
 622 was calculated by multiplying  $N_{\text{mass}}$  by  $M_{\text{area}}$ .

623 We used leaf  $\delta^{13}\text{C}$  values to estimate  $\chi$  (unitless), which is an isotope-  
 624 derived estimate of the leaf  $C_i:C_a$  ratio. While intercellular and atmospheric CO<sub>2</sub>  
 625 concentrations were directly measured during each  $A_{\text{net}}/C_i$  curve, deriving  $\chi$  from  
 626  $\delta^{13}\text{C}$  provides a more integrative estimate of the  $C_i:C_a$  over an individual leaf's  
 627 lifespan. We derived  $\chi$  following the approach of Farquhar et al. (1989) described  
 628 in Cernusak et al. (2013):

$$\chi = \frac{\Delta^{13}C - a}{b - a} \quad (3.1)$$

629 where  $\Delta^{13}\text{C}$  represents the relative difference between leaf  $\delta^{13}\text{C}$  (‰) and air  $\delta^{13}\text{C}$   
 630 (‰), and is calculated from the following equation:

$$\Delta^{13}C = \frac{\delta^{13}C_{\text{air}} - \delta^{13}C_{\text{leaf}}}{1 + \delta^{13}C_{\text{leaf}}} \quad (3.2)$$

631 where  $\delta^{13}C_{\text{air}}$  is assumed to be -8‰ (Keeling et al. 1979; Farquhar et al. 1989), a  
 632 represents the fractionation between <sup>12</sup>C and <sup>13</sup>C due to diffusion in air, assumed  
 633 to be 4.4‰, and b represents the fractionation caused by Rubisco carboxylation,  
 634 assumed to be 27‰ (Farquhar et al. 1989).

**635** 3.2.4  $A_{net}/C_i$  curve-fitting and parameter estimation

**636** We fit  $A_{net}/C_i$  curves of each individual using the ‘fitaci’ function in the  
**637** ‘plantecophys’ R package (Duursma 2015). This function estimates the maximum  
**638** rate of Rubisco carboxylation  $V_{cmax}$ ;  $\mu\text{mol m}^{-2} \text{s}^{-1}$ ) and maximum rate of electron  
**639** transport for RuBP regeneration ( $J_{max}$ ;  $\mu\text{mol m}^{-2} \text{s}^{-1}$ ) based on the Farquhar,  
**640** von Caemmerer, and Berry biochemical model of C<sub>3</sub> photosynthesis (Farquhar  
**641** et al. 1980). For each curve fit, we included triose phosphate utilization (TPU)  
**642** limitation to avoid underestimating  $J_{max}$  (Gregory et al. 2021). Curves were  
**643** visually examined to confirm the likely presence of TPU limitation.

**644** We determined Michaelis-Menten coefficients for Rubisco affinity to CO<sub>2</sub>  
**645** ( $K_c$ ;  $\mu\text{mol mol}^{-1}$ ) and O<sub>2</sub> ( $K_o$ ;  $\mu\text{mol mol}^{-1}$ ), and the CO<sub>2</sub> compensation point  
**646** ( $\Gamma^*$ ;  $\mu\text{mol mol}^{-1}$ ) using leaf temperature and equations described in Medlyn et al.  
**647** (2002) and derived in Bernacchi et al. (2001). Specifically,  $K_c$  and  $K_o$  were  
**648** calculated as:

$$K_c = 404.9 * \exp^{\frac{79430(T_k - 298)}{298RT_k}} \quad (3.3)$$

**649** and

$$K_o = 278.4 * \exp^{\frac{36380(T_k - 298)}{298RT_k}} \quad (3.4)$$

**650** while  $\Gamma^*$  was calculated as:

$$\Gamma^* = 42.75 * \exp^{\frac{37830(T_k - 298)}{298RT_k}} \quad (3.5)$$

**651** In all three equations,  $T_k$  is the leaf temperature (in Kelvin) during each  $A_{\text{net}}/C_i$

**652** curve and R is the universal gas constant ( $8.314 \text{ J mol}^{-1} \text{ K}^{-1}$ ).

**653** We standardized  $V_{\text{cmax}}$  and  $J_{\text{max}}$  estimates to  $25^\circ\text{C}$  using a modified Ar-

**654** rhenius equation (Kattge and Knorr 2007):

$$k_{25} = \frac{k_{\text{obs}}}{e^{\frac{H_a(T_{\text{obs}} - T_{\text{ref}})}{T_{\text{ref}}RT_{\text{obs}}}} * \frac{1+e^{\frac{T_{\text{ref}}\Delta S - H_d}{T_{\text{obs}}}}}{1+e^{\frac{T_{\text{obs}}\Delta S - H_d}{T_{\text{obs}}}}}} \quad (3.6)$$

**655**  $k_{25}$  represents the standardized  $V_{\text{cmax}}$  or  $J_{\text{max}}$  rate at  $25^\circ\text{C}$ ,  $k_{\text{obs}}$  represents

**656** the  $V_{\text{cmax}}$  or  $J_{\text{max}}$  estimate at the average leaf temperature measured inside the

**657** cuvette during the  $A_{\text{net}}/C_i$  curve.  $H_a$  is the activation energy of  $V_{\text{cmax}}$  ( $71,513$

**658**  $\text{J mol}^{-1}$ ) Kattge and Knorr (2007) or  $J_{\text{max}}$  ( $49,884 \text{ J mol}^{-1}$ ) (Kattge and Knorr

**659** 2007).  $H_d$  represents the deactivation energy of both  $V_{\text{cmax}}$  and  $J_{\text{max}}$  ( $200,000 \text{ J}$

**660**  $\text{mol}^{-1}$ ) (Medlyn et al. 2002), and R represents the universal gas constant ( $8.314$

**661**  $\text{J mol}^{-1} \text{ K}^{-1}$ ).  $T_{\text{ref}}$  represents the standardized temperature of  $298.15 \text{ K}$  ( $25^\circ\text{C}$ )

**662** and  $T_{\text{obs}}$  represents the mean leaf temperature (in K) during each  $A_{\text{net}}/C_i$  curve.

**663**  $\Delta S$  is an entropy term that (Kattge and Knorr 2007) derived as a linear relation-

**664** ship with average growing season temperature ( $T_g$ ;  $^\circ\text{C}$ ), where:

$$\Delta S_{v_{\text{cmax}}} = -1.07 T_g + 668.39 \quad (3.7)$$

**665** and

$$\Delta S_{j_{\text{max}}} = -0.75 T_g + 659.70 \quad (3.8)$$

**666** We estimated  $T_g$  in Equations 3.7 and 3.8 based on mean daily (24-hour) air  
**667** temperature of the 30 days leading up to the day of each sample collection using  
**668** the same weather station reported in the site description. We then used  $V_{cmax25}$   
**669** and  $J_{max25}$  estimates to calculate the ratio of  $J_{max25}$  to  $V_{cmax25}$  ( $J_{max25}:V_{cmax25}$ ;  
**670** unitless).

**671** 3.2.5 *Proportion of leaf nitrogen allocated to photosynthesis and structure*

**672** We used equations from Niinemets and Tenhunen (1997) to estimate the  
**673** proportion of leaf N content allocated to Rubisco and bioenergetics. The propor-  
**674** tion of leaf N allocated to Rubisco ( $\rho_{rub}$ ; gN gN $^{-1}$ ) was calculated as a function  
**675** of  $V_{cmax25}$  and  $N_{area}$ :

$$\rho_{rubisco} = \frac{V_{cmax25} N_r}{V_{cr} N_{area}} \quad (3.9)$$

**676** where  $N_r$  is the amount of nitrogen in Rubisco, set to 0.16 gN (gN in Rubisco) $^{-1}$   
**677** and  $V_{cr}$  is the maximum rate of RuBP carboxylation per unit Rubisco protein,  
**678** set to 20.5  $\mu$ mol CO $_2$  (g Rubisco) $^{-1}$ . The proportion of leaf nitrogen allocated to  
**679** bioenergetics ( $\rho_{bioe}$ ; gN gN $^{-1}$ ) was similarly calculated as a function of  $J_{max25}$  and  
**680**  $N_{area}$ :

$$\rho_{bioe} = \frac{J_{max25} N_b}{J_{mc} N_{area}} \quad (3.10)$$

**681** where  $N_b$  is the amount of nitrogen in cytochrome f, set to 0.12407 gN ( $\mu$ mol  
**682** cytochrome f) $^{-1}$  assuming a constant 1: 1: 1.2 cytochrome f: ferredoxin NADP  
**683** reductase: coupling factor molar ratio (Evans and Seemann 1989; Niinemets and

684 Tenhunen 1997), and  $J_{mc}$  is the capacity of electron transport per cytochrome f,  
685 set to  $156 \mu\text{mol electron} (\mu\text{mol cytochrome f})^{-1}\text{s}^{-1}$ .

686 We estimated the proportion of leaf N content allocated to photosynthetic  
687 tissue ( $\rho_{photo}$ ;  $\text{gN gN}^{-1}$ ) as the sum of  $\rho_{rub}$  and  $\rho_{bioe}$ . This calculation is an un-  
688 derestimate of the proportion of leaf N allocated to photosynthetic tissue because  
689 it does not include N allocated to light harvesting proteins. This leaf N pool was  
690 not included because we did not perform chlorophyll extractions on focal leaves.  
691 However, the proportion of leaf N content allocated to light harvesting proteins  
692 tends to be small relative to  $\rho_{rub}$  and  $\rho_{bioe}$ , and may scale with changes in  $\rho_{rub}$   
693 and  $\rho_{bioe}$  (Niinemets and Tenhunen 1997).

694 Finally, we estimated the proportion of leaf N content allocated to struc-  
695 tural tissue ( $\rho_{str}$ ;  $\text{gN gN}^{-1}$ ) using an empirical equation from Onoda et al. (2017):

$$N_{cw} = 0.000355 * M_{area}^{1.39} \quad (3.11)$$

696 where  $N_{cw}$  is the leaf N content allocated to cell walls ( $\text{gN m}^{-2}$ ).  $\rho_{str}$  was estimated  
697 by dividing  $N_{cw}$  by  $N_{area}$ .

### 698 3.2.6 *Tradeoffs between nitrogen and water use*

699 Photosynthetic nitrogen use efficiency (PNUE;  $\mu\text{mol CO}_2 \text{ mol}^{-1} \text{ N s}^{-1}$ )  
700 was calculated by dividing  $A_{net}$  by  $N_{area}$ , first converting  $N_{area}$  to  $\text{mol N m}^{-2}$   
701 using the molar mass of N ( $14 \text{ g mol}^{-1}$ ). We used  $\chi$  as an indicator of water  
702 use efficiency, which exploratory analyses suggest had similar responses to soil N  
703 availability and pH as intrinsic water use efficiency measured from gas exchange

704 ( $A_{\text{net}}/g_s$ ). Tradeoffs between nitrogen and water use were determined by cal-  
705 culating the ratio of  $N_{\text{area}}$  to  $\chi$  ( $N_{\text{area}}:\chi$ ; g N m<sup>-2</sup>) and  $V_{\text{cmax25}}$  to  $\chi$  ( $V_{\text{cmax25}}:\chi$ ;  
706  $\mu\text{mol m}^{-2} \text{s}^{-1}$ ). This approach is similar to tradeoff calculations in which nitrogen-  
707 water use tradeoffs are measured as the ratio of  $N_{\text{area}}$  or  $V_{\text{cmax25}}$  to  $g_s$  (Paillassa  
708 et al. 2020; Bialic-Murphy et al. 2021). In this study, we quantify these re-  
709 lationships using  $\chi$  in lieu of  $g_s$  because  $g_s$  rapidly changes with environmental  
710 conditions and therefore may have been altered by recent tree branch severance  
711 and/or placement in the cuvette.

712 3.2.7 *Soil nitrogen availability and pH*

713 To characterize soil N availability at the time of our leaf gas exchange  
714 measurements, we used mixed bed resin bags to quantify mobile ammonium-N  
715 and nitrate-N concentrations in each plot. Lycra mesh bags were filled with 5 g  
716 of Dowex® Marathon MR-3 hydrogen and hydroxide form resin (MilliporeSigma,  
717 Burlington, MA USA) and sealed with a zip tie. Each bag was activated by  
718 soaking in 0.5 M HCl for 20 minutes, then in 2 M NaCl until pH of the saline  
719 solution stabilized, as described in Allison et al. (2008). Five resin bags were  
720 inserted about 10 cm below the soil surface at each plot on June 25, 2019: one  
721 near each of the four plot corners and one near the plot center. All resin bags  
722 were collected 24 days later on July 19, 2019 and were frozen until extracted.

723 Prior to anion and cation extraction, each resin bag was rinsed with ul-  
724 trapure water (MilliQ IQ 7000; Millipore Sigma, Burlington, MA) to remove any  
725 surface soil residues. Anions and cations were extracted from surface-cleaned resin  
726 bags by individually soaking and shaking each bag in 100 mL of a 0.1 M HCl/2.0

727 M NaCl matrix for one hour. Using a microplate reader (Biotek Synergy H1;  
728 Biotek Instruments, Winooski, VT USA), nitrate-N concentrations were quanti-  
729 fied spectrophotometrically at 540 nm with the end product of a single reagent  
730 vanadium (III) chloride reaction (Doane and Horwáth 2003), and ammonium-N  
731 concentrations quantified at 650 nm with the end product of a modified phenol-  
732 hypochlorite reaction (Weatherburn 1967; Rhine et al. 1998). Both the single  
733 reagent vanadium (III) chloride and modified phenol-hypochlorite methodologies  
734 have been well established for determining nitrate-N and ammonium-N concen-  
735 trations in resin bag extracts (Arnone 1997; Allison et al. 2008). We used a  
736 series of negative and positive controls throughout each well plate to verify the  
737 accuracy and precision of our measurements, assaying each resin bag extract and  
738 control in triplicate. Soil N availability was estimated as the sum of the nitrate-N  
739 and ammonium-N concentration in each resin bag, normalized per g of resin and  
740 duration in the field ( $\mu\text{g N g}^{-1} \text{ resin d}^{-1}$ ), then subsequently averaged across all  
741 resin bags in a plot for a plot-level mean.

742 Soil pH was measured on 0-10 cm mineral soil samples collected prior to  
743 fertilization in 2019. Near each of the four plot corners, three 5.5 cm diameter soil  
744 cores were collected after first removing the forest floor where present. Each set  
745 of three cores was placed in a plastic bag, and later composited by hand mixing  
746 and sieved to 4mm. Soil pH was determined for a 1:2 soil:water slurry (10 g field-  
747 moist soil to 20 mL DI water) of each sample using an Accumet AB15 pH meter  
748 with flushable junction probe (Fisher Scientific; Hampton, NH, USA), and was  
749 estimated at the plot level as the mean soil pH within each plot.

**750** 3.2.8 *Statistical analyses*

**751** We built two separate series of linear mixed-effects models to explore effects  
**752** of soil N availability, soil pH, species, and leaf N content on leaf physiological  
**753** traits. In the first series of linear mixed-effects models, we explored the effect  
**754** of soil N availability, soil pH, and species on leaf N content, leaf photosynthesis,  
**755** stomatal conductance, and nitrogen-water use tradeoffs. Models included plot-  
**756** level soil N availability and plot-level soil pH as continuous fixed effects, species  
**757** as a categorical fixed effect, and site as a categorical random intercept term.  
**758** Interaction terms between fixed effects were not included due to the small number  
**759** of experimental plots. We built a series of separate models with this independent  
**760** variable structure to quantify individual effects of soil N availability, soil pH,  
**761** and species on  $N_{\text{area}}$ ,  $M_{\text{area}}$ ,  $N_{\text{mass}}$ ,  $A_{\text{net}}$ ,  $V_{\text{cmax25}}$ ,  $J_{\text{max25}}$ ,  $J_{\text{max25}}:V_{\text{cmax25}}$ ,  $\rho_{\text{rubisco}}$ ,  
**762**  $\rho_{\text{bioenergetics}}$ ,  $\rho_{\text{photo}}$ ,  $\rho_{\text{structure}}$ ,  $\chi$ , PNUE,  $N_{\text{area}}:\chi$ , and  $V_{\text{cmax25}}:\chi$ .

**763** A second series of linear mixed-effects models were built to investigate  
**764** relationships between leaf N content and photosynthetic parameters. Statistical  
**765** models included  $N_{\text{area}}$  as a single continuous fixed effect with species and site des-  
**766** ignated as individual random intercept terms. We used this independent variable  
**767** structure to quantify individual effects of leaf N content on  $A_{\text{net}}$ ,  $V_{\text{cmax25}}$ ,  $J_{\text{max25}}$ ,  
**768**  $J_{\text{max25}}:V_{\text{cmax25}}$ , and  $\chi$ .

**769** For all linear mixed-effects models, we used Shapiro-Wilk tests of normal-  
**770** ity to determine whether linear mixed-effects models satisfied residual normality  
**771** assumptions. If residual normality assumptions were not met, then models were  
**772** fit using dependent variables that were natural log transformed. If residual nor-  
**773** mality assumptions were still not met (Shapiro-Wilk:  $p < 0.05$ ), then models were

774 fit using dependent variables that were square root transformed. All residual nor-  
775 mality assumptions for both sets of models that did not originally satisfy residual  
776 normality assumptions were met with either a natural log or square root data  
777 transformation (Shapiro-Wilk:  $p > 0.05$  in all cases).

778 In the first series of models, models for  $N_{\text{area}}$ ,  $M_{\text{area}}$ ,  $N_{\text{mass}}$ ,  $V_{\text{cmax25}}$ ,  $J_{\text{max25}}$ ,  
779  $\chi$ ,  $N_{\text{area}}:\chi$ , and  $V_{\text{cmax25}}:\chi$ ,  $\rho_{\text{rubisco}}$ ,  $\rho_{\text{bioenergetics}}$ ,  $\rho_{\text{photo}}$ ,  $\rho_{\text{structure}}$  satisfied residual  
780 normality assumptions without data transformations (Shapiro-Wilk:  $p > 0.05$  in  
781 all cases). The model for  $J_{\text{max25}}:V_{\text{cmax25}}$  satisfied residual normality assumptions  
782 with a natural log data transformation, while models for  $A_{\text{net}}$  and PNUE each  
783 satisfied residual normality assumptions with square root data transformations.  
784 In the second series of models, models for  $V_{\text{cmax25}}$ ,  $J_{\text{max25}}$ ,  $\chi$ , and  $V_{\text{cmax25}}:\chi$  satisfied  
785 residual normality assumptions without data transformations (Shapiro-Wilk:  $p$   
786  $> 0.05$  in all cases). The model for  $J_{\text{max25}}:V_{\text{cmax25}}$  required a natural log data  
787 transformation and the model for  $A_{\text{net}}$  required a square root data transformation  
788 (Shapiro-Wilk:  $p > 0.05$  in both cases).

789 In all models, we used the ‘lmer’ function in the ‘lme4’ R package (Bates  
790 et al. 2015) to fit each model and the ‘Anova’ function in the ‘car’ R package (Fox  
791 and Weisberg 2019) to calculate Type II Wald’s  $\chi^2$  and determine the significance  
792 level ( $\alpha = 0.05$ ) of each fixed effect coefficient. Finally, we used the ‘emmeans’  
793 R package (Lenth, 2019) to conduct post-hoc comparisons using Tukey’s tests,  
794 where degrees of freedom were approximated using the Kenward-Roger approach  
795 (Kenward and Roger 1997). All analyses and plots were conducted in R version  
796 4.1.1 (R Core Team 2021)). All figure regression lines and associated 95% confi-  
797 dence interval error bars were plotted using predictions generated across the soil

**798** nitrogen availability gradient using the ‘emmeans’ R package (Lenth 2019).

**799** 3.3 Results

**800** 3.3.1 *Leaf N content*

**801** Increasing soil N availability generally increased  $N_{\text{area}}$  (Table 3.1; Fig.  
**802** 3.1a). This pattern was driven by an increase in  $N_{\text{mass}}$  (Table 3.1; Fig. 3.1c)  
**803** and a marginal increase in  $M_{\text{area}}$  (Table 3.1; Fig. 3.1e) with increasing soil N  
**804** availability. There was no effect of soil pH on  $N_{\text{area}}$ ,  $N_{\text{mass}}$ , or  $M_{\text{area}}$  (Table 3.1);  
**805** however, we did observe strong differences in  $N_{\text{area}}$  (Fig. 3.1b),  $N_{\text{mass}}$  (Fig. 3.1d),  
**806** and  $M_{\text{area}}$  (Fig. 3.1e) between species (Table 3.1).

**Table 3.1.** Effects of soil N availability, soil pH, and species on leaf N content per unit leaf area ( $N_{\text{area}}$ ), leaf N content per unit leaf mass ( $N_{\text{mass}}$ ), and leaf mass per unit leaf area ( $M_{\text{area}}$ )

	df	$N_{\text{area}}$			$N_{\text{mass}}$			$M_{\text{area}}$		
		Coefficient	$\chi^2$	p	Coefficient	$\chi^2$	p	Coefficient	$\chi^2$	p
Intercept	-	9.03E-01	-	-	1.68E+00	-	-	4.60E+01	-	-
Soil N	1	1.68E-02	11.990	<b>0.001</b>	1.25E-02	6.902	<b>0.009</b>	4.87E-01	4.143	<b>0.042</b>
Soil pH	1	9.28E-02	0.836	0.361	8.08E-02	0.663	0.415	4.05E+00	0.653	0.419
Species	4	-	72.128	<b>&lt;0.001</b>	-	35.074	<b>&lt;0.001</b>	-	29.869	<b>&lt;0.001</b>

\*Significance determined using Type II Wald  $\chi^2$  tests ( $\alpha = 0.05$ ). P-values  $< 0.05$  are in bold.

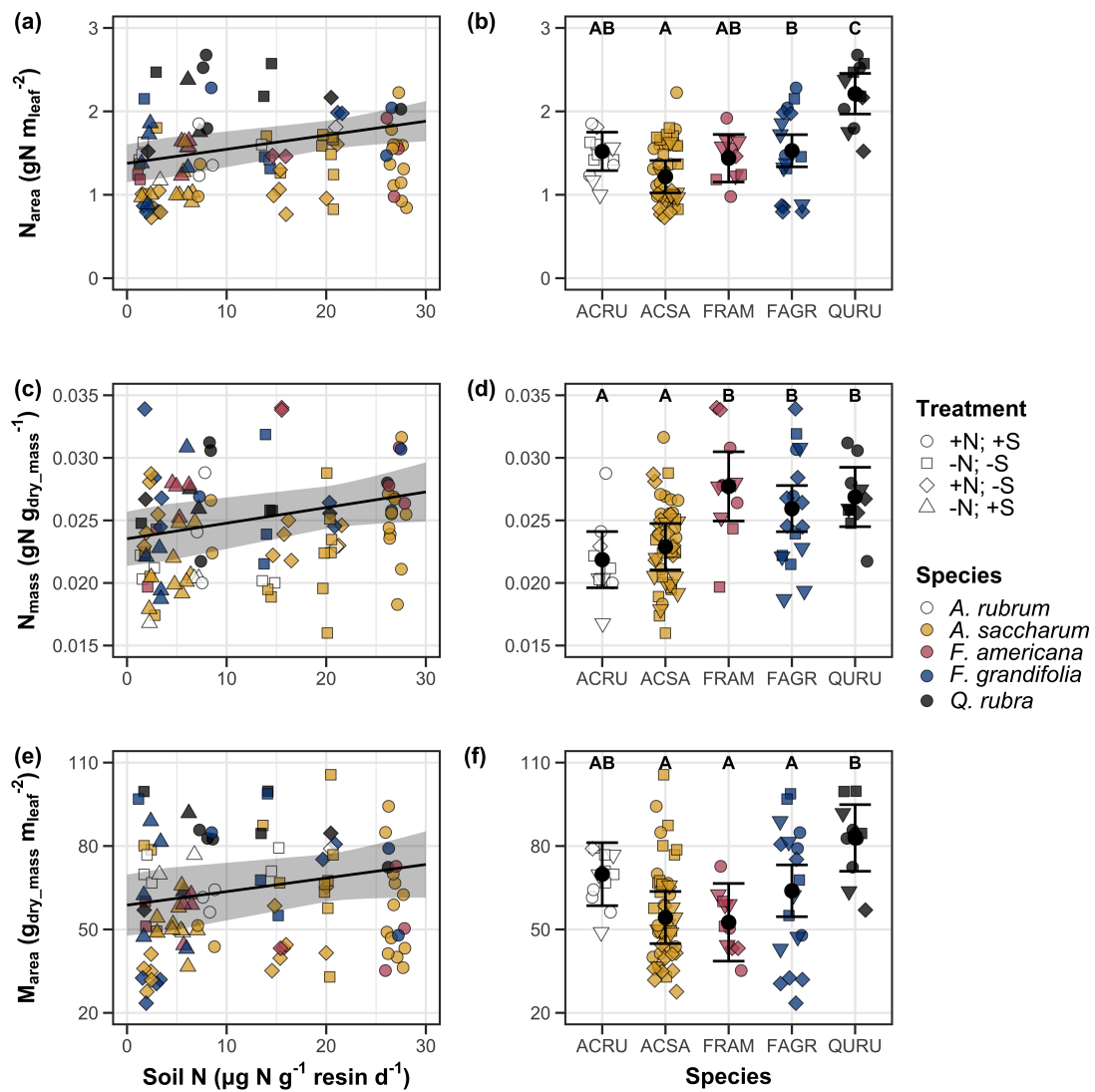


**Figure 3.1.** Effects of soil N availability and species on leaf N content per unit leaf area (a-b), leaf nitrogen content per unit leaf biomass (c-d), and leaf mass per unit leaf area (e-f). Soil N availability is represented on the x-axis in the left column of panels, while species is represented on the x-axis in the right column of panels. Tree species are represented as colored points and treatment plots are represented as shaped points, jittered for visibility. Species are abbreviated in the right column of panels through their assigned NRCS PLANTS Database symbol (USDA NRCS 2022), grouped along the x-axis per common mycorrhizal association, where the first three species commonly associate with arbuscular mycorrhizae (ACRU, ASCA, FAGR) and the second two species with ectomycorrhizae (FAGR, QURU). Trendlines are only included when the regression slope is statistically different from zero ( $p < 0.05$ ).

**807** 3.3.2 *Net photosynthesis and leaf biochemistry*

**808** Increasing soil N availability generally had no effect on  $A_{\text{net}}$ ,  $V_{\text{cmax25}}$ ,  $J_{\text{max25}}$ ,  
**809** or  $J_{\text{max25}}:V_{\text{cmax25}}$  (Table 3.2, Figs. 3.2a, 3.2d, 3.2g). We also observed strong  
**810** species effects on all measured leaf photosynthetic traits (Table 3.2; Figs. 3.2b,  
**811** 3.2e, 3.2h). Increasing soil pH had a marginal negative effect on  $A_{\text{net}}$ , but had no  
**812** effect on  $V_{\text{cmax25}}$ ,  $J_{\text{max25}}$ , or  $J_{\text{max25}}:V_{\text{cmax25}}$  (Table 3.2). There was a weak positive  
**813** effect of increasing  $N_{\text{area}}$  on  $A_{\text{net}}$  (Fig. 3.2c), but quite strong positive effects of  
**814** increasing  $N_{\text{area}}$  on  $V_{\text{cmax25}}$  and  $J_{\text{max25}}$  (Table 3.2; Fig. 3.2f and 3.2i).

**Table 3.2.** Effects of soil N availability, soil pH, species, and  $N_{\text{area}}$  on leaf biochemistry

	$A_{\text{net}}$			$V_{\text{cmax25}}$			$J_{\text{max25}}$			
	df	Coefficient	$\chi^2$	p	Coefficient	$\chi^2$	p	Coefficient	$\chi^2$	p
(Intercept)	-	3.29E+00 <sup>b</sup>	-	-	6.38E+01	-	-	1.12E+02	-	-
Soil N	1	-1.23E-03 <sup>b</sup>	1.798	0.180	-3.84E-01	1.745	0.187	-6.70E-01	2.172	0.141
Soil pH	1	-3.09E-01 <sup>b</sup>	3.312	0.069	-4.91E+00	0.655	0.418	-8.18E+00	0.742	0.389
Species	4	-	11.838	<b>0.019</b>	-	31.748	<0.001	-	27.291	<0.001
( $N_{\text{area}}$ int.)	-	6.59E-01 <sup>b</sup>	-	-	1.45E-01	-	-	2.86E+01	-	-
$N_{\text{area}}$	4	3.13E-01 <sup>b</sup>	4.790	<b>0.029</b>	2.43E+01	22.616	<0.001	4.04E+01	28.259	<0.001

	$J_{\text{max25}}:V_{\text{cmax25}}$			
	df	Coefficient	$\chi^2$	p
(Intercept)	-	6.59E-01 <sup>a</sup>	-	-
Soil N	1	7.04E-04 <sup>a</sup>	0.088	0.767
Soil pH	1	-7.84E-03 <sup>a</sup>	0.025	0.874
Species	4	-	12.745	<b>0.013</b>
( $N_{\text{area}}$ int.)	-	6.69E-01 <sup>a</sup>	-	-
$N_{\text{area}}$	4	-4.69E-02 <sup>a</sup>	1.142	0.285

\*Significance determined using Type II Wald  $\chi^2$  tests ( $\alpha = 0.05$ ).  $P$ -values  $< 0.05$  are in bold, while  $p$ -values between 0.05 and 0.1 are italicized. Superscript letters indicate model coefficients fit to natural-log (<sup>a</sup>) or square-root (<sup>b</sup>) transformed data. Relationships between  $N_{\text{area}}$  and each response variable were fit using the second series of bivariate mixed-effects models, so model coefficients and results are independent from model coefficients and results reported for relationships between soil N, soil pH, and species for each response variable. Key:  $A_{\text{net}}$  – light saturated net photosynthesis rate;  $V_{\text{cmax25}}$  – maximum rate of Rubisco carboxylation at 25°C;  $J_{\text{max25}}$  – maximum rate of electron transport for RuBP regeneration at 25°C,  $J_{\text{max25}}:V_{\text{cmax25}}$  – the ratio of  $J_{\text{max25}}$  to  $V_{\text{cmax25}}$ .

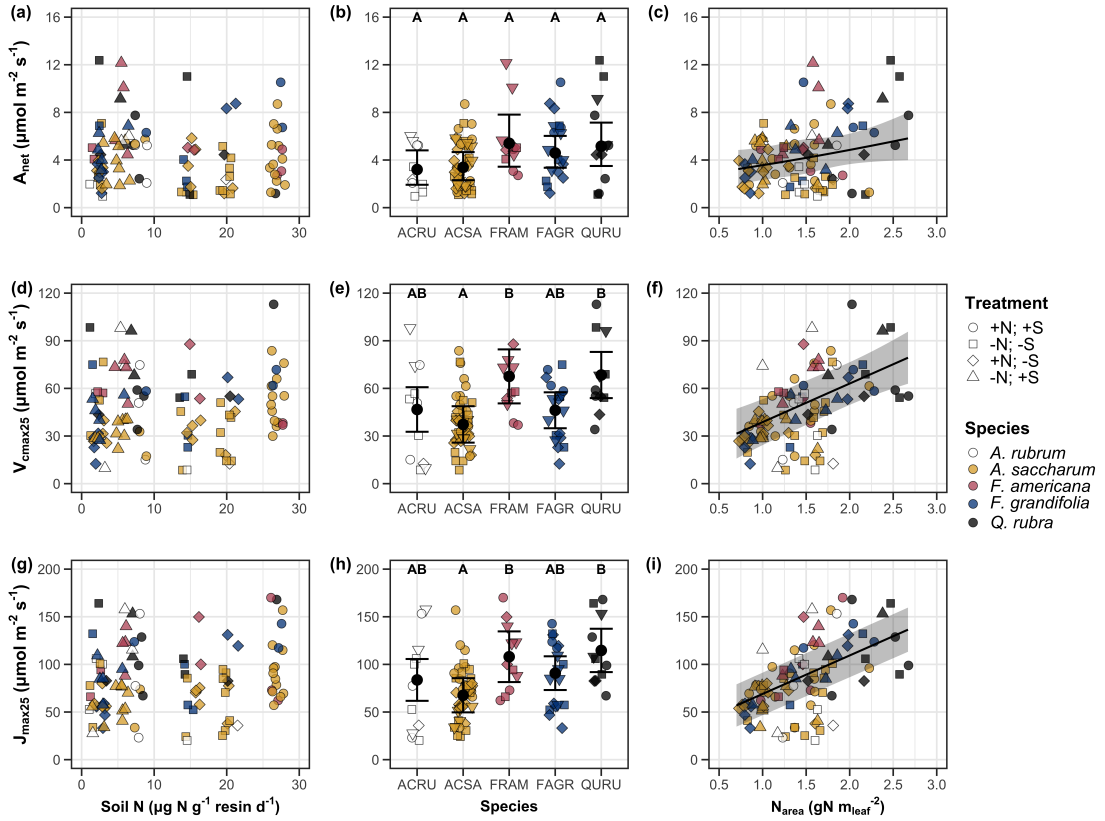


**Figure 3.2.** Effects of soil N availability (left column of panels), species (middle column of panels), and leaf N content per unit leaf area (right column of panels) on net photosynthesis (a-c), maximum Rubisco carboxylation rate (d-f), and maximum RuBP regeneration rate (g-i). Soil N availability is represented on the x-axis in the left column of panels, species is represented on the x-axis in the middle column of panels, and leaf N content per unit leaf area is represented continuously on the x-axis in the right column of panels. Species abbreviations and position along the x-axis in the middle column of panels, colored points, shapes, and trendlines are as explained in Figure 3.1.

**815** 3.3.3 *Leaf N allocation*

**816** Neither soil N availability nor soil pH affected the proportion of leaf N  
**817** allocated to Rubisco or bioenergetics (Table 3.3; Fig. 3.3a, Fig. 3.3c), nor was  
**818** there any subsequent effect on the proportion of leaf N allocated to photosynthesis  
**819** (Table 3.3; Fig. 3.3f). We also found no effect of soil N availability or soil pH on  
**820** the proportion of leaf N allocated to structure (Table 3.3; Fig 3.3g). Species varied  
**821** in the proportion of leaf N allocated to Rubisco, photosynthesis, and structure (Fig  
**822** 3.3b, Fig. 3.3d, Fig 3.3h), with no detectable species effect on the proportion of  
**823** leaf N allocated to bioenergetics (Table 3.3).

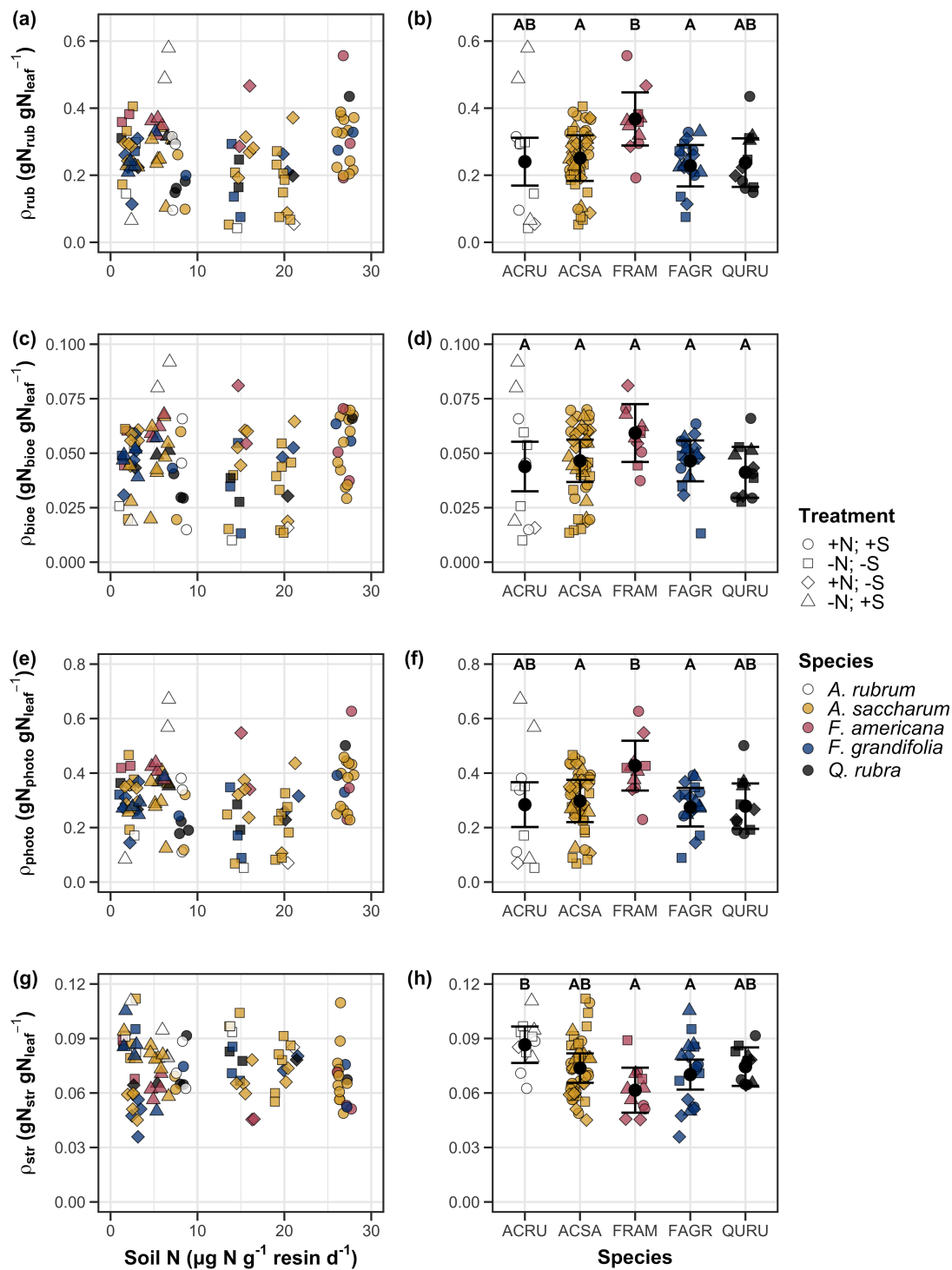
**Table 3.3.** Effects of soil N availability, soil pH, and species on the proportion of leaf nitrogen content allocated to photosynthesis, Rubisco, bioenergetics, and structure

	$\rho_{\text{photo}}$			$\rho_{\text{rub}}$			$\rho_{\text{bioe}}$			
	df	Coefficient	$\chi^2$	p	Coefficient	$\chi^2$	p	Coefficient	$\chi^2$	p
Intercept	-	4.93E-01	-	-	4.17E-01	-	-	7.64E-02	-	-
Soil N	1	-1.23E-03	0.521	0.470	-1.04E-03	0.501	0.479	-1.77E-04	0.557	0.455
Soil pH	1	-4.37E-02	1.581	0.209	-3.70E-02	1.511	0.219	-6.84E-03	1.941	0.164
Species	4	-	13.106	<b>0.011</b>	-	14.152	<b>0.007</b>	-	7.300	0.121

	$\rho_{\text{str}}$			
	df	Coefficient	$\chi^2$	p
Intercept	-	9.77E-02	-	-
Soil N	1	-2.29E-04	1.165	0.280
Soil pH	1	-1.87E-03	0.179	0.672
Species	4	-	16.428	<b>0.002</b>

\*Significance determined using Type II Wald  $\chi^2$  tests ( $\alpha = 0.05$ ). P-values  $< 0.05$  are in bold. Key:  $\rho_{\text{photo}}$  - proportion of leaf nitrogen content allocated to photosynthesis;  $\rho_{\text{rub}}$  - proportion of leaf nitrogen content allocated to Rubisco;  $\rho_{\text{bioe}}$  - proportion of leaf nitrogen content allocated to bioenergetics;  $\rho_{\text{str}}$  - proportion of leaf nitrogen content allocated to structure.



**Figure 3.3.** Effects of soil nitrogen availability and species on the proportion of leaf nitrogen content allocated to Rubisco (a-b), bioenergetics (c-d), photosynthesis (e-f), and structure (g-h)

**824** 3.3.4 *Tradeoffs between nitrogen and water use*

**825** Although soil N availability did not affect  $\chi$  (Table 3.4; Fig. 3.4a), increasing  
**826** soil N availability decreased PNUE (Table 3.4; Fig. 3.4d) and increased the  
**827** ratio of  $N_{\text{area}}:\chi$  (Table 3.4; Fig. 3.4f). Specifically, this response yielded a 26%  
**828** reduction in PNUE and 37% stimulation in  $N_{\text{area}}:\chi$  across the soil nitrogen avail-  
**829** ability gradient. There was no apparent effect of soil N availability on  $V_{\text{cmax25}}:\chi$   
**830** (Table 3.4; Fig. 3.4h). Increasing soil pH had a weak marginal negative effect  
**831** on PNUE, but did not influence  $\chi$ ,  $N_{\text{area}}:\chi$ , or  $V_{\text{cmax25}}:\chi$  (Table 3.4). We also  
**832** observed differences in  $\chi$  (Fig. 3.4b), PNUE (Fig. 3.4e),  $N_{\text{area}}:\chi$  (Fig. 3.4g), and  
**833**  $V_{\text{cmax25}}:\chi$  (Fig. 3.4i) between species (Table 3.4). Finally, increasing  $N_{\text{area}}$  had a  
**834** strong negative effect on  $\chi$  (Table 3.4; Fig. 3.4c) and a strong positive effect on  
**835**  $V_{\text{cmax25}}:\chi$  (Table 3.4; Fig. 3.4j).

**Table 3.4.** Effects of soil N availability, soil pH, species, and  $N_{\text{area}}$  on tradeoffs between nitrogen and water use

	$\chi$			PNUE			$N_{\text{area}}:\chi$			
	df	Coefficient	$\chi^2$	p	Coefficient	$\chi^2$	p	Coefficient	$\chi^2$	p
(Intercept)	-	8.12E-01	-	-	9.57E+00	-	-	9.19E-01	-	-
Soil N	1	-1.14E-03	1.698	0.193	-6.63E-02	6.396	<b>0.011</b>	2.60E-02	9.533	<b>0.002</b>
Soil pH	1	-1.91E-02	1.087	0.297	-9.25E-01	2.843	<i>0.092</i>	2.03E-01	1.321	0.250
Species	4	-	18.843	<b>0.001</b>	-	13.454	<b>0.009</b>	-	52.983	<b>&lt;0.001</b>
( $N_{\text{area}}$ int.)	-	8.93E-01	-	-	-	-	-	-	-	-
$N_{\text{area}}$	1	-1.11E-01	80.606	<b>&lt;0.001</b>	-	-	-	-	-	-

	$V_{\text{cmax}25}:\chi$			
	df	Coefficient	$\chi^2$	p
(Intercept)	-	7.20E+01	-	-
Soil N	1	3.99E-01	0.963	0.326
Soil pH	1	-3.12E+00	0.138	0.711
Species	4	-	31.450	<b>&lt;0.001</b>
( $N_{\text{area}}$ int.)	-	1.18E+01	-	-
$N_{\text{area}}$	4	3.87E+01	32.797	<b>&lt;0.001</b>

\*Significance determined using Type II Wald  $\chi^2$  tests ( $\alpha = 0.05$ ).  $P$ -values  $< 0.05$  are in bold, while  $p$ -values between 0.05 and 0.1 are italicized. Superscript letters indicate model coefficients fit to natural-log <sup>(a)</sup> or square-root <sup>(b)</sup> transformed data. Relationships between  $N_{\text{area}}$  and each response variable were fit using the second series of bivariate mixed-effects models, so model coefficients and results are independent from model coefficients and results reported for relationships between soil N, soil pH, and species for each response variable. Key:  $\chi$  - isotope-derived estimate of the  $C_i:C_a$ ; PNUE - photosynthetic N use efficiency, ratio of net photosynthesis to leaf N content per unit leaf area;  $N_{\text{area}}:\chi$  - ratio of  $N_{\text{area}}$  to  $\chi$ ;  $V_{\text{cmax}25}:\chi$  - ratio of  $V_{\text{cmax}25}$  to  $\chi$ .

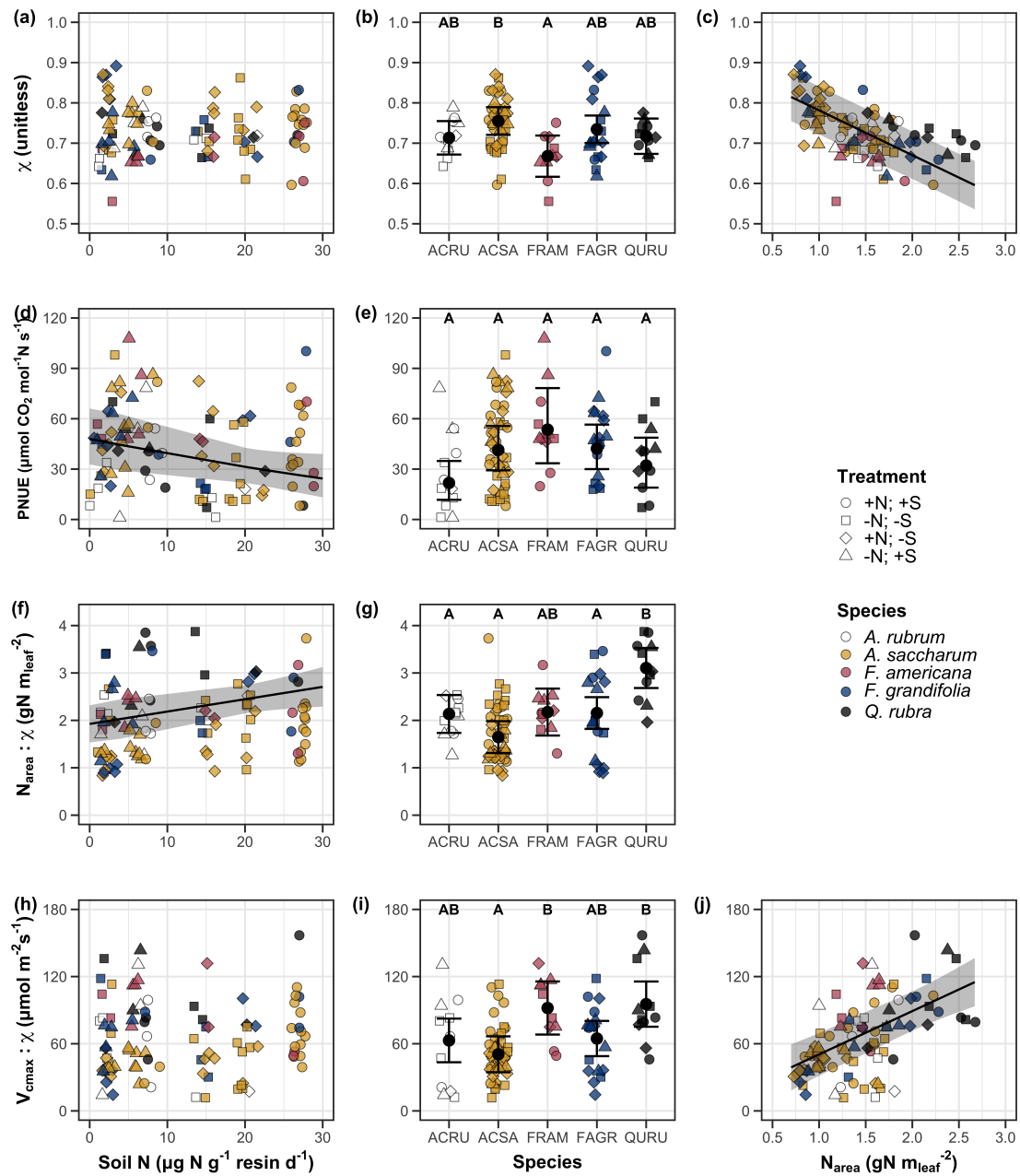


**Figure 3.4.** Effects of soil nitrogen availability and species on the proportion of leaf nitrogen content allocated to Rubisco (a-b), bioenergetics (c-d), photosynthesis (Rubisco + bioenergetics; e-f), and structure (g-h). Soil nitrogen availability is represented on the x-axis in the left column of panels and species are represented on the x-axis in the right column of panels. Species abbreviations and position along the x-axis in the middle column of panels, colored points, shapes, trendlines, error bars, and compact lettering are as explained in Figure 3.1.

**836** 3.4 Discussion

**837** Photosynthetic least-cost theory provides an explanation for understand-  
**838** ing relationships between soil nutrient availability, leaf nutrient allocation, and  
**839** photosynthetic capacity. The theory suggests that plants acclimate to a given  
**840** environment by optimizing leaf photosynthesis rates at the lowest summed cost  
**841** of using nutrients and water Prentice et al. (2014), Wang et al. (2017), Smith  
**842** et al. (2019), Paillassa et al. (2020). The theory predicts that an increase in  
**843** soil nutrient availability should allow similar photosynthesis rates to be achieved  
**844** with increased leaf nutrient content and photosynthetic capacity (i.e.,  $V_{cmax25}$  and  
**845**  $J_{max25}$ ) at lower leaf  $C_i:C_a$  ( $\chi$ ), resulting in an increase in water use efficiency,  
**846** decrease in nutrient use efficiency, and increase in both leaf nutrient content and  
**847** photosynthetic capacity per unit  $\chi$ . The theory predicts similar leaf responses to  
**848** increasing soil pH under acidic conditions, presumably due to generally faster nu-  
**849** trient cycle dynamics and consequent reductions in the cost of acquiring nutrients  
**850** relative to water with increasing soil pH (Wang et al. 2017; Paillassa et al. 2020;  
**851** Dong et al. 2020).

**852** Supporting the theory, we showed that increasing soil N availability was  
**853** associated with increased leaf N content (Fig 3.1a, 3.1c), a pattern that reduced  
**854** photosynthetic N use efficiency (Fig 3.4d) and increased leaf N content per unit  
**855**  $\chi$  (Fig 3.4f). Increasing soil N coincided with slight, but non-significant decreases  
**856** in  $\chi$  and increases in  $V_{cmax25}$  and  $J_{max25}$  ( $p < 0.2$ , Table 3.2). The positive trend  
**857** between soil N availability and photosynthetic capacity was supported by the con-  
**858** current strong increase in leaf N content with increasing soil N availability, which  
**859** resulted in no change in the proportion of leaf N content allocated to photosynthe-

860 sis across the soil N availability gradient. Additionally, leaf N content exhibited a  
861 strong negative correlation with  $\chi$ , indicative of strong nitrogen-water use trade-  
862 offs at the leaf level. Responses tended to vary more due to soil N availability  
863 than soil pH. Overall, these findings are consistent with the nutrient-water use  
864 tradeoffs predicted from theory.

865 3.4.1 *Soil nitrogen availability modifies tradeoffs between nitrogen and water use*

866 In support of expected least-cost outcomes and past environmental gradient  
867 studies (Dong et al. 2017; Paillassa et al. 2020), we found that increasing soil N  
868 availability was associated with increased leaf N content. Soil N availability had  
869 smaller impacts on measures of net photosynthesis and  $\chi$ , which led to reductions  
870 in PNUE and increases in leaf N content per unit  $\chi$ , as expected from theory.  
871 Photosynthetic least-cost theory suggests that reductions in PNUE should be  
872 driven by an increase in the proportion of leaf N allocated to photosynthetic tissue,  
873 a pattern that should allow plants to achieve optimal photosynthetic rates with  
874 greater photosynthetic capacity to make better use of available light. Contrasting  
875 theory predictions, we found no effect of soil N availability on photosynthetic  
876 capacity. However, photosynthetic capacity did tend to increase with increasing  
877 soil N availability ( $p < 0.20$ ; Table 3.2) resulting in no effect of soil N availability on  
878 the relative fraction of leaf N allocated to photosynthesis, Rubisco, or bioenergetics  
879 (Fig. 3.3). These lines of evidence support the idea that trees use additional N  
880 to support increased leaf N allocation toward photosynthetic tissue and enhance  
881 photosynthetic capacity (Wright et al. 2003).

882 Soil N availability had a stronger effect on leaf N than photosynthetic ca-

883 pacity. This pattern suggests that additional plant N uptake due to increased  
884 soil N availability was also being used to support non-photosynthetic N pools,  
885 possibly to structural tissue or stress-induced amino acid and polyamine synthe-  
886 sis (Minocha et al. 2000; Onoda et al. 2004; Bubier et al. 2011). While we  
887 found no change in the proportion of leaf N allocated to leaf structural tissue, the  
888 overall stimulation in leaf N content with increasing soil N availability suggests an  
889 increase in the net amount of N invested in leaf structural tissue along the N avail-  
890 ability gradient. Importantly, leaf N allocated to structure was calculated using  
891 an empirical relationship between  $M_{\text{area}}$  and the amount of leaf N allocated to cell  
892 walls (Onoda et al. 2017). As the generality of relationships between  $M_{\text{area}}$  and  
893 the amount of leaf N allocated to cell walls has been called into question (Harrison  
894 et al. 2009), future work should consider explicitly measuring N allocation to cell  
895 wall tissue and stress-induced amino acid synthesis to confirm these patterns.

896 In opposition to patterns expected from least cost theory, increasing soil  
897 N availability had no apparent effect on  $\chi$  (Fig. 3.4a). Interestingly, despite  
898 the null effect of soil N availability on  $\chi$ , we observed a strong negative effect of  
899 increasing  $N_{\text{area}}$  on  $\chi$  (Fig. 3.4c), consistent with the nitrogen-water use tradeoffs  
900 expected from theory. The null response of  $\chi$  to increasing soil N availability may  
901 have been due to a lack of water limitation in the system, given that the area  
902 received approximately 20% more precipitation (1167 mm) during the 12-month  
903 period leading up to our measurement period than normally expected (972 mm).  
904 However, droughts can and do occur in temperate forests of the northeastern  
905 United States (Sweet et al. 2017), so the observed increase in leaf N content  
906 with increasing soil N availability could be a strategy that allows trees to hedge

907 bets against drier than normal growing seasons (Onoda et al. 2004; Onoda et al.  
908 2017; Hallik et al. 2009). As was suggested in Paillassa et al. (2020), and more  
909 recently by Querejeta et al. (2022), negative effects of soil N availability on  $\chi$  may  
910 increase with increasing aridity. This strategy would be especially advantageous if  
911 it allows individuals growing in arid regions to maintain carbon assimilation rates  
912 with reduced water loss. Future work should attempt to quantify interactive roles  
913 of climate and soil nitrogen availability on nitrogen-water use tradeoffs, which  
914 could be done by leveraging coordinated and multi-factor nutrient (Borer et al.  
915 2014) and water (Knapp et al. 2017) manipulation experiments across broad  
916 climatic gradients.

917 3.4.2 *Soil pH did not modify tradeoffs between nitrogen and water usage*

918 While the primary purpose of this study was to examine the role of soil N  
919 availability on nitrogen-water use tradeoffs, our experimental design manipulated  
920 both soil N and pH, providing an opportunity to isolate the roles of these variables.  
921 Previous correlational studies along environmental gradients identified soil pH as  
922 a particularly important factor that can modify tradeoffs between nutrient and  
923 water use (Smith et al. 2019; Paillassa et al. 2020; Westerband et al. 2023)  
924 and the proportion of leaf nitrogen allocated to photosynthesis (Luo et al. 2021).  
925 Such studies implied that these patterns may be driven by reductions in the cost of  
926 acquiring nutrients relative to water with increasing pH, which may be exacerbated  
927 in acidic soils.

928 Consistent with theory (Wright et al. 2003; Prentice et al. 2014), our  
929 results indicate that increasing soil pH was negatively associated with PNUE.

930 However, there was no effect of soil pH on leaf N content,  $\chi$ , or leaf N content per  
931 unit  $\chi$ , most likely because the experimental N additions increased soil N sup-  
932 ply while both increasing (sodium nitrate) and decreasing (ammonium sulfate)  
933 soil pH. These results suggest that soil pH did not play a major role in modify-  
934 ing expected photosynthetic least-cost theory patterns, contrasting findings from  
935 Paillassa et al. (2020) and other gradient studies that note positive effects of in-  
936 creasing soil pH on leaf N content, Rubisco carboxylation, and  $\chi$  (Viet et al. 2013;  
937 Cornwell et al. 2018; Luo et al. 2021). Instead, null responses to soil pH show  
938 that leaf photosynthetic parameters depend more on soil N availability than pH  
939 per se, and that inferences from gradient studies might be confounding covariation  
940 between N availability and soil acidity.

941 3.4.3 *Species identity explains a large amount of variation in leaf and whole*  
942 *plant traits*

943 Species generally explained a larger amount of variation in measured leaf  
944 traits than soil N availability or soil pH. Interspecies variation is an important  
945 factor to consider when deducing mechanisms that drive photosynthetic least-  
946 cost theory, particularly for species that form distinct mycorrhizal associations or  
947 have different photosynthetic pathways, growth forms, or leaf habit (Espelta et al.  
948 2005; Adams et al. 2016; Bialic-Murphy et al. 2021; Scott and Smith 2022). The  
949 need to consider species may also be important when comparing nutrient-water  
950 use tradeoffs in early and late successional species, or in species with different  
951 resource economic strategies (Abrams and Mostoller 1995; Ellsworth and Reich  
952 1996; Wright et al. 2004; Reich 2014; Onoda et al. 2017; Ziegler et al. 2020).

953        A strength of the study design and sampling effort is that it controls for  
954    many species differences that should modify nitrogen-water use tradeoffs expected  
955    from theory. All tree species measured in this study shared the leaf habit of decid-  
956    uous broadleaves, were growing in forests of similar successional stage, but differed  
957    in mycorrhizal association and consequent resource economic strategies. As stands  
958    tended to be dominated by trees that associate with arbuscular mycorrhizae (*Frax-*  
959    *inus* and both *Acer* species made up 70% of total aboveground biomass across  
960    stands), ecosystem biogeochemical cycle dynamics may be more closely aligned  
961    to the inorganic nutrient economy proposed in Phillips et al. (2013), which may  
962    promote stronger nitrogen-water use tradeoffs in tree species that associate with  
963    arbuscular mycorrhizae. This result was not observed here, as photosynthetic  
964    properties varied as much within as across the two mycorrhizal associations rep-  
965    resented. Given the high variability in measured photosynthetic traits within  
966    and across species, effects of mycorrhizal association likely require more intensive  
967    sampling efforts to detect than were possible here.

968 3.4.4 *Implications for photosynthetic least-cost theory model development*

969        In the field, soil nutrient availability is heterogeneous across time and space  
970    (Table S4). Unaccounted within-plot heterogeneity may have contributed to the  
971    low amount of variation explained by soil N availability in our statistical mod-  
972    els, as resin bags are a coarse surrogate for soil N availability. Despite this, we  
973    still observed evidence for nutrient-water use tradeoffs, suggesting that observed  
974    responses reported here may be an underestimate toward the net effect of soil  
975    N availability on these tradeoffs. While we urge caution in the interpretation of

976 these results, they do provide a promising baseline for future studies investigating  
977 patterns expected from photosynthetic least-cost theory at finer spatiotemporal  
978 resolutions.

979 The general stronger relationship between leaf N content and photosynthetic parameters versus between leaf N content and soil N availability suggests  
980 that leaf N content is more directly tied to photosynthesis than soil N availability.  
981 While this could be due to the high spatiotemporal heterogeneity of soil N availability,  
982 principles from photosynthetic least-cost theory suggest that leaf N content is the downstream product of leaf nutrient demand to build and maintain  
983 photosynthetic machinery, which is set by aboveground environmental conditions  
984 such as light availability, CO<sub>2</sub>, temperature, or vapor pressure deficit (Smith  
985 et al. 2019; Paillassa et al. 2020; Peng et al. 2021; Westerband et al. 2023). The  
986 stronger relationship between leaf N and photosynthetic parameters paired with  
987 the strong negative relationship between leaf N and  $\chi$  could indicate a relatively  
988 stronger effect of climate on leaf N-photosynthesis relationships than soil resource  
989 availability. However, the short distance between plots and across sites limited  
990 our ability to test this mechanism.

993 Variation in soil pH affected least cost responses less than variations in  
994 soil N availability, in part because experimental treatments directly increased soil  
995 N and affected soil pH in opposite directions. While soil pH has been shown  
996 to drive nitrogen-water tradeoffs in global gradient analyses (Viet et al. 2013;  
997 Paillassa et al. 2020), these responses may be due to covariations between soil pH  
998 and nutrient cycling rather than a role of pH per se. The direct manipulations  
999 of soil pH and soil N availability in this study allowed us to partly disentangle

**1000** these factors and show that variation in N availability matters more for least-cost  
**1001** tradeoffs than pH alone.

**1002** 3.4.5 *Conclusions*

**1003** Increasing soil N availability generally increased leaf N content (both area-  
**1004** and mass-based), but did not significantly influence  $\chi$ . This shift in leaf N led  
**1005** to a reduction in PNUE, and an increase in leaf N per unit  $\chi$  with increasing  
**1006** soil N availability. Despite null effects of soil N availability on  $\chi$ , we observed a  
**1007** strong negative relationship between leaf N content and  $\chi$ . These results provide  
**1008** empirical support for the nutrient-water use tradeoffs expected from photosyn-  
**1009** thetic least-cost theory in response to soil nutrient availability, but suggest that  
**1010** all tenets of the theory may not hold in every environment. These results exper-  
**1011** imentially test previous work suggesting that leaf water-nitrogen economies vary  
**1012** across gradients of soil nutrient availability and pH, and show that variations in  
**1013** nutrient availability matter more for determining variation in leaf photosynthetic  
**1014** traits than soil pH.

1015

## Chapter 4

1016 The relative cost of resource use for photosynthesis drives variance in  
1017 leaf nitrogen content across climate and soil resource availability  
1018 gradients

1019 4.1 Introduction

1020 Terrestrial biosphere models, which comprise the land surface component of  
1021 Earth system models, are sensitive to the formulation of photosynthetic processes  
1022 (Knorr 2000; Ziehn et al. 2011; Booth et al. 2012). This is because photosynthe-  
1023 sis is the largest carbon flux between the atmosphere and terrestrial biosphere,  
1024 and is constrained by ecosystem carbon and nutrient cycles (Hungate et al. 2003;  
1025 LeBauer and Treseder 2008; IPCC 2021; Fay et al. 2015). Many terrestrial bio-  
1026 sphere models formulate photosynthesis by parameterizing photosynthetic capac-  
1027 ity within plant functional groups through empirical linear relationships between  
1028 area-based leaf nitrogen content ( $N_{\text{area}}$ ) and the maximum carboxylation rate  
1029 of Ribulose-1,5-bisphosphate carboxylase/oxygenase (Kattge et al. 2009; Rogers  
1030 2014; Rogers et al. 2017). Models are also beginning to include connected carbon-  
1031 nitrogen cycles (Wieder et al. 2015; Shi et al. 2016; Davies-Barnard et al. 2020;  
1032 Braghieri et al. 2022), which allows leaf photosynthesis to be predicted directly  
1033 through changes in  $N_{\text{area}}$  and indirectly through changes in soil nitrogen avail-  
1034 ability (e.g., LPJ-GUESS, Smith et al., 2014; CLM5.0, Lawrence et al., 2019).  
1035 Despite recent model developments, open questions remain regarding the gen-  
1036 erality of ecological relationships between soil nitrogen availability, leaf nitrogen  
1037 content, and leaf photosynthesis across edaphic and climatic gradients.  
1038 Empirical support for positive relationships between soil nitrogen avail-

ability and  $N_{\text{area}}$  is abundant (Firn et al. 2019; Liang et al. 2020), and is a result often attributed to the high nitrogen cost of building and maintaining Rubisco (Evans 1989; Evans and Seemann 1989; Onoda et al. 2004; Onoda et al. 2017; Dong et al. 2020). Such patterns imply that positive relationships between soil nitrogen availability and  $N_{\text{area}}$  should cause an increase in leaf photosynthesis and photosynthetic capacity by increasing the maximum rate of Rubisco carboxylation through increased investments to Rubisco construction and maintenance. This integrated  $N_{\text{area}}$ -photosynthesis response to soil nitrogen availability has been observed both in manipulative experiments and across environmental gradients (Field and Mooney 1986; Evans 1989; Walker et al. 2014; Li et al. 2020), and is thought to be driven by ecosystem nitrogen limitation, which limits its primary productivity globally (LeBauer and Treseder 2008; Fay et al. 2015). However, this response is not consistently observed, as recent studies note variable  $N_{\text{area}}$ -photosynthesis relationships across soil nitrogen availability gradients (Liang et al. 2020; Luo et al. 2021) and that aboveground growing conditions (e.g., light availability, temperature, vapor pressure deficit) or species identity traits (e.g., photosynthetic pathway, nitrogen acquisition strategy) may be more important for explaining variance in  $N_{\text{area}}$  and photosynthetic capacity across time and space (Adams et al. 2016; Dong et al. 2017; Dong et al. 2020; Dong et al. 2022; Smith et al. 2019; Peng et al. 2021; Westerband et al. 2023).

**1059** 4.2 Methods

**1060** 4.2.1 textit{Site descriptions and sampling methodology}

**1061** We collected leaf and soil samples from 24 open grassland sites across cen-  
**1062** tral and eastern Texas in summer 2020 and summer 2021 (Fig. 4.1). Twelve  
**1063** sites were visited between June and July 2020 and 14 sites (11 unique from 2020)  
**1064** were visited between May and June 2021 (Table 1). We explicitly chose sites  
**1065** that maximized variability in precipitation and edaphic variability between sites  
**1066** while minimizing temperature variability across the environmental gradient (Ta-  
**1067** ble 1). No site with personally communicated or anecdotal evidence of grazing  
**1068** or disturbance (e.g., mowing, feral hog activity, etc.) were used. We collected  
**1069** leaf material from three individuals each of the five most abundant species at ran-  
**1070** dom locations at each site, only selecting species that were broadly classified as  
**1071** graminoid, forb/herb, shrub, or subshrub growth habits per the USDA PLANTS  
**1072** database (USDA NRCS 2022). All collected leaves were fully expanded with no  
**1073** visible herbivory or other external damage and also free from shading by nearby  
**1074** shrubs or trees. Five soil samples were collected from 0-15cm below the soil sur-  
**1075** face at each site near the leaf collection sample locations. Soil samples were later  
**1076** mixed together by hand to create one composite soil sample per site.

**1077** 4.2.2 *Leaf trait measurements*

**1078** Images of each leaf were taken immediately following each site visit using  
**1079** a flat-bed scanner. Fresh leaf area was determined from each image using the  
**1080** 'LeafArea' R package (Katabuchi 2015), which automates leaf area calculations  
**1081** using ImageJ software (Schneider et al. 2012). Each leaf was dried at 65°C for at

**1082** least 48 hours to a constant mass, weighed, and manually ground in a mortar and  
**1083** pestle until homogenized. Leaf mass per area ( $M_{\text{area}}$ ; g m<sup>-2</sup>) was calculated as the  
**1084** ratio of dry leaf biomass to fresh leaf area. Subsamples of dried and homogenized  
**1085** leaf tissue were used to measure leaf nitrogen content ( $N_{\text{mass}}$ ; gN g<sup>-1</sup>) through el-  
**1086** emental combustion analysis (Costech-4010, Costech Instruments, Valencia, CA).  
**1087** Leaf nitrogen content per unit leaf area ( $N_{\text{area}}$ ; gN m<sup>-2</sup>) was then calculated as  
**1088** the product of  $N_{\text{mass}}$  and  $M_{\text{area}}$ .

**1089** Subsamples of dried and homogenized leaf tissue were sent to the University  
**1090** of California-Davis Stable Isotope Facility to determine leaf  $\delta^{13}\text{C}$ . Leaf  $\delta^{13}\text{C}$  values  
**1091** were determined using an elemental analyzer (PDZ Europa ANCA-GSL; Sercon  
**1092** Ltd., Chestshire, UK) interfaced to an isotope ratio mass spectrometer (PDZ  
**1093** Europa 20-20 Isotope Ratio Mass Spectrometer, Sercon Ltd., Chestshire, UK).  
**1094** We used leaf  $\delta^{13}\text{C}$  values (‰; relative to Vienna Pee Dee Belemnite international  
**1095** reference standard) to estimate the ratio of intercellular ( $C_i$ ) to extracellular ( $C_a$ )  
**1096** CO<sub>2</sub> ratio (leaf  $C_i:C_a$ ,  $\chi$ ; unitless) following the approach of Farquhar et al. (1989)  
**1097** described in Cernusak et al. (2013). We derived  $\chi$  as:

$$\chi = \frac{C_i}{C_a} = \frac{\Delta^{13}\text{C} - a}{b - a} \quad (4.1)$$

**1098** where  $\Delta^{13}\text{C}$  represents the relative difference between leaf  $\delta^{13}\text{C}$  (‰) and air  $\delta^{13}\text{C}$   
**1099** (‰), and is calculated as:

$$\Delta^{13}\text{C} = \frac{\delta^{13}\text{C}_{\text{air}} - \delta^{13}\text{C}_{\text{leaf}}}{1 + \delta^{13}\text{C}_{\text{leaf}}} \quad (4.2)$$

**1100**  $\delta^{13}\text{C}_{\text{air}}$ , traditionally assumed to be -8‰ (Keeling et al. 1979; Farquhar et al.

**1101** 1989), was calculated as a function of calendar year  $t$  using an empirical equation  
**1102** derived in Feng (1999):

$$\delta^{13}C_{air} = -6.429 - 0.006e^{0.0217(t-1740)} \quad (4.3)$$

**1103** This calculation resulted in  $\delta^{13}C_{air}$  values for 2020 and 2021 as -9.04 and -9.09,  
**1104** respectively.  $a$  represents the fractionation between  $^{12}C$  and  $^{13}C$  due to diffusion  
**1105** in air, assumed to be 4.4‰, and  $b$  represents the fractionation caused by Rubisco  
**1106** carboxylation, assumed to be 27‰ (Farquhar et al. 1989). For  $C_4$  species,  $b$  in  
**1107** Eqn. 4.1 was set to 6.3‰, and was derived from:

$$b = c + (d \cdot \phi) \quad (4.4)$$

**1108** Where  $c$  was set to -5.7‰ and  $d$  was set to 30‰ (Farquhar et al. 1989).  $\phi$ , which  
**1109** is the bundle sheath leakiness term, was set to 0.4. All  $\chi$  values less than 0.2 and  
**1110** greater than 1.0 were assumed to be incorrect and removed.

**1111** We derived the unit cost of resource use ( $\beta$ ) using leaf  $\chi$  and site climate  
**1112** data with equations first described in Prentice et al. (2014) and simplified in  
**1113** Lavergne et al. (2020):

$$\beta = 1.6\eta^*D \frac{\chi - (\frac{\Gamma^*}{C_a})^2}{(1 - \chi)^2(K_m + \Gamma^*)} \quad (4.5)$$

**1114** where  $\eta^*$  is the viscosity of water relative to 25°C, calculated using elevation and  
**1115** mean air temperature of the seven days leading up to each site visit following  
**1116** equations in Huber et al. (2009).  $D$  represents vapor pressure deficit (Pa), set

**1117** to the mean vapor pressure deficit of the seven days leading up to each site visit,  
**1118**  $C_a$  represents atmospheric CO<sub>2</sub> concentration, arbitrarily set to 420  $\mu\text{mol mol}^{-1}$   
**1119** CO<sup>2</sup>.  $K_m$  (Pa) is the Michaelis-Menten coefficient for Rubisco affinity to CO<sub>2</sub> and  
**1120** O<sub>2</sub>, calculated as:

$$K_m = K_c \cdot \left(1 + \frac{O_i}{K_o}\right) \quad (4.6)$$

**1121** where  $K_c$  (Pa) and  $K_o$  (Pa) are the Michaelis-Menten coefficients for Rubisco  
**1122** affinity to CO<sub>2</sub> and O<sub>2</sub>, respectively, and  $O_i$  is the intercellular O<sub>2</sub> concentration.  
**1123**  $\Gamma^*$  (Pa) is the CO<sub>2</sub> compensation point in the absence of dark respiration.  $K_c$ ,  $K_o$ ,  
**1124** and  $\Gamma^*$  were determined using equations described in Medlyn et al. (2002) and  
**1125** derived in Bernacchi et al. (2001), invoking an elevation correction for atmospheric  
**1126** pressure as explained in Stocker et al. (2020).

**1127**

placeholder for Table 1

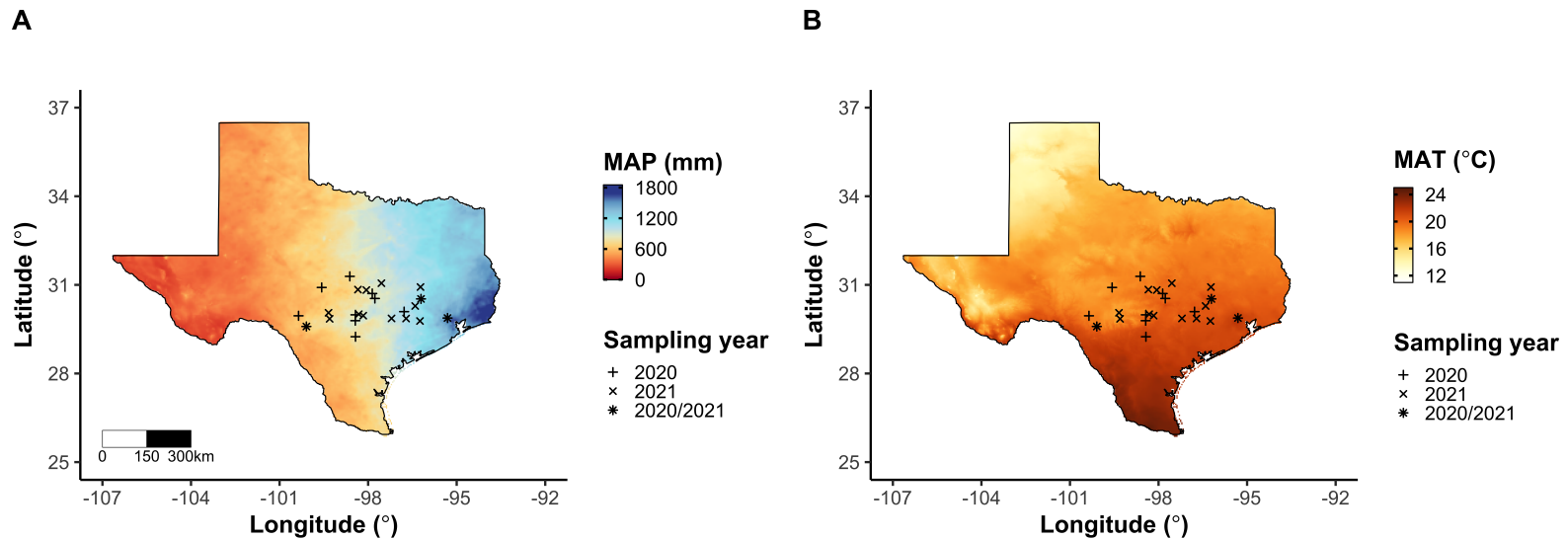


**Figure 4.1.** Maps that detail site locations along 2006-2020 mean annual precipitation (panel A) and mean annual temperature (panel B) gradients in Texas, USA. Precipitation and temperature data were plotted at a 4-km grid resolution and are masked to include only grid cells that occur in the Texas state boundary in the United States. In both panels, open circles refer to sites visited in 2020, open triangles to sites visited in 2021, and closed circles to sites visited in 2020 and 2021. The scale bar in panel A also applies to panel B.

**1128** 4.2.3 *Site climate data*

**1129** We used the Parameter-elevation Regressions on Independent Slopes Model  
**1130** (PRISM) (Daly et al. 2008) climate product to access gridded daily temperature  
**1131** and precipitation data for the coterminous United States at a 4-km grid resolution  
**1132** between January 1, 2006 and July 31, 2021 (PRISM Climate Group, Oregon State  
**1133** University, <https://prism.oregonstate.edu>, data created 4 Feb 2014, accessed 24  
**1134** Mar 2022). Daily mean air temperature, mean VPD, and total precipitation  
**1135** data were extracted from the grid cell that contained the latitude and longitude  
**1136** of each property using the ‘extract’ function in the ‘terra’ R package (Hijmans  
**1137** 2022). PRISM data were used in lieu of local weather station data because several  
**1138** rural sites did not have a local weather station present within a 20-km radius of  
**1139** the site. Daily site climate data were used to estimate mean annual precipitation  
**1140** and mean annual temperature for each site between 2006 and 2020 (Table 1). We  
**1141** then calculated total precipitation and mean daily VPD for the prior 1, 2, 3, 4, 5,  
**1142** 6, 7, 8, 9, 10, 15, 20, 25, 30, 60, and 90 days leading up to each site visit.

**1143** 4.2.4 *Site edaphic characteristics*

**1144** Subsamples of composited soil samples were sent to the Texas A & M  
**1145** Soil, Water and Forage Laboratory to quantify soil nitrate concentration (NO<sub>3</sub>-N;  
**1146** ppm). Soil NO<sub>3</sub>-N was determined by extracting composite soil samples in 1 M  
**1147** KCl, measuring absorbance values of extracts at 520 nm using the end product of  
**1148** a NO<sub>3</sub>-N to NO<sub>2</sub>-N cadmium reduction reaction (Kachurina et al. 2000). Soil tex-  
**1149** ture data from 0-15cm below the soil surface were accessed using the SoilGrids2.0  
**1150** data product (Poggio et al. 2021) through the ‘fetchSoilGrids’ function in the

1151 ‘soilDB’ R package (Beaudette et al. 2022). We used SoilGrids2.0 to access soil  
1152 texture data in lieu of analyses using the collected composite soil sample due to  
1153 a lack of soil material from some sites after sending samples for soil NO<sub>3</sub>-N.

1154 Soil moisture was not measured in the field, but was estimated using  
1155 the ‘Simple Process-Led Algorithms for Simulating Habitats’ model (‘SPLASH’)  
1156 (Davis et al. 2017). This model, derived from the STASH model (Cramer and  
1157 Prentice 1988), spins up a bucket model using Priestley-Taylor equations (Priest-  
1158 ley and Taylor 1972) to calculate daily soil moisture ( $W_n$ ; mm) as a function  
1159 of the previous day’s soil moisture ( $W_{n-1}$ ; mm), daily precipitation ( $P_n$ ; mm),  
1160 condensation ( $C_n$ ; mm), actual evapotranspiration ( $E_n^a$ ; mm), and runoff (RO;  
1161 mm):

$$W_n = W_{n-1} + P_n + C_n - E_n^a - RO \quad (4.7)$$

1162 Models were spun up by equilibrating the previous day’s soil moisture using  
1163 successive model iterations with daily mean air temperature, daily precipitation  
1164 total, the number of daily sunlight hours, and latitude as model inputs (Davis et al.  
1165 2017). Daily sunlight hours were estimated for each day at each site using the  
1166 ‘getSunlightTimes’ function in the ‘suncalc’ R package, which estimated sunrise  
1167 and sunset times of each property using date and site coordinates (Thieurmel and  
1168 Elmarhraoui 2019). Water holding capacity (mm), or bucket size, was estimated  
1169 as a function of soil texture using pedotransfer equations explained in Saxton and  
1170 Rawls (2006), as done in Stocker et al. (2020) and Bloomfield et al. (2022). A  
1171 summary of these equations is included in the Supplemental Information.

1172 Daily soil moisture outputs from the SPLASH model for each site were  
1173 used to calculate mean daily soil moisture for the prior 1, 2, 3, 4, 5, 6, 7, 8, 9,  
1174 10, 15, 20, 25, 30, 60, and 90 days leading up to each site visit. Mean daily  
1175 soil moisture values were then expressed as a fraction of water holding capacity  
1176 to normalize across sites with different bucket depths, as done in Stocker et al.  
1177 (2018).

1178 4.2.5 *Plant functional group assignments*

1179 Plant functional group was assigned to each species and used as the pri-  
1180 mary descriptor of species identity. Specifically, we assigned plant functional  
1181 groups based on photosynthetic pathway ( $C_3$ ,  $C_4$ ) and ability to form associations  
1182 with symbiotic nitrogen-fixing bacteria. The ability to form associations with  
1183 symbiotic nitrogen-fixing bacteria was assigned based on whether species were in  
1184 the *Fabaceae* family, and photosynthetic pathway of each species was determined  
1185 from past literature and confirmed through leaf  $\delta^{13}\text{C}$  values. We chose these plant  
1186 functional groups based on *a priori* hypotheses regarding the functional role of  
1187 nitrogen fixation and photosynthetic pathway on the sensitivity of plant nitrogen  
1188 uptake and leaf nitrogen allocation to soil nutrient availability and aboveground  
1189 growing conditions. These plant functional group classifications resulted in three  
1190 distinct plant functional groups within our dataset:  $C_3$  legumes ( $n = 53$ ),  $C_3$   
1191 non-legumes ( $n = 350$ ), and  $C_4$  non-legumes ( $n = 117$ ).

**1192** 4.2.6 *Data analysis*

**1193** All analyses and plotting were conducted in R version 4.1.1 (R Core Team  
**1194** 2021). We constructed a series of separate linear mixed-effects models to inves-  
**1195** tigate environmental drivers of  $\beta$ ,  $\chi$ ,  $N_{\text{area}}$ ,  $N_{\text{mass}}$ , and  $M_{\text{area}}$ , followed by a path  
**1196** analysis using a piecewise structural equation model to investigate direct and  
**1197** indirect effects of climate and soil resource availability on  $N_{\text{area}}$ .

**1198** To explore environmental drivers of  $\beta$ , we built a linear mixed-effects model  
**1199** that included soil moisture, soil nitrogen availability, and plant functional group  
**1200** as fixed effect coefficients. Species were designated as a random intercept term.  
**1201** Interaction coefficients between all possible combinations of the three fixed effect  
**1202** coefficients were also included.  $\beta$  was natural log transformed to linearize data.  
**1203** We used an information-theoretic model selection approach to determine whether  
**1204** 90-, 60-, 30-, 20-, 15-, 10-, 9-, 8-, 7-, 6-, 5-, 4-, 3-, 2-, or 1-day mean daily  
**1205** soil moisture conferred the best model fit for  $\beta$ . To do this, we constructed 16  
**1206** separate linear mixed-effects models where log-transformed  $\beta$  was included as the  
**1207** response variable and each soil moisture timestep was separately included as a  
**1208** single continuous fixed effect. Species were included as a random intercept term  
**1209** for all models. We used corrected Akaike Information Criterion (AICc) to select  
**1210** the soil moisture timescale that conferred the best model fit, indicated by the  
**1211** model with the lowest AICc score (Table S2; Fig. S2).

**1212** To explore environmental drivers of  $\chi$ , we constructed a second linear mixed  
**1213** effects model that included VPD, soil moisture, soil nitrogen availability, and plant  
**1214** functional group as fixed effect coefficients. Two-way interactions between plant  
**1215** functional group and VPD, soil nitrogen availability, or soil moisture were also

1216 included as fixed effect coefficients, in addition to a three-way interaction between  
1217 soil moisture, soil nitrogen availability, and plant functional group. Species were  
1218 included as a random intercept term. We used an information-theoretic model  
1219 selection approach to determine whether 90-, 60-, 30-, 20-, 15-, 10-, 9-, 8-, 7-, 6-,  
1220 5-, 4-, 3-, 2-, or 1-day mean daily VPD conferred the best model fit for  $\chi$  using  
1221 the same approach explained above for the soil moisture effect on  $\beta$ . The soil  
1222 moisture timescale was set to the same timescale that conferred the best fit for  $\beta$ .

1223 To explore environmental drivers of  $N_{\text{area}}$ ,  $N_{\text{mass}}$ , and  $M_{\text{area}}$ , we constructed  
1224 three separate linear mixed effects model that each included  $\chi$ , soil nitrogen avail-  
1225 ability, soil moisture, and plant functional group as fixed effect coefficients. Two-  
1226 way interactions between plant functional group and  $\beta$ ,  $\chi$ , soil nitrogen availability,  
1227 or soil moisture were included as additional fixed effect coefficients, in addition to  
1228 a three-way interaction between soil nitrogen availability, soil moisture, and plant  
1229 functional group. Species were included as a random intercept term, with the soil  
1230 moisture timescale set to the same timescale that conferred the best fit for  $\beta$ .

1231 In all linear mixed-effects models explained above, including those to select  
1232 relevant timescales, we used the 'lmer' function in the 'lme4' R package (Bates  
1233 et al. 2015) to fit each model and the 'Anova' function in the 'car' R package (Fox  
1234 and Weisberg 2019) to calculate Type II Wald's  $\chi^2$  and determine the significance  
1235 level ( $\alpha = 0.05$ ) of each fixed effect coefficient. We also used the 'emmeans'  
1236 R package (Lenth 2019) to conduct post-hoc comparisons using Tukey's tests,  
1237 where degrees of freedom were approximated using the Kenward-Roger approach  
1238 (Kenward and Roger 1997). Trendlines and error ribbons for all plots were drawn  
1239 using a series of 'emmeans' outputs across the range in plotted x-axis values.

Finally, we conducted a path analysis using a piecewise structural equation model to examine direct and indirect pathways that determined variance in  $N_{\text{area}}$ . Seven separate linear mixed effects models were loaded into the piecewise structural equation model. Models were constructed per our *a priori* hypotheses following patterns expected from photosynthetic least-cost theory. The first model regressed  $N_{\text{area}}$  against  $\chi$ ,  $N_{\text{mass}}$ , and  $M_{\text{area}}$ . The second model regressed  $M_{\text{area}}$  against  $\chi$ . The third model regressed  $N_{\text{mass}}$  against  $\chi$  and  $M_{\text{area}}$  (Dong et al. 2017; Dong et al. 2020). The fourth model regressed  $\chi$  against  $\beta$  and VPD. The fifth model regressed  $\beta$  against soil nitrogen availability, soil moisture, ability to associate with symbiotic nitrogen-fixing bacteria, and photosynthetic pathway. The sixth model regressed soil nitrogen availability against soil moisture, while the seventh model regressed VPD against soil moisture (Novick et al. 2016; Sulman et al. 2016). All models included the relevant timescale selected in the individual linear mixed effect models explained above (2-day soil moisture, 4-day vapor pressure deficit). Models also included species as a random intercept term, were built using the ‘lme’ function in the ‘nlme’ R package (Pinheiro and Bates 2022), and subsequently loaded into the piecewise structural equation model using the ‘psem’ function in the ‘piecewiseSEM’ R package (Lefcheck 2016).

## 1258 4.3 Results

### 1259 4.3.1 Cost to acquire nitrogen relative to water ( $\beta$ )

Model selection indicated that 2-day soil moisture was the timescale that conferred the best model fit for  $\beta$  ( $AIC_c = 1227.83$ ; Table S2; Fig. S1). Increasing soil nitrogen availability generally decreased  $\beta$  ( $p < 0.001$ ; Table 2), a

**1263** pattern driven by a negative effect of increasing soil nitrogen availability on  $\beta$  in  
**1264** C<sub>3</sub> nonlegumes (Tukey:  $p < 0.001$ ) and C<sub>3</sub> legumes (Tukey:  $p = 0.004$ ; Fig. 2a).  
**1265** C<sub>4</sub> nonlegumes also demonstrated a negative trend in the effect of increasing soil  
**1266** nitrogen availability on  $\beta$ , but this pattern was not significantly different from  
**1267** zero (Tukey:  $p = 0.307$ ; Fig. 2a). There was no apparent effect of soil moisture  
**1268** on  $\beta$  ( $p = 0.264$ ; Table 1; Fig. 2b). A functional group effect ( $p < 0.001$ ; Ta-  
**1269** ble 1) indicated that C<sub>4</sub> nonlegumes generally had lower  $\beta$  values than both C<sub>3</sub>  
**1270** legumes and C<sub>3</sub> non-legumes when averaged across soil moisture and soil nitrogen  
**1271** availability values (Tukey:  $p < 0.001$  in both cases), while average  $\beta$  values in C<sub>3</sub>  
**1272** legumes did not differ from C<sub>3</sub> nonlegumes (Tukey:  $p = 0.691$ ).

**1273**

placeholder Table 2

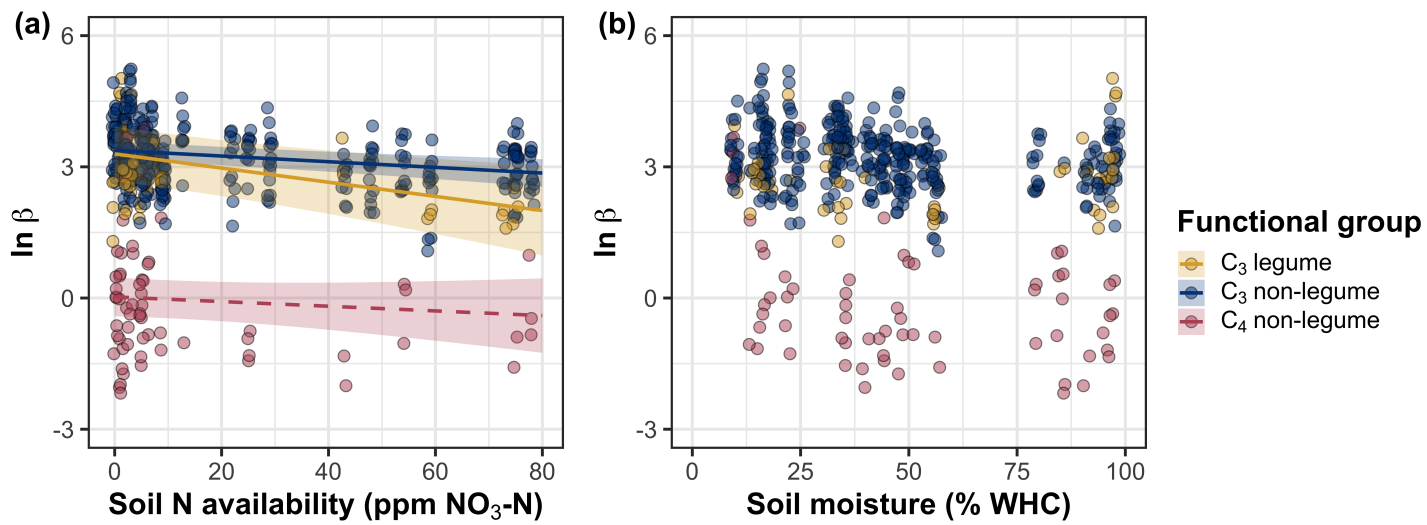


**Figure 4.2.** Effects of soil nitrogen availability (a) and soil moisture (b) on the unit cost ratio  $\beta$ . In (b), soil moisture is represented as a percent of site water holding capacity. Yellow shading and trendlines indicate C<sub>3</sub> legumes, blue shading and trendlines indicate C<sub>3</sub> non-legumes, and red shading and trendlines indicate C<sub>4</sub> non-legumes. Points are jittered for visibility. Variably colored trendlines are only included if there is an interaction between the x-axis and plant functional group, where solid trendlines indicate slopes that are different from zero ( $p < 0.05$ ) and dashed trendlines indicate slopes that are not different from zero ( $p > 0.05$ ). Error ribbons represent the upper and lower 95% confidence intervals of each fitted trendline.

**1274** 4.3.2 *Leaf C<sub>i</sub>:C<sub>a</sub>*

**1275** Model selection indicated that 4-day daily VPD was the timescale that  
**1276** conferred the best model fit for  $\chi$  (AICc = -883.97; Table S1; Fig. S2).

**1277** Variance in  $\chi$  was driven by a series of two-way interactions between func-  
**1278** tional group and VPD ( $p = 0.006$ ; Table 3), soil moisture ( $p = 0.033$ , Table 3),  
**1279** and soil nitrogen availability ( $p = 0.022$ ; Table 3). The interaction between 4-day  
**1280** VPD and functional group revealed that the general negative effect of increasing  
**1281** VPD ( $p < 0.001$ ; Table 3) was driven by a negative effect of increasing VPD  
**1282** on  $\chi$  in C<sub>3</sub> nonlegumes (Tukey:  $p < 0.001$ ) and marginal negative effect in C<sub>3</sub>  
**1283** legumes (Tukey:  $p = 0.074$ ) paired with a positive trending, but insignificant  
**1284** effect of increasing VPD in C<sub>4</sub> nonlegumes (Tukey:  $p = 0.130$ ; Fig. 3a). The  
**1285** interaction between 2-day soil moisture and functional group indicated that the  
**1286** general negative effect of increasing soil moisture on  $\chi$  was driven by a positive  
**1287** effect of increasing soil moisture on  $\chi$  in C<sub>4</sub> nonlegumes (Tukey:  $p = 0.009$ ) de-  
**1288** spite a positive trending but insignificant effect of increasing soil moisture on  $\chi$   
**1289** in C<sub>3</sub> legumes (Tukey:  $p = 0.116$ ) and a null effect of soil moisture on  $\chi$  in C<sub>3</sub>  
**1290** nonlegumes (Tukey:  $p = 0.693$ ; Fig. 3c). The interaction between soil nitrogen  
**1291** availability and plant functional group revealed a weak negative effect of increas-  
**1292** ing soil nitrogen availability on  $\chi$  in C<sub>3</sub> legumes (Tukey:  $p = 0.045$ ), with no  
**1293** apparent effect in C<sub>3</sub> nonlegumes (Tukey:  $p = 0.706$ ) or C<sub>4</sub> nonlegumes (Tukey:  
**1294**  $p = 0.757$ ). Finally, an individual effect of functional group ( $p < 0.001$ ; Table 3)  
**1295** revealed that C<sub>4</sub> nonlegumes generally had lower  $\chi$  than C<sub>3</sub> legumes and C<sub>3</sub> non-  
**1296** legumes (Tukey:  $p < 0.001$  in both cases), with no apparent difference between  
**1297** C<sub>3</sub> legumes and C<sub>3</sub> nonlegumes (Tukey:  $p = 0.831$ ).

**1298**

placeholder Table 3



**1299** 4.3.3 *Leaf nitrogen content*

**1300** An interaction between  $\chi$  and plant functional group ( $p < 0.001$ ; Table  
**1301** 4) revealed that the general negative effect of increasing  $\chi$  on  $N_{\text{area}}$  ( $p < 0.001$ ;  
**1302** Table 4) was driven by a negative effect of increasing  $\chi$  on  $N_{\text{area}}$  in C<sub>3</sub> nonlegumes  
**1303** (Tukey:  $p < 0.001$ ) and C<sub>3</sub> legumes (Tukey:  $p = 0.002$ ) despite a null effect of  $\chi$   
**1304** on  $N_{\text{area}}$  in C<sub>4</sub> nonlegumes (Tukey:  $p = 0.795$ ; Fig. 4a). An interaction between  
**1305** soil nitrogen availability and soil moisture ( $p = 0.028$ ; Table 4) indicated that the  
**1306** marginal positive effect of increasing soil nitrogen availability on  $N_{\text{area}}$  ( $p = 0.091$ ;  
**1307** Table 4) decreased with increasing soil moisture, despite no apparent individual  
**1308** effect of soil moisture on  $N_{\text{area}}$  ( $p = 0.692$ ; Table 4). Finally, a plant functional  
**1309** group effect ( $p < 0.001$ ; Table 4) indicated that C<sub>4</sub> nonlegumes had lower  $N_{\text{area}}$   
**1310** values on average compared to C<sub>3</sub> legumes (Tukey:  $p < 0.001$ ) and C<sub>3</sub> nonlegumes  
**1311** (Tukey:  $p = 0.001$ ), while C<sub>3</sub> legumes had lower average  $N_{\text{area}}$  values compared  
**1312** to C<sub>3</sub> nonlegumes (Tukey:  $p = 0.012$ ).

**1313** A marginal interaction between  $\chi$  and plant functional group ( $p = 0.088$ ;  
**1314** Table 4) revealed that, despite no apparent general effect of  $\chi$  on  $N_{\text{mass}}$  ( $p = 0.273$ ;  
**1315** Table 4), increasing  $\chi$  decreased  $N_{\text{mass}}$  in C<sub>3</sub> nonlegumes (Tukey:  $p = 0.021$ ), but  
**1316** this effect was not apparent in C<sub>4</sub> nonlegumes (Tukey:  $p = 0.693$ ) or C<sub>3</sub> legumes  
**1317** (Tukey:  $p = 0.477$ ). An interaction between soil nitrogen availability and soil  
**1318** moisture ( $p < 0.001$ ; Table 4) indicated that the general positive effect of increas-  
**1319** ing soil nitrogen availability on  $N_{\text{mass}}$  ( $p < 0.001$ ; Table 4) generally decreased  
**1320** with increasing soil moisture, despite an apparent general positive effect of in-  
**1321** creasing soil moisture on  $N_{\text{mass}}$  ( $p < 0.001$ ; Table 4). This interaction indicated  
**1322** that the positive effect of increasing soil nitrogen availability on  $N_{\text{mass}}$  was only

1323 apparent when soil moisture was less than 70% the maximum water holding ca-  
1324 pacity (Tukey:  $p < 0.05$  in all cases) despite a positive effect of increasing soil  
1325 moisture on  $N_{\text{mass}}$  ( $p < 0.001$ ; Table 4). Finally, a plant functional group effect  
1326 ( $p < 0.001$ ; Table 4) indicated that C<sub>4</sub> nonlegumes had lower  $N_{\text{mass}}$  values on  
1327 average compared to C<sub>3</sub> legumes (Tukey:  $p = 0.002$ ) and C<sub>3</sub> nonlegumes (Tukey:  
1328  $p = 0.019$ ), while  $N_{\text{mass}}$  did not differ between C<sub>3</sub> legumes and C<sub>3</sub> nonlegumes  
1329 (Tukey:  $p = 0.149$ ).

1330 An interaction between  $\chi$  and functional group ( $p = 0.005$ ; Table 4) indi-  
1331 cated that the general negative effect of increasing  $\chi$  on  $M_{\text{area}}$  ( $p < 0.001$ ; Table  
1332 4; Fig. 4c) was driven by a negative effect of increasing  $\chi$  on  $M_{\text{area}}$  in C<sub>3</sub> legumes  
1333 and C<sub>3</sub> nonlegumes (Tukey:  $p < 0.001$  in both cases) despite a nonsignificant  
1334 effect of increasing  $\chi$  on  $M_{\text{area}}$  in C<sub>4</sub> nonlegumes (Tukey:  $p = 0.724$ ). An in-  
1335 teraction between soil nitrogen and soil moisture ( $p < 0.001$ ; Table 4) indicated  
1336 that the general negative effect of increasing soil nitrogen availability on  $M_{\text{area}}$  ( $p$   
1337  $< 0.001$ ; Table 4) decreased with increasing soil moisture, despite an apparent  
1338 general negative effect of increasing soil moisture on  $M_{\text{area}}$  ( $p = 0.002$ ; Table 4).  
1339 Specifically, the negative effect of increasing soil nitrogen availability on  $M_{\text{area}}$  was  
1340 only apparent when soil moisture was less than 65% the maximum water holding  
1341 capacity (Tukey:  $p < 0.05$  in all cases). An additional interaction between soil  
1342 nitrogen availability and functional group ( $p = 0.034$ ; Table 4) indicated that the  
1343 general negative effect of increasing soil nitrogen availability on  $M_{\text{area}}$  was driven  
1344 by decreases in C<sub>3</sub> nonlegumes (Tukey:  $p < 0.001$ ) and C<sub>4</sub> nonlegumes (Tukey:  
1345  $p = 0.003$ ), with no apparent effect of soil nitrogen availability on  $M_{\text{area}}$  in C<sub>3</sub>  
1346 legumes (Tukey:  $p = 0.997$ ).

**1347**

placeholder Table 4

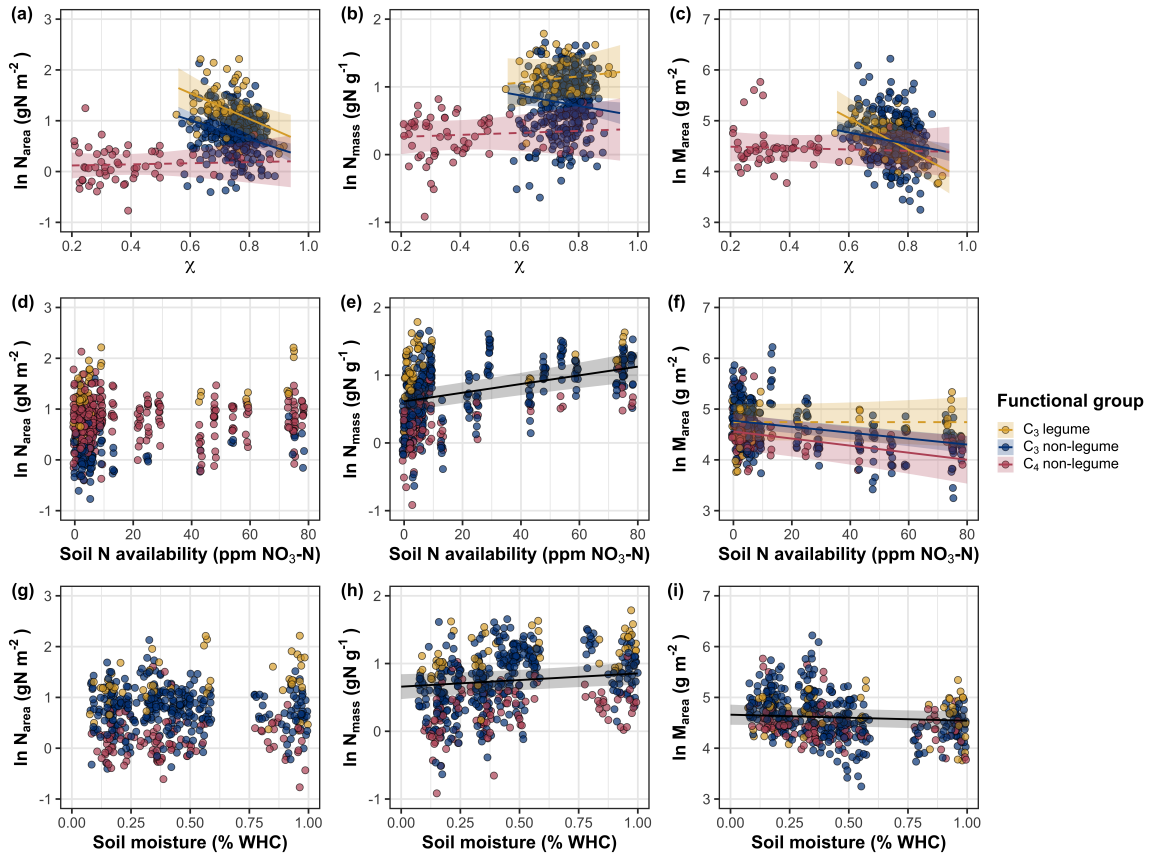


**Figure 4.4.** Effects of  $\chi$  (a-c), soil nitrogen availability (d-f), and soil moisture (g-i) on leaf nitrogen content per unit leaf area (a, d, g), leaf nitrogen content per unit leaf biomass (b, e, h), and leaf mass per area (c, f, i). A solid black trendline indicates the bivariate relationship between the fixed effect the x-axis and response variable on the y-axis and is only included when there is no interaction between the x-axis and plant functional group.

**1348** 4.3.4 *Structural equation model*

**1349** The piecewise structural equation model explained 90%, 54%, 80%, 92%,  
**1350** and 41% of variance in  $N_{\text{area}}$ ,  $N_{\text{mass}}$ ,  $M_{\text{area}}$ ,  $\chi$ , and  $\beta$ , respectively (Table 5; Fig.  
**1351** 5). Variance in  $N_{\text{area}}$  was driven by a negative effect of increasing  $\chi$  ( $p < 0.001$ ;  
**1352** Table 5) paired with positive effects of increasing  $N_{\text{mass}}$  and  $M_{\text{area}}$  ( $p < 0.001$  in  
**1353** both cases; Table 5; Fig. 5). Model results indicated that the negative effect  
**1354** of  $\chi$  on  $N_{\text{area}}$  was driven by a strong reduction in  $M_{\text{area}}$  with increasing  $\chi$  ( $p <$   
**1355** 0.001; Table 5) paired with no change in  $\chi$  due to Nmass ( $p = 0.150$ ; Table 5).  
**1356** However, there was a strong negative effect of increasing  $M_{\text{area}}$  on  $N_{\text{mass}}$  ( $p <$   
**1357** 0.001; Table 5; Fig. 5).  $\chi$  generally increased with increasing  $\beta$  ( $p < 0.001$ ; Table  
**1358** 5) and decreased with increasing VPD ( $p < 0.001$ ; Table 5; Fig. 5). Variance in  $\beta$   
**1359** was driven by a negative effect of increasing soil nitrogen availability ( $p < 0.001$ ;  
**1360** Table 5) and was generally higher in C<sub>3</sub> species ( $p < 0.001$ ; Table 5; Fig. 5).  
**1361** However,  $\beta$  did not change with soil moisture ( $p = 0.332$ ; Table 5) or with ability  
**1362** to acquire nitrogen via symbiotic nitrogen fixation ( $p = 0.546$ ; Table 5). Finally,  
**1363** soil nitrogen availability was positively associated with increasing soil moisture ( $p$   
**1364** < 0.001; Table 5; Fig. 5), while VPD was negatively associated with increasing  
**1365** soil moisture ( $p < 0.001$ ; Table 5; Fig. 5).

**1366**

placeholder Table 5

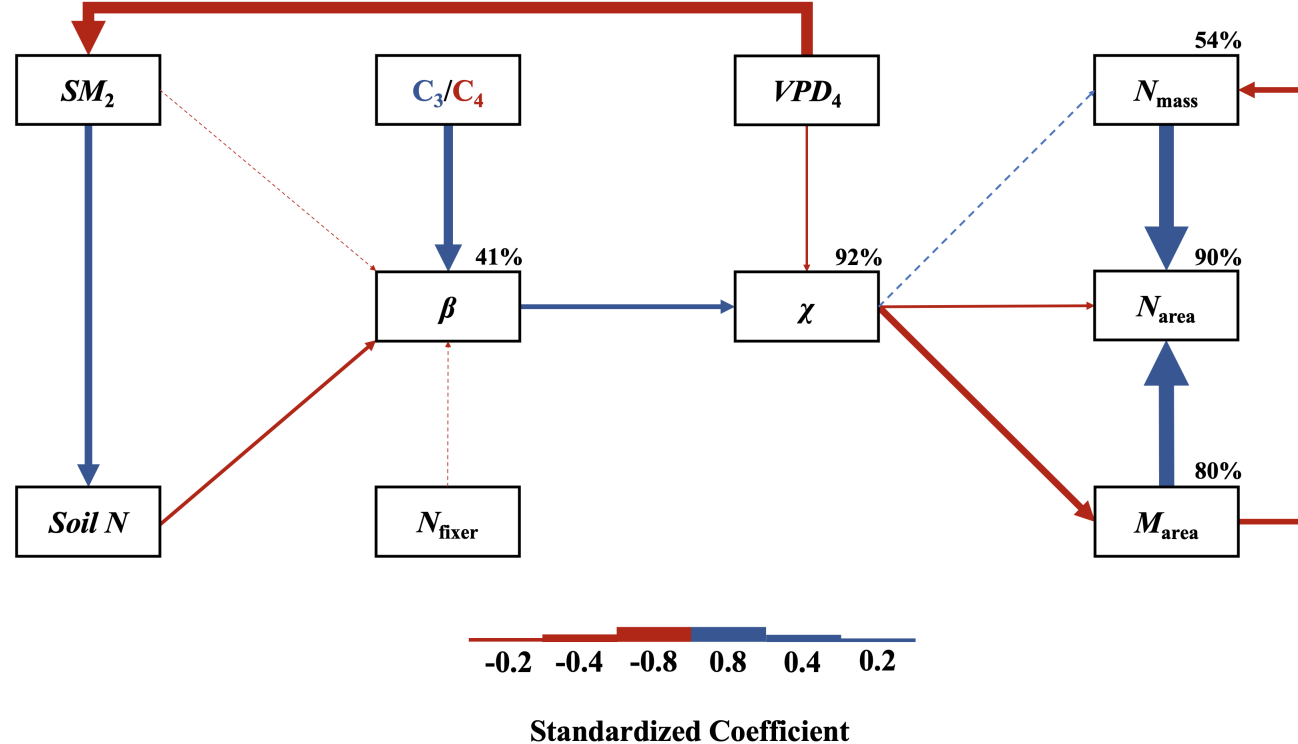


**Figure 4.5.** Structural equation model results exploring direct and indirect drivers of  $N_{area}$ . Boxes indicate measured edaphic factors, climatic factors, and leaf traits. Percentages above boxes indicate conditional  $R^2$  values of each respective leaf trait. Solid arrows indicate bivariate relationships where  $p < 0.05$ , while dashed arrows indicate bivariate relationships where  $p > 0.05$ . Positive model coefficients are indicated through blue arrows, while negative model coefficients are indicated through red arrows. Arrow thickness scales with the standardized model coefficient of each bivariate relationship. A positive coefficient for photosynthetic pathway indicates generally larger values in  $C_3$  species, while a positive coefficient for  $N_{fixer}$  indicates generally larger values in N-fixing species. Standardized model coefficients and associated  $p$ -values are reported in Table 5.

**1367** 4.4 Discussion

1368

## Chapter 5

1369  
1370

Optimal resource investment to photosynthetic capacity maximizes  
nutrient allocation to whole plant growth under elevated CO<sub>2</sub>

1371 5.1 Introduction

1372 Terrestrial ecosystems are regulated by complex carbon and nitrogen cy-  
1373 cles. As a result, terrestrial biosphere models, which are beginning to include  
1374 coupled carbon and nitrogen cycles (Shi et al. 2016; Davies-Barnard et al. 2020;  
1375 Braghieri et al. 2022), must accurately represent these cycles under different  
1376 environmental scenarios to reliably simulate carbon and nitrogen atmosphere-  
1377 biosphere fluxes (Hungate et al. 2003; Prentice et al. 2015). While the inclusion  
1378 of coupled carbon and nitrogen cycles tends to reduce model uncertainty (Arora  
1379 et al. 2020), large uncertainty in role of soil nitrogen availability and nitrogen ac-  
1380 quisition strategy on leaf and whole plant acclimation responses to CO<sub>2</sub> remains  
1381 (Smith and Dukes 2013; Terrer et al. 2018; Smith and Keenan 2020). This source  
1382 of uncertainty likely contributes to the widespread divergence in future carbon  
1383 and nitrogen flux simulations across terrestrial biosphere models (Friedlingstein  
1384 et al. 2014; Zaehle et al. 2014; Meyerholt et al. 2020).

1385 Plants grown under elevated CO<sub>2</sub> generally have less leaf nitrogen content  
1386 than those grown under ambient CO<sub>2</sub>, a response that often corresponds with  
1387 reductions in photosynthetic capacity and stomatal conductance at the leaf-level  
1388 and biomass stimulation over time at the whole plant level (Curtis 1996; Drake  
1389 et al. 1997; Ainsworth et al. 2002; Makino 2003; Morgan et al. 2004; Ainsworth  
1390 and Long 2005; Ainsworth and Rogers 2007; Smith and Dukes 2013; Poorter et al.  
1391 2022). As net primary productivity is generally limited by nitrogen availability

1392 (Vitousek and Howarth 1991; LeBauer and Treseder 2008; Fay et al. 2015), and  
1393 soil nitrogen availability is often positively correlated with leaf nitrogen content  
1394 and photosynthetic capacity (Field and Mooney 1986; Evans and Seemann 1989;  
1395 Evans 1989; Walker et al. 2014; Firn et al. 2019; Liang et al. 2020), some  
1396 have hypothesized that leaf and whole plant acclimation responses to CO<sub>2</sub> are  
1397 constrained by soil nitrogen availability. The progressive nitrogen limitation hy-  
1398 pothesis predicts that elevated CO<sub>2</sub> will increase plant nitrogen demand, which  
1399 will increase plant nitrogen uptake and progressively deplete soil nitrogen if soil  
1400 nitrogen supply does not exceed plant nitrogen demand (Luo et al. 2004). The  
1401 hypothesis predicts that this response should result in strong acute stimulations in  
1402 whole plant growth and primary productivity that diminish over time as nitrogen  
1403 becomes more limiting. Assuming a positive relationship between soil nitrogen  
1404 availability, leaf nitrogen content, and photosynthetic capacity, this hypothesis  
1405 also implies that progressive reductions in soil nitrogen availability should be the  
1406 mechanism that drives the downregulation in leaf nitrogen content and photosyn-  
1407 thetic capacity under elevated CO<sub>2</sub>. This hypothesis has received some support  
1408 from free air CO<sub>2</sub> enrichment experiments (Reich et al. 2006; Norby et al. 2010),  
1409 although is not consistently observed across experiments (Finzi et al. 2006; Moore  
1410 et al. 2006; Liang et al. 2016).

1411 While possible that progressive nitrogen limitation may determine leaf and  
1412 whole plant acclimation responses to CO<sub>2</sub>, growing evidence indicates that leaf ni-  
1413 trogen and photosynthetic capacity are more strongly determined through above-  
1414 ground growing conditions than by soil resource availability (Dong et al. 2017;  
1415 Dong et al. 2020; Dong et al. 2022; Smith et al. 2019; Smith and Keenan 2020;

1416 Paillassa et al. 2020; Peng et al. 2021; Querejeta et al. 2022; Westerband et al.  
1417 2023), and satellite-derived chlorophyll fluorescence data indicate that increasing  
1418 atmospheric CO<sub>2</sub> may decrease leaf and canopy demand for nitrogen (Dong et al.  
1419 2022). Together, results from these studies suggest that the downregulation in  
1420 leaf nitrogen content and photosynthetic capacity due to increasing CO<sub>2</sub> may not  
1421 be as tightly linked to progressive nitrogen limitation as previously hypothesized.

1422 A unification of optimal coordination and photosynthetic least-cost the-  
1423 ories predicts that leaves acclimate to elevated CO<sub>2</sub> by downregulating nitrogen  
1424 allocation to Ribulose-1,5-bisphosphate (RuBP) carboxylase/oxygenase (Rubisco)  
1425 to optimize resource use efficiencies at the leaf level, which allows for greater re-  
1426 source allocation to whole plant growth (Drake et al. 1997; Wright et al. 2003;  
1427 Prentice et al. 2014; Smith et al. 2019). The theory predicts that the downregu-  
1428 lation in nitrogen allocation to Rubisco results in a stronger downregulation in the  
1429 maximum rate of Rubisco carboxylation ( $V_{cmax}$ ) than the maximum rate of RuBP  
1430 regeneration ( $J_{max}$ ), which maximizes photosynthetic efficiency by allowing net  
1431 photosynthesis rates to be equally co-limited by Rubisco carboxylation and RuBP  
1432 regeneration (Chen et al. 1993; Maire et al. 2012). This acclimation response  
1433 allows plants to make more efficient use of available light while avoiding overin-  
1434 vestment in Rubisco, which has high nitrogen and energetic costs of building and  
1435 maintaining (Evans 1989; Evans and Clarke 2019). Instead, additional acquired  
1436 resources not needed to optimize leaf photosynthesis are allocated to the mainte-  
1437 nance of structures that support whole plant growth (e.g., total leaf area, whole  
1438 plant biomass, etc.) or to allocation processes not related to leaf photosynthesis  
1439 or growth, such as plant defense mechanisms or leaf structural tissue. Regardless,

**1440** optimized resource allocation at the leaf level should allow for greater resource  
**1441** allocation to whole plant growth. The theory indicates that leaf acclimation re-  
**1442** sponses to CO<sub>2</sub> should be independent of changes in soil nitrogen availability.  
**1443** While this leaf acclimation response maximizes nitrogen allocation to structures  
**1444** that support whole plant growth, the theory suggests that the positive effect of  
**1445** elevated CO<sub>2</sub> on whole plant growth may be further stimulated by soil nitrogen  
**1446** availability through a reduction in the cost of acquiring nitrogen (Bae et al. 2015;  
**1447** Perkowski et al. 2021; Lu et al. 2022).

**1448** Plants acquire nitrogen by allocating photosynthetically derived carbon be-  
**1449** lowground in exchange for nitrogen through different nitrogen acquisition strate-  
**1450** gies. These nitrogen acquisition strategies can include direct uptake pathways  
**1451** such as mass flow or diffusion (Barber 1962), symbioses with mycorrhizal fungi or  
**1452** symbiotic nitrogen-fixing bacteria (Vance and Heichel 1991; Marschner and Dell  
**1453** 1994; Smith and Read 2008; Udvardi and Poole 2013), or through the release  
**1454** of root exudates that prime free-living soil microbial communities (Phillips et al.  
**1455** 2011; Wen et al. 2022). Plants cannot acquire nitrogen without first allocating  
**1456** carbon belowground, which implies an inherent carbon cost to the plant for acquir-  
**1457** ing nitrogen regardless of nitrogen acquisition strategy. Carbon costs to acquire  
**1458** nitrogen often vary in species with different nitrogen acquisition strategies and  
**1459** are dependent on external environmental factors such as atmospheric CO<sub>2</sub>, light  
**1460** availability, and soil nitrogen availability (Brzostek et al. 2014; Terrer et al. 2016;  
**1461** Terrer et al. 2018; Allen et al. 2020; Perkowski et al. 2021; Lu et al. 2022), which  
**1462** suggests that acquisition strategy may be an important factor in determining ef-  
**1463** fects of soil nitrogen availability on leaf and whole plant acclimation responses to

1464 elevated CO<sub>2</sub>.

1465 A recent meta-analysis using data across 20 grassland and forest CO<sub>2</sub> en-  
1466 richment experiments suggested that species which acquire nitrogen from sym-  
1467 biotic nitrogen-fixing bacteria had reduced costs of nitrogen acquisition under  
1468 elevated CO<sub>2</sub> (Terrer et al. 2018). Findings from this meta-analysis indicated  
1469 that reductions in costs of nitrogen acquisition in species that form associations  
1470 with symbiotic nitrogen-fixing bacteria under elevated CO<sub>2</sub> may drive stronger  
1471 stimulations in whole plant growth and downregulations in  $V_{cmax}$  than species that  
1472 associate with arbuscular mycorrhizal fungi (Smith and Keenan 2020), which gen-  
1473 erally have higher costs of nitrogen acquisition under elevated CO<sub>2</sub> (Terrer et al.  
1474 2018). However, plant investments in symbiotic nitrogen fixation generally de-  
1475 cline with increasing nitrogen availability (Dovrat et al. 2018; Perkowski et al.  
1476 2021), a response that has been previously inferred to be the result of a shift in  
1477 the dominant mode of nitrogen acquisition to direct uptake pathways as costs of  
1478 direct uptake decrease with increasing soil nitrogen availability (Rastetter et al.  
1479 2001; Perkowski et al. 2021). Thus, effects of symbiotic nitrogen fixation on plant  
1480 acclimation responses to CO<sub>2</sub> should decline with increasing soil nitrogen avail-  
1481 ability, although manipulative experiments that directly test these patterns are  
1482 rare.

1483 Here, we conducted a 7-week growth chamber experiment using *Glycine*  
1484 *max* L. (Merr.) to examine the effects of soil nitrogen fertilization and inocula-  
1485 tion with symbiotic nitrogen-fixing bacteria on leaf and whole plant acclimation  
1486 responses to elevated CO<sub>2</sub>. Following patterns expected from theory, we hypoth-  
1487 esized that individual leaves should acclimate to elevated CO<sub>2</sub> by more strongly

1488 downregulating  $V_{cmax}$  relative to  $J_{max}$ , allowing leaf photosynthesis to approach  
1489 optimal coordination. We expected this response to correspond with a stronger  
1490 downregulation in leaf nitrogen content than  $V_{cmax}$  and  $J_{max}$ , which would in-  
1491 crease the fraction of leaf nitrogen content allocated to photosynthesis and photo-  
1492 synthetic nitrogen use efficiency. At the whole-plant level, we hypothesized that  
1493 plants would acclimate to elevated CO<sub>2</sub> by stimulating whole plant growth and  
1494 productivity, a response that would be driven by a strong positive response of  
1495 total leaf area and aboveground biomass to elevated CO<sub>2</sub>. We predicted that  
1496 leaf acclimation responses to elevated CO<sub>2</sub> would be independent of soil nitro-  
1497 gen fertilization and inoculation with symbiotic nitrogen-fixing bacteria; however,  
1498 we expected that increasing soil nitrogen fertilization would increase the posi-  
1499 tive effect of elevated CO<sub>2</sub> on measures of whole plant growth due to a stronger  
1500 reduction in the cost of acquiring nitrogen under elevated CO<sub>2</sub> with increasing  
1501 fertilization. We also expected stronger stimulations in whole plant growth due  
1502 to inoculation, but that this effect would only be apparent under low fertilization  
1503 due to a reduction in root nodulation with increasing fertilization.

1504 5.2 Methods

1505 5.2.1 *Seed treatments and experimental design*

1506 *Glycine max* L. (Merr) seeds were planted in 144 6-liter surface sterilized  
1507 pots (NS-600, Nursery Supplies, Orange, CA, USA) containing a steam-sterilized  
1508 70:30 v:v mix of Sphagnum peat moss (Premier Horticulture, Quakertown, PA,  
1509 USA) to sand (Pavestone, subsidiary of Quikrete Companies, Atlanta, GA, USA).  
1510 Before planting, all *G. max* seeds were surface sterilized in 2% sodium hypochlorite

**1511** for 3 minutes, followed by three separate 3-minute washes with ultrapure water  
**1512** (MilliQ 7000; MilliporeSigma, Burlington, MA USA). A subset of surface steril-  
**1513** ized seeds were inoculated with *Bradyrhizobium japonicum* (Verdesian N-Dure™  
**1514** Soybean, Cary, NC, USA) in a slurry following manufacturer recommendations  
**1515** (3.12 g inoculant and 241 g deionized water per 1 kg seed).

**1516** Seventy-two pots were randomly planted with surface-sterilized seeds inoc-  
**1517** ulated with *B. japonicum*, while the remaining 72 pots were planted with surface-  
**1518** sterilized uninoculated seeds. Thirty-six pots within each inoculation treatment  
**1519** were randomly placed in one of two atmospheric CO<sub>2</sub> treatments (ambient and  
**1520** 1000 μmol mol<sup>-1</sup> CO<sub>2</sub>). Pots within each unique inoculation-by-CO<sub>2</sub> treatment  
**1521** combination randomly received one of nine soil nitrogen fertilization treatments  
**1522** equivalent to 0, 35, 70, 105, 140, 210, 280, 350, or 630 ppm N. Nitrogen fertil-  
**1523** ization treatments were created using a modified Hoagland solution (Hoagland  
**1524** and Arnon 1950) designed to keep concentrations of other macronutrients and  
**1525** micronutrients equivalent across treatments (Table S1). Pots received the same  
**1526** fertilization treatment throughout the entire duration experiment, which were ap-  
**1527** plied twice per week in 150 mL doses as topical agents to the soil surface through-  
**1528** out the duration of the experiment. This experimental design yielded a fully  
**1529** factorial experiment with four replicates per unique fertilization-by-inoculation-  
**1530** by-CO<sub>2</sub> combination.

**1531** 5.2.2 *Growth chamber conditions*

**1532** Upon experiment initiation, pots were randomly placed in one of six Per-  
**1533** cival LED-41L2 growth chambers (Percival Scientific Inc., Perry, IA, USA) over

1534 two experimental iterations due to chamber space limitation. two iterations were  
1535 conducted such that one iteration included all elevated CO<sub>2</sub> pots and the second  
1536 iteration included all ambient CO<sub>2</sub> pots. Average ( $\pm$  SD) CO<sub>2</sub> concentrations  
1537 across chambers throughout the experiment were  $439 \pm 5 \mu\text{mol mol}^{-1}$  for the  
1538 ambient CO<sub>2</sub> treatment and  $989 \pm 4 \mu\text{mol mol}^{-1}$  for the elevated CO<sub>2</sub> treatment.

1539 Daytime growing conditions were simulated using a 16-hour photoperiod,  
1540 with incoming light radiation set to chamber maximum (mean  $\pm$  SD:  $1240 \pm 32$   
1541  $\mu\text{mol m}^{-2} \text{s}^{-1}$  across chambers), air temperature set to 25°C, and relative humid-  
1542 ity set to 50%. The remaining 8 hours simulated nighttime growing conditions,  
1543 with incoming light radiation set to 0  $\mu\text{mol m}^{-2} \text{s}^{-1}$ , chamber temperature set  
1544 to 17°C, and relative humidity set to 50%. Transitions between daytime and  
1545 nighttime growing conditions were simulated by ramping incoming light radiation  
1546 in 45-minute increments and temperature in 90-minute increments over a 3-hour  
1547 period (Table S2).

1548 Including the two, 3-hour ramping periods, pots grew under average ( $\pm$   
1549 SD) daytime light intensity of  $1049 \pm 27 \mu\text{mol m}^{-2} \text{s}^{-1}$ . In the elevated CO<sub>2</sub>  
1550 iteration, pots grew under  $24.0 \pm 0.2^\circ\text{C}$  during the day,  $16.4 \pm 0.8^\circ\text{C}$  during the  
1551 night, and  $51.6 \pm 0.4\%$  relative humidity. In the ambient CO<sub>2</sub> iteration, pots grew  
1552 under  $23.9 \pm 0.2^\circ\text{C}$  during the day,  $16.0 \pm 1.4^\circ\text{C}$  during the night, and  $50.3 \pm 0.2\%$   
1553 relative humidity. We accounted for climatic differences across the six chambers  
1554 by shuffling the same group of pots daily throughout the growth chambers. This  
1555 process was done by iteratively moving the group of pots on the top rack of a  
1556 chamber to the bottom rack of the same chamber, while simultaneously moving  
1557 the group of pots on the bottom rack of a chamber to the top rack of the adjacent

1558 chamber. We moved pots within and across chambers every day throughout the  
1559 course of each experiment iteration.

1560 5.2.3 *Leaf gas exchange measurements*

1561 Gas exchange measurements were collected for all individuals on the sev-  
1562 enth week of development. All gas exchange measurements were collected on  
1563 the center leaf of the most recent fully expanded trifoliate leaf set. Specifi-  
1564 cally, we measured net photosynthesis ( $A_{\text{net}}$ ;  $\mu\text{mol m}^{-2} \text{s}^{-1}$ ), stomatal conduc-  
1565 tance ( $g_{\text{sw}}$ ;  $\text{mol m}^{-2} \text{s}^{-1}$ ), and intercellular  $\text{CO}_2$  ( $C_i$ ;  $\mu\text{mol mol}^{-1}$ ) concentrations  
1566 across a range of atmospheric  $\text{CO}_2$  concentrations (i.e., an  $A_{\text{net}}/C_i$  curve) using the  
1567 Dynamic Assimilation Technique™. The Dynamic Assimilation Technique™ has  
1568 been shown to correspond well with traditional steady-state  $\text{CO}_2$  response curves  
1569 in *G. max* (Saathoff and Welles 2021).  $A_{\text{net}}/C_i$  curves were generated along a  
1570 reference  $\text{CO}_2$  ramp down from  $420 \mu\text{mol mol}^{-1} \text{CO}_2$  to  $20 \mu\text{mol mol}^{-1} \text{CO}_2$ , fol-  
1571 lowed by a ramp up from  $420 \mu\text{mol mol}^{-1} \text{CO}_2$  to  $1620 \mu\text{mol mol}^{-1} \text{CO}_2$  after  
1572 a 90-second wait period at  $420 \mu\text{mol mol}^{-1} \text{CO}_2$ . The ramp rate for each curve  
1573 was set to  $200 \mu\text{mol mol}^{-1} \text{min}^{-1}$ , logging every five seconds, which generated 96  
1574 data points per response curve. All  $A_{\text{net}}/C_i$  curves were generated after  $A_{\text{net}}$  and  
1575  $g_{\text{sw}}$  stabilized in a LI-6800 cuvette set to a  $500 \text{ mol s}^{-1}$ , 10,000 rpm mixing fan  
1576 speed, 1.5 kPa vapor pressure deficit,  $25^\circ\text{C}$  leaf temperature,  $2000 \mu\text{mol m}^{-2} \text{s}^{-1}$   
1577 incoming light radiation, and initial reference  $\text{CO}_2$  set to  $420 \mu\text{mol mol}^{-1}$ .

1578 With the same focal leaf used to generate  $A_{\text{net}}/C_i$  curves, we measured  
1579 dark respiration ( $R_{\text{d25}}$ ;  $\mu\text{mol m}^{-2} \text{s}^{-1}$ ) following at least a 30-minute period of  
1580 darkness. Measurements were collected on a 5-second log interval for 60 seconds

1581 after stabilizing in a LI-6800 cuvette set to a  $500 \text{ mol s}^{-1}$ , 10,000 rpm mixing fan  
1582 speed, 1.5 kPa vapor pressure deficit, 25°C leaf temperature, and  $420 \mu\text{mol mol}^{-1}$   
1583 reference CO<sub>2</sub> concentration (for both CO<sub>2</sub> concentrations), with incoming light  
1584 radiation set to  $0 \mu\text{mol m}^{-2} \text{ s}^{-1}$ . A single dark respiration value was determined  
1585 for each focal leaf by calculating the mean dark respiration value (i.e. the absolute  
1586 value of  $A_{\text{net}}$  during the logging period) across the logging interval.

1587 5.2.4 *Leaf trait measurements*

1588 The focal leaf used to generate  $A_{\text{net}}/C_i$  curves and dark respiration was  
1589 harvested immediately following gas exchange measurements. Images of each focal  
1590 leaf were curated using a flat-bed scanner to determine wet leaf area using the  
1591 'LeafArea' R package (Katabuchi 2015), which automates leaf area calculations  
1592 using ImageJ software (Schneider et al. 2012). Each leaf was dried at 65°C for  
1593 at least 48 hours, and subsequently weighed and ground until homogenized. Leaf  
1594 mass per area ( $M_{\text{area}}$ ; g m<sup>-2</sup>) was calculated as the ratio of dry leaf biomass  
1595 to fresh leaf area. Using subsamples of ground and homogenized leaf tissue, we  
1596 measured leaf nitrogen content ( $N_{\text{mass}}$ ; gN g<sup>-1</sup>) through elemental combustion  
1597 analysis (Costech-4010, Costech, Inc., Valencia, CA, USA). Leaf nitrogen content  
1598 per unit leaf area ( $N_{\text{area}}$ ; gN m<sup>-2</sup>) was calculated by multiplying  $N_{\text{mass}}$  and  $M_{\text{area}}$ .

1599 We extracted chlorophyll content from a second leaf in the same trifoliolate  
1600 leaf set as the focal leaf used to generate  $A_{\text{net}}/C_i$  curves. Prior to chlorophyll  
1601 extraction, we used a cork borer to punch between 3 and 5 0.6 cm<sup>2</sup> disks from  
1602 the leaf. Separate images of each punched leaf and set of leaf disks were curated  
1603 using a flat-bed scanner to determine wet leaf area, again quantified using the

**1604** 'LeafArea' R package (Katabuchi 2015). The punched leaf was dried and weighed  
**1605** after at least 65°C in the drying oven to determine Marea of the chlorophyll leaf.

**1606** Leaf disks were shuttled into a test tube containing 10mL dimethyl sul-  
**1607** foxide, vortexed, and incubated at 65degreeC for 120 minutes (Barnes et al.  
**1608** 1992). Incubated test tubes were vortexed again before loaded in 150  $\mu$ L trip-  
**1609** licate aliquots to a 96-well plate. Dimethyl sulfoxide was also loaded in a 150  
**1610**  $\mu$ L triplicate aliquot as a blank. Absorbance measurements at 649.1 nm ( $A_{649.1}$ )  
**1611** and 665.1 nm ( $A_{665.1}$ ) were read in each well using a plate reader (Biotek Synergy  
**1612** H1; Biotek Instruments, Winooski, VT USA) (Wellburn 1994), with triplicates  
**1613** subsequently averaged and corrected by the mean of the blank absorbance value.  
**1614** Blank-corrected absorbance values were used to estimate  $Chl_a$  ( $\mu$ g mL $^{-1}$ ) and  
**1615**  $Chl_b$  ( $\mu$ g mL $^{-1}$ ) following equations from Wellburn (1994):

$$Chl_a = 12.47A_{665.1} - 3.62A_{649.1} \quad (5.1)$$

**1616** and

$$Chl_b = 25.06A_{665.1} - 6.50A_{649.1} \quad (5.2)$$

**1617**  $Chl_a$  and  $Chl_b$  were converted to mmol mL $^{-1}$  using the molar mass of chlorophyll a  
**1618** (893.51 g mol $^{-1}$ ) and the molar mass of chlorophyll b (907.47 g mol $^{-1}$ ), then added  
**1619** together to calculate total chlorophyll content in the dimethyl sulfoxide extractant  
**1620** (mmol mL $^{-1}$ ). Total chlorophyll content was multiplied by the volume of the  
**1621** dimethyl sulfoxide extractant (10 mL) and converted to area-based chlorophyll  
**1622** content by dividing by the total area of the leaf disks ( $Chl_{area}$ ; mmol m $^{-2}$ ). Mass-  
**1623** based chlorophyll content ( $Chl_{mass}$ ; mmol g $^{-1}$ ) was calculated by dividing  $Chl_{area}$

**1624** by the leaf mass per area of the punched leaf.

**1625** 5.2.5 *A/C<sub>i</sub> curve fitting and parameter estimation*

**1626** We fit  $A_{\text{net}}/C_i$  curves of each individual using the ‘fitaci’ function in the  
**1627** ‘plantecophys’ R package (Duursma 2015). This function estimates the maximum  
**1628** rate of Rubisco carboxylation  $V_{\text{cmax}}$ ;  $\mu\text{mol m}^{-2} \text{s}^{-1}$ ) and maximum rate of electron  
**1629** transport for RuBP regeneration ( $J_{\text{max}}$ ;  $\mu\text{mol m}^{-2} \text{s}^{-1}$ ) based on the Farquhar bio-  
**1630** chemical model of C<sub>3</sub> photosynthesis (Farquhar et al. 1980). Triose phosphate  
**1631** utilization (TPU) limitation was included in all curve fits, and all curve fits in-  
**1632** cluded measured dark respiration values. As  $A_{\text{net}}/C_i$  curves were generated using  
**1633** a common leaf temperature, curves were fit using Michaelis-Menton coefficients  
**1634** for Rubisco affinity to CO<sub>2</sub> ( $K_c$ ;  $\mu\text{mol mol}^{-1}$ ) and O<sub>2</sub> ( $K_o$ ;  $\mu\text{mol mol}^{-1}$ ), and the  
**1635** CO<sub>2</sub> compensation point ( $\Gamma^*$ ;  $\mu\text{mol mol}^{-1}$ ) reported in Bernacchi et al. (2001).  
**1636** Specifically,  $K_c$  was set to 404.9  $\mu\text{mol mol}^{-1}$ ,  $K_o$  was set to 278.4  $\mu\text{mol mol}^{-1}$ , and  
**1637**  $\Gamma^*$  was set to 42.75  $\mu\text{mol mol}^{-1}$ . The use of a common leaf temperature across  
**1638** curves and dark respiration measurements also eliminated the need to manually  
**1639** temperature standardize rate estimates. For clarity, we reference  $V_{\text{cmax}}$ ,  $J_{\text{max}}$ , and  
**1640**  $R_d$  estimates throughout the rest of the paper as  $V_{\text{cmax}25}$ ,  $J_{\text{max}25}$ , and  $R_{d25}$ .

**1641** 5.2.6 Stomatal limitation

**1642** We quantified the extent by which stomatal conductance limited photo-  
**1643** synthesis (l; unitless) following equations originally described in Farquhar and  
**1644** Sharkey (1982). Stomatal limitation was calculated as:

$$l = 1 - \frac{A_{net}}{A_{mod}} \quad (5.3)$$

**1645** where  $A_{mod}$  represents the photosynthetic rate where  $C_i = C_a$ .  $A_{mod}$  was calcu-

**1646** lated as:

$$A_{mod} = V_{cmax25} - \frac{420 - \Gamma^*}{420 + K_m} - R_{d25} \quad (5.4)$$

**1647**  $K_m$  is the Michaelis-Menten coefficient for Rubisco-limited photosynthesis, calcu-

**1648** lated as:

$$K_m = K_c \cdot \left(1 + \frac{O_i}{K_o}\right) \quad (5.5)$$

**1649** where  $O_i$  refers to leaf intercellular  $O_2$  concentrations, set to  $210 \mu\text{mol mol}^{-1}$ .

**1650** 5.2.7 *Proportion of leaf nitrogen allocated to photosynthesis and structure*

**1651** We used equations from Niinemets and Tenhunen (1997) to estimate the

**1652** proportion of leaf N content allocated to Rubisco bioenergetics, and light harvest-

**1653** ing proteins. The proportion of leaf N allocated to Rubisco ( $\rho_{rub}$ ;  $\text{gN gN}^{-1}$ ) was

**1654** calculated as a function of  $V_{cmax25}$  and  $N_{area}$ :

$$\rho_{rubisco} = \frac{V_{cmax25} N_r}{V_{cr} N_{area}} \quad (5.6)$$

**1655** where  $N_r$  is the amount of nitrogen in Rubisco, set to  $0.16 \text{ gN (gN in Rubisco)}^{-1}$

**1656** and  $V_{cr}$  is the maximum rate of RuBP carboxylation per unit Rubisco protein,

**1657** set to  $20.5 \mu\text{mol CO}_2 (\text{g Rubisco})^{-1}$ . The proportion of leaf nitrogen allocated to

**1658** bioenergetics ( $\rho_{bioe}$ ;  $\text{gN gN}^{-1}$ ) was similarly calculated as a function of  $J_{max25}$  and

**1659**  $N_{\text{area}}$ :

$$\rho_{\text{bioe}} = \frac{J_{\text{max}25} N_b}{J_{\text{mc}} N_{\text{area}}} \quad (5.7)$$

**1660** where  $N_b$  is the amount of nitrogen in cytochrome f, set to 0.12407 gN ( $\mu\text{mol}$   
**1661** cytochrome f) $^{-1}$  assuming a constant 1: 1: 1.2 cytochrome f: ferredoxin NADP  
**1662** reductase: coupling factor molar ratio (Evans and Seemann 1989; Niinemets and  
**1663** Tenhunen 1997), and  $J_{\text{mc}}$  is the capacity of electron transport per cytochrome f,  
**1664** set to 156  $\mu\text{mol}$  electron ( $\mu\text{mol}$  cytochrome f) $^{-1}\text{s}^{-1}$ .

**1665** The proportion of leaf nitrogen allocated to light harvesting proteins was  
**1666** calculated as a function of  $Chl_{\text{mass}}$  and  $N_{\text{mass}}$ :

$$\rho_{\text{light}} = \frac{Chl_{\text{mass}}}{N_{\text{mass}} c_b} \quad (5.8)$$

**1667** where  $c_b$  is the stoichiometry of the light-harvesting chlorophyll complexes of  
**1668** photosystem II, set to 2.75 mmol chlorophyll (gN in chlorophyll) $^{-1}$ . We used the  
**1669**  $N_{\text{mass}}$  value of the focal leaf used to generate  $A_{\text{net}}/C_i$  curves instead of the leaf  
**1670** used to extract chlorophyll content, as the two leaves are from the same trifoliolate  
**1671** leaf set and are highly correlated with each other (Figure SX).

**1672** The proportion of leaf nitrogen content allocated to photosynthetic tissue  
**1673** ( $\rho_{\text{photo}}$ ; gN gN $^{-1}$ ) was estimated as the sum of  $\rho_{\text{rubisco}}$ ,  $\rho_{\text{bioe}}$ , and  $\rho_{\text{light}}$ .

**1674** Finally, the proportion of leaf N content allocated to structural tissue ( $\rho_{\text{str}}$ ;  
**1675** gN gN $^{-1}$ ) was estimated as:

$$\rho_{\text{structure}} = \frac{N_{\text{cw}}}{N_{\text{area}}} \quad (5.9)$$

1676 where  $N_{cw}$  is the leaf N content allocated to cell walls ( $\text{gN m}^{-2}$ ), calculated as a  
1677 function of  $M_{area}$  using an empirical equation from Onoda et al. (2017):

$$N_{cw} = 0.000355 * M_{area}^{1.39} \quad (5.10)$$

1678 5.2.8 *Whole plant traits*

1679 Seven weeks after experiment initiation and immediately following gas ex-  
1680 change measurements, we harvested all experimental individuals and separated  
1681 biomass of each experimental individual into major organ types (leaves, stems,  
1682 roots, and nodules when present). Fresh leaf area of all harvested leaves was mea-  
1683 sured using an LI-3100C (Li-COR Biosciences, Lincoln, Nebraska, USA). Total  
1684 fresh leaf area ( $\text{cm}^2$ ) was calculated as the sum of all leaf areas, including the focal  
1685 leaf used to collect gas exchange data and the focal leaf used to extract chlorophyll  
1686 content. All harvested material was dried in an oven set to 65°C for at least 48  
1687 hours, weighed, and ground to homogeneity. Leaves and nodules were manually  
1688 ground either with a mortar and pestle, while stems and roots were ground using  
1689 a Wiley mill (E3300 Mini Mill; Eberbach Corp., MI, USA). Total dry biomass (g)  
1690 was calculated as the sum of dry leaf (including focal leaf for both the  $A_{net}/C_i$   
1691 curve and leaf used to extract chlorophyll content), stem, root, and root nodule  
1692 biomass. We also quantified carbon and nitrogen content of each respective organ  
1693 type through elemental combustion (Costech-4010, Costech, Inc., Valencia, CA,  
1694 USA) using subsamples of ground and homogenized organ tissue.

1695 Following the approach explained in Perkowski et al. (2021), we calcu-  
1696 lated structural carbon costs to acquire nitrogen as the ratio of total belowground

**1697** carbon biomass to whole plant nitrogen biomass ( $N_{\text{cost}}$ ; gC gN<sup>-1</sup>). Belowground  
**1698** carbon biomass ( $C_{\text{bg}}$ ; gC) was calculated as the sum of root carbon biomass  
**1699** and root nodule carbon biomass. Root carbon biomass and root nodule carbon  
**1700** biomass was calculated as the product of the organ biomass and the respective  
**1701** organ carbon content. Whole plant nitrogen biomass ( $N_{\text{wp}}$ ; gN) was similarly  
**1702** calculated as the sum of total leaf, stem, root, and root nodule nitrogen biomass,  
**1703** including the focal leaf used for  $A_{\text{net}}/C_i$  curve and chlorophyll extractions. Leaf,  
**1704** stem, root, and root nodule nitrogen biomass was calculated as the product of  
**1705** the organ biomass and the respective organ nitrogen content. This calculation  
**1706** only quantifies plant structural carbon costs to acquire nitrogen and does not  
**1707** include any additional costs of nitrogen acquisition associated with respiration,  
**1708** root exudation, or root turnover. An explicit explanation of the limitations for  
**1709** interpreting this calculation can be found in Perkowski et al. (2021) and Terrer  
**1710** et al. (2018).

**1711** Finally, plant investments in nitrogen fixation were calculated as the ratio  
**1712** of root nodule biomass to root biomass, where increasing values indicate an in-  
**1713** crease in plant investments to nitrogen fixation (Dovrat et al. 2018; Dovrat et al.  
**1714** 2020; Perkowski et al. 2021). We also calculated the percent of leaf nitrogen  
**1715** acquired from the atmosphere (% $N_{\text{dfa}}$ ) using leaf  $\delta^{15}\text{N}$  and the following equation  
**1716** from Andrews et al. (2011):

$$\%N_{\text{dfa}} = \frac{\delta^{15}N_{\text{reference}} - \delta^{15}N_{\text{sample}}}{\delta^{15}N_{\text{reference}} - B} \quad (5.11)$$

**1717** where  $\delta^{15}\text{N}_{\text{reference}}$  refers to a reference plant that exclusively acquires nitrogen via

1718 direct uptake,  $\delta^{15}\text{N}_{\text{sample}}$  refers to an individual's leaf  $\delta^{15}\text{N}$ , and B refers to individuals  
1719 that are entirely reliant on nitrogen fixation. Within each unique nitrogen  
1720 fertilization treatment-by-CO<sub>2</sub> treatment combination, we calculated the mean  
1721 leaf  $\delta^{15}\text{N}$  for individuals growing in the non-inoculated treatment for  $\delta^{15}\text{N}_{\text{reference}}$ .  
1722 Any individuals with visual confirmation of root nodule formation or nodule initia-  
1723 tion were omitted from the calculation of  $\delta^{15}\text{N}_{\text{reference}}$ . Following recommendations  
1724 from Andrews et al. (2011) we calculated B within each CO<sub>2</sub> treatment using the  
1725 mean leaf  $\delta^{15}\text{N}$  of inoculated individuals that received 0 ppm N. We did not calcu-  
1726 late B within each unique soil nitrogen x CO<sub>2</sub> treatment combination, as previous  
1727 studies suggest decreased reliance on nitrogen fixation with increasing soil nitro-  
1728 gen availability (Perkowski et al. 2021). This approach for estimating nitrogen  
1729 fixation standardizes values such that approaching 1 indicates increasing reliance  
1730 on nitrogen fixation.

1731 5.2.9 *Statistical analyses*

1732 Any uninoculated pots that had substantial root nodule formation (nodule  
1733 biomass: root biomass values greater than 0.05 g g<sup>-1</sup>) were removed from our  
1734 analyses. This was because they were assumed to have been colonized by symbiotic  
1735 nitrogen-fixing bacteria from outside sources. This decision resulted in the removal  
1736 of sixteen pots from our analysis: two pots in the elevated CO<sub>2</sub> treatment that  
1737 received 35 ppm N, three pots in the elevated CO<sub>2</sub> treatment that received 70  
1738 ppm N, one pot in the elevated CO<sub>2</sub> treatment that received 210 ppm N, two pots  
1739 in the elevated CO<sub>2</sub> treatment that received 280 ppm N, two pots in the ambient  
1740 CO<sub>2</sub> treatment that received 0 ppm N, three pots in the ambient CO<sub>2</sub> treatment

1741 that received 70 ppm N, two pots in the ambient CO<sub>2</sub> treatment that received  
1742 105 ppm N, and one pot in the ambient CO<sub>2</sub> treatment that received 280 ppm N.

1743 We built a series of linear mixed effects models to investigate the impacts of  
1744 CO<sub>2</sub> concentration, soil nitrogen fertilization, and inoculation with *B. japonicum*  
1745 on *G. max* gas exchange, tradeoffs between nitrogen and water use, whole plant  
1746 growth, and investment in nitrogen fixation. All models included CO<sub>2</sub> treatment  
1747 as a categorical fixed effect, inoculation treatment as a categorical fixed effect,  
1748 soil nitrogen fertilization as a continuous fixed effect, with interaction terms be-  
1749 tween all three fixed effects. All models also accounted for climatic difference  
1750 between chambers across experiment iterations by including a random intercept  
1751 term that nested starting chamber rack by CO<sub>2</sub> treatment. Models with this  
1752 independent variable structure were created for each of the following dependent  
1753 variables:  $N_{\text{area}}$ ,  $M_{\text{area}}$ ,  $N_{\text{mass}}$ ,  $Chl_{\text{area}}$ ,  $V_{\text{cmax25}}$ ,  $J_{\text{max25}}$ ,  $J_{\text{max25}}:V_{\text{cmax25}}$ ,  $R_{\text{d25}}$ ,  $g_{\text{sw}}$ ,  
1754 stomatal limitation,  $\rho_{\text{rubisco}}$ ,  $\rho_{\text{bioe}}$ ,  $\rho_{\text{light}}$ ,  $\rho_{\text{photo}}$ ,  $\rho_{\text{structure}}$ ,  $N_{\text{cost}}$ ,  $C_{\text{bg}}$ ,  $N_{\text{wp}}$ , total  
1755 biomass, total leaf area, nodule biomass, and the ratio of nodule biomass to root  
1756 biomass.

1757 We used Shapiro-Wilk tests of normality to determine whether linear mixed  
1758 effects models satisfied residual normality assumptions. If residual normality as-  
1759 sumptions were not met (Shapiro-Wilk:  $p < 0.05$ ), then models were fit using  
1760 dependent variables that were natural log transformed. All residual normality  
1761 assumptions that did not originally satisfy residual normality assumptions were  
1762 met with either a natural log or square root data transformation (Shapiro-Wilk:  
1763  $p > 0.05$  in all cases). Specifically, models for  $N_{\text{area}}$ ,  $N_{\text{mass}}$ ,  $Chl_{\text{area}}$ ,  $V_{\text{cmax25}}$ ,  
1764  $J_{\text{max25}}$ ,  $J_{\text{max25}}:V_{\text{cmax25}}$ ,  $g_{\text{sw}}$ , stomatal limitation,  $\rho_{\text{rubisco}}$ ,  $\rho_{\text{bioe}}$ ,  $\rho_{\text{light}}$ ,  $\rho_{\text{photo}}$ , and to-

1765 tal leaf area satisfied residual normality assumptions without data transformation.  
1766 Models for  $M_{\text{area}}$ ,  $\rho_{\text{structure}}$ ,  $N_{\text{cost}}$ ,  $C_{\text{bg}}$ ,  $N_{\text{wp}}$ , and total biomass satisfied residual  
1767 normality assumptions with a natural log data transformation, while models for  
1768 nodule biomass and nodule biomass: root biomass satisfied residual normality  
1769 assumptions with a square root data transformation.

1770 In all statistical models, we used the 'lmer' function in the 'lme4' R package  
1771 (Bates et al. 2015) to fit each model and the 'Anova' function in the 'car' R  
1772 package (Fox and Weisberg 2019) to calculate Type II Wald's  $\chi^2$  and determine the  
1773 significance ( $\alpha = 0.05$ ) of each fixed effect coefficient. We then used the 'emmeans'  
1774 R package (Lenth 2019) to conduct post-hoc comparisons using Tukey's tests,  
1775 where degrees of freedom were approximated using the Kenward-Roger approach  
1776 (Kenward and Roger 1997). All analyses and plots were conducted in R version  
1777 4.2.0 (R Core Team 2021).

1778 5.3 Results

1779 5.3.1 Leaf nitrogen content, chlorophyll content, and mass per area

1780 Elevated CO<sub>2</sub> reduced  $N_{\text{area}}$ ,  $N_{\text{mass}}$ , and  $Chl_{\text{area}}$  by 29%, 50%, and 31%,  
1781 respectively, and stimulated  $M_{\text{area}}$  by 44% ( $p < 0.001$  in all cases; Table 1). An in-  
1782 teraction between fertilization and CO<sub>2</sub> (CO<sub>2</sub>-by-fertilization interaction:  $p_{N_{\text{area}}} =$   
1783 0.017,  $p_{N_{\text{mass}}} < 0.001$ ,  $p_{M_{\text{area}}} = 0.006$ ,  $p_{Chl_{\text{area}}} = 0.083$ ; Table 1) indicated that the  
1784 general positive effect of increasing fertilization on  $N_{\text{area}}$ ,  $N_{\text{mass}}$ , and  $Chl_{\text{area}}$  ( $p <$   
1785 0.001 in all cases; Table 1) was generally stronger under ambient CO<sub>2</sub> (Tukey <sub>$N_{\text{area}}$</sub> :  
1786  $p = 0.026$ ; Tukey <sub>$N_{\text{mass}}$</sub> :  $p < 0.001$ ; Tukey <sub>$M_{\text{area}}$</sub> :  $p = 0.009$ ; Tukey <sub>$Chl_{\text{area}}$</sub> :  $p = 0.065$ ;  
1787 Table 1; Figs. 1a-d). This pattern resulted in a stronger reduction in  $N_{\text{area}}$ ,  $N_{\text{mass}}$ ,

1788 and  $Chl_{area}$  as well as a stronger stimulation in  $M_{area}$  under elevated CO<sub>2</sub> with  
1789 increasing fertilization. An additional interaction between inoculation and CO<sub>2</sub>  
1790 on  $N_{area}$  (CO<sub>2</sub>-by-inoculation interaction:  $p = 0.030$ ; Table 1) indicated that the  
1791 general positive effect of inoculation on  $N_{area}$  ( $p < 0.001$ ; Table 1) was stronger  
1792 under elevated CO<sub>2</sub> (45% increase; Tukey:  $p < 0.001$ ) than under ambient CO<sub>2</sub>  
1793 (18% increase; Tukey:  $p < 0.001$ ), a result that increased the reduction in  $N_{area}$   
1794 in inoculated pots under elevated CO<sub>2</sub>. Inoculation treatment did not modify the  
1795 downregulation in  $N_{mass}$  (CO<sub>2</sub>-by-inoculation interaction:  $p = 0.148$ ; Table 1) and  
1796  $Chl_{area}$  ( $p = 0.147$ ; Table 1) or the stimulation in  $M_{area}$  ( $p = 0.866$ ; Table 1) un-  
1797 der elevated CO<sub>2</sub>. However, interactions between fertilization and inoculation on  
1798  $N_{area}$  (fertilization-by-inoculation interaction:  $p < 0.001$ ; Table 1; Fig. 1a),  $N_{mass}$   
1799 ( $p = 0.001$ ; Table 1; Fig. 1b),  $M_{area}$  ( $p = 0.025$ ; Table 1; Fig. 1c), and  $Chl_{area}$  ( $p$   
1800  $< 0.001$ ; Table 1; Fig. 1d) indicated that the general positive effect of increasing  
1801 fertilization on each trait was stronger in uninoculated pots (Tukey <sub>$N_{area}$</sub> :  $p <$   
1802 0.001; Tukey <sub>$N_{mass}$</sub> :  $p = 0.001$ ; Tukey <sub>$M_{area}$</sub> :  $p = 0.031$ ; Tukey <sub>$Chl_{area}$</sub> :  $p < 0.001$ ).

**Table 5.1.** Effects of soil nitrogen fertilization, inoculation, and CO<sub>2</sub> treatments on  $N_{\text{area}}$ ,  $N_{\text{mass}}$ ,  $M_{\text{area}}$ , and  $Chl_{\text{area}}$ 

	$N_{\text{area}}$			$N_{\text{mass}}$			$M_{\text{area}}^a$			
	df	Coefficient	$\chi^2$	p	Coefficient	$\chi^2$	p	Coefficient	$\chi^2$	p
(Intercept)	-	1.10E+00	-	-	3.05E-02	-	-	3.64E+00	-	-
CO <sub>2</sub>	1	-5.67E-01	155.908	<0.001	-1.80E-02	272.362	<0.001	3.04E-01	151.319	<0.001
Inoculation (I)	1	6.21E-01	86.029	<0.001	7.54E-03	15.576	<0.001	1.81E-01	19.158	<0.001
Fertilization (N)	1	3.06E-03	316.408	<0.001	5.78E-05	106.659	<0.001	3.10E-04	21.440	<0.001
CO <sub>2</sub> *I	1	2.63E-01	4.729	0.030	3.96E-03	2.025	0.155	-3.37E-02	0.029	0.866
CO <sub>2</sub> *N	1	-3.68E-04	5.723	0.017	-2.85E-05	22.542	<0.001	2.80E-04	7.619	0.006
I*N	1	-1.36E-03	43.381	<0.001	-2.00E-05	11.137	0.001	-3.36E-04	5.022	0.025
CO <sub>2</sub> *I*N	1	-3.23E-04	0.489	0.484	-2.59E-06	0.041	0.839	1.15E-04	0.208	0.649

	$Chl_{\text{area}}$			
	df	Coefficient	$\chi^2$	p
(Intercept)	-	2.13E-02	-	-
CO <sub>2</sub>	1	-1.33E-02	69.233	<0.001
Inoculation (I)	1	1.24E-01	136.341	<0.001
Fertilization (N)	1	3.35E-04	163.111	<0.001
CO <sub>2</sub> *I	1	-3.18E-02	2.102	0.147
CO <sub>2</sub> *N	1	-8.79E-05	2.999	0.083
I*N	1	-2.65E-04	75.769	<0.001
CO <sub>2</sub> *I*N	1	7.68E-05	2.144	0.147

\*Significance determined using Type II Wald  $\chi^2$  tests ( $\alpha = 0.05$ ). P-values  $< 0.05$  are in bold, while p-values between 0.05 and 0.1 are italicized. A superscript “a” is included after trait labels to indicate if models were fit with natural log transformed response variables. Key: df = degrees of freedom,  $N_{\text{area}}$  = leaf nitrogen content per unit leaf area,  $N_{\text{mass}}$  = leaf nitrogen content,  $M_{\text{area}}$  = leaf mass per unit leaf area.

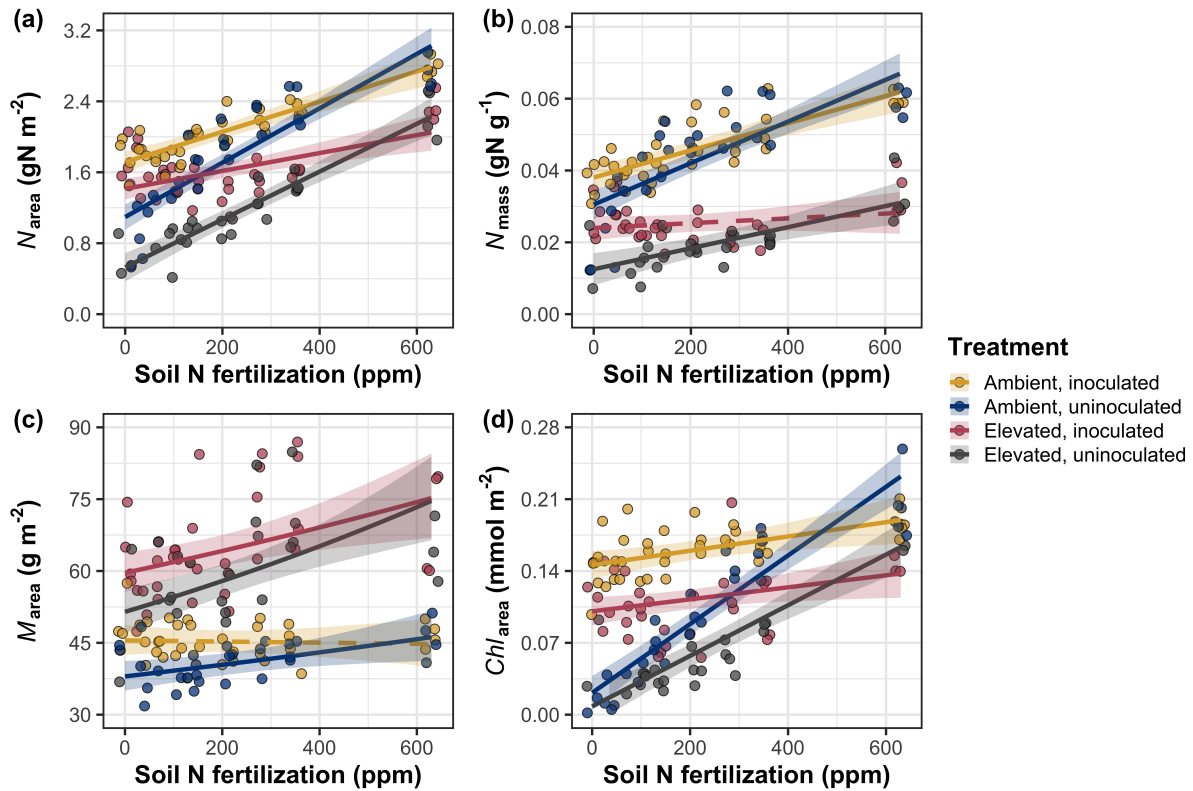


**Figure 5.1.** Effects of CO<sub>2</sub>, fertilization, and inoculation on leaf nitrogen per unit leaf area (a), leaf nitrogen content (b), leaf mass per unit leaf area (c), and chlorophyll content per unit leaf area (d). Soil nitrogen fertilization is represented on the x-axis in all panels. Yellow points and trendlines indicate inoculated individuals grown under ambient CO<sub>2</sub>, blue points and trendlines indicate uninoculated individuals grown under ambient CO<sub>2</sub>, red points and trendlines indicate inoculated individuals grown under elevated CO<sub>2</sub>, and grey points indicate uninoculated individuals grown under elevated CO<sub>2</sub>. Solid trendlines indicate regression slopes that are different from zero ( $p < 0.05$ ), while dashed trendlines indicate slopes that are not distinguishable from zero ( $p > 0.05$ ).

**1803** 5.3.2 *Leaf biochemistry and stomatal conductance*

**1804** Elevated CO<sub>2</sub> resulted in plants with 16% lower  $V_{cmax25}$  ( $p < 0.001$ ; Table  
**1805** 2) and 10% lower  $J_{max25}$  ( $p = 0.014$ ; Table 2) as compared to those grown un-  
**1806** der ambient CO<sub>2</sub>, but did not influence  $R_{d25}$  ( $p = 0.613$ ; Table 2). A relatively  
**1807** stronger downregulation in  $V_{cmax25}$  than  $J_{max25}$  resulted in an 8% stimulation in  
**1808**  $J_{max25}:V_{cmax25}$  under elevated CO<sub>2</sub> ( $p < 0.001$ ; Table 2; Fig. 2E). The downregu-  
**1809** latory effect of CO<sub>2</sub> on  $V_{cmax25}$  and  $J_{max25}$  was not modified across the fertilization  
**1810** gradient (CO<sub>2</sub>-by-fertilization interaction:  $p = 0.185$ ,  $p = 0.389$  for  $V_{cmax25}$  and  
**1811**  $J_{max25}$ , respectively; Table 2; Fig. 2A, 2C) or between inoculation treatments  
**1812** (CO<sub>2</sub>-by-inoculation interaction:  $p = 0.799$  and  $p = 0.714$  for  $V_{cmax25}$  and  $J_{max25}$ ,  
**1813** respectively; Table 2). However, a strong interaction between fertilization and  
**1814** inoculation (fertilization-by-inoculation interaction:  $p \leq 0.001$  in all cases; Table  
**1815** 2) indicated that the general positive effect of increasing fertilization on  $V_{cmax25}$  ( $p$   
**1816**  $< 0.001$ ; Table 2),  $J_{max25}$  ( $p < 0.001$ ; Table 2), and  $R_{d25}$  ( $p = 0.015$ ; Table 2) was  
**1817** only observed in uninoculated pots (Tukey:  $p \leq 0.001$  in all cases), as there was  
**1818** no apparent effect of fertilization on  $V_{cmax25}$  (Tukey:  $p = 0.456$ ),  $J_{max25}$  (Tukey:  $p$   
**1819** = 0.180), or  $R_{d25}$  (Tukey:  $p = 0.443$ ) in inoculated pots (Figs. 2B, 2D, 2F, 2H). A  
**1820** relatively stronger positive effect of increasing fertilization on  $V_{cmax25}$  than  $J_{max25}$   
**1821** resulted in a general reduction in  $J_{max25}:V_{cmax25}$  with increasing fertilization ( $p <$   
**1822** 0.001), though this pattern was only seen in uninoculated pots (Tukey:  $p = 0.003$ )  
**1823** and not inoculated plants (Tukey:  $p > 0.05$ ).

**1824** Elevated CO<sub>2</sub> reduced stomatal conductance by 20% ( $p < 0.001$ ; Table 2)  
**1825** compared to ambient CO<sub>2</sub>, but this downregulation did not influence stomatal  
**1826** limitation of photosynthesis ( $p = 0.355$ ; Table 2). As with  $V_{cmax25}$  and  $J_{max25}$ , the

1827 downregulation of stomatal conductance due to elevated CO<sub>2</sub> was not modified  
1828 across the fertilization gradient (CO<sub>2</sub>-by-fertilization interaction:  $p = 0.141$ ; Table  
1829 2) or between inoculation treatments (CO<sub>2</sub>-by-inoculation interaction:  $p = 0.179$ ;  
1830 Table 2). Fertilization also did not modify the general null effect of CO<sub>2</sub> on stom-  
1831 atal limitation (CO<sub>2</sub>-by-fertilization interaction:  $p = 0.554$ ; Table 2), although  
1832 an interaction between CO<sub>2</sub> and inoculation (CO<sub>2</sub>-by-inoculation interaction:  $p$   
1833 = 0.043; Table 2) indicated that inoculation increased stomatal limitation un-  
1834 der ambient CO<sub>2</sub> (Tukey:  $p = 0.021$ ), but not under elevated CO<sub>2</sub> (Tukey:  $p$   
1835 > 0.999). An interaction between inoculation and fertilization on stomatal con-  
1836 ductance (fertilization-by-inoculation interaction:  $p < 0.001$ ; Table 2) indicated  
1837 that increasing fertilization increased stomatal conductance in uninoculated pots  
1838 (Tukey:  $p = 0.003$ ) but decreased stomatal conductance in inoculated pots (Tukey:  
1839  $p = 0.021$ ). The similar in magnitude, but opposite direction, trend in the effect of  
1840 increasing fertilization on stomatal conductance between inoculation treatments  
1841 likely drove a null general response of stomatal conductance to increasing fertil-  
1842 ization ( $p = 0.642$ ; Table 2).

**Table 5.2.** Effects of soil nitrogen fertilization, inoculation, and CO<sub>2</sub> on leaf biochemistry

	<i>V</i> <sub>cmax25</sub>			<i>J</i> <sub>max25</sub>			<i>R</i> <sub>d25</sub>			
	df	Coefficient	$\chi^2$	p	Coefficient	$\chi^2$	p	Coefficient	$\chi^2$	p
(Intercept)	-	4.36E+01	-	-	8.30E+01	-	-	1.69E+00	-	-
CO <sub>2</sub>	1	-7.05E+00	18.039	<0.001	-9.11E+00	6.042	0.014	4.53E-01	0.256	0.613
Inoculation (I)	1	5.87E+01	98.579	<0.001	9.62E+01	85.064	<0.001	1.04E+00	3.094	0.079
Fertilization (N)	1	1.32E-01	37.053	<0.001	2.09E-01	25.356	<0.001	2.86E-03	5.965	0.015
CO <sub>2</sub> *I	1	-4.65E+00	0.065	0.799	7.84E-01	0.667	0.414	-5.71E-01	2.563	0.109
CO <sub>2</sub> *N	1	-3.58E-02	1.758	0.185	-4.33E-02	0.742	0.389	-1.55E-03	2.675	0.102
I*N	1	-1.35E-01	60.394	<0.001	-2.30E-01	57.410	<0.001	-2.84E-03	12.083	0.001
CO <sub>2</sub> *I*N	1	2.73E-02	0.748	0.387	3.46E-02	0.377	0.539	7.21E-04	0.244	0.622

119

	<i>J</i> <sub>max25</sub> : <i>V</i> <sub>cmax25</sub>			<i>g</i> <sub>sw</sub>			Stomatal limitation			
	df	Coefficient	$\chi^2$	p	Coefficient	$\chi^2$	p	Coefficient	$\chi^2$	p
(Intercept)	-	1.92E+00	-	-	1.95E-01	-	-	2.12E-01	-	-
CO <sub>2</sub>	1	5.71E-02	92.010	<0.001	-6.23E-02	9.718	0.002	3.91E-02	0.856	0.355
Inoculation (I)	1	-1.79E-01	27.768	<0.001	1.30E-01	22.351	<0.001	7.87E-02	4.582	0.032
Fertilization (N)	1	-4.61E-04	28.147	<0.001	2.50E-04	0.066	0.797	2.60E-04	32.218	<0.001
CO <sub>2</sub> *I	1	8.94E-02	2.916	0.088	6.69E-02	1.810	0.179	-7.84E-02	4.093	0.043
CO <sub>2</sub> *N	1	2.35E-04	3.210	0.073	-8.50E-05	2.165	0.141	-1.24E-04	0.350	0.554
I*N	1	3.27E-04	9.607	0.002	-3.09E-04	14.696	<0.001	-1.67E-04	2.547	0.110
CO <sub>2</sub> *I*N	1	-1.66E-04	1.102	0.294	-8.89E-05	0.234	0.629	1.67E-04	2.231	0.135

\*Significance determined using Type II Wald  $\chi^2$  tests ( $\alpha = 0.05$ ). P-values < 0.05 are in bold, while p-values between 0.05 and 0.1 are italicized. Key: *V*<sub>cmax25</sub> – maximum rate of Rubisco carboxylation at 25°C; *J*<sub>max25</sub> – maximum rate of electron transport for RuBP regeneration at 25°C, *R*<sub>d25</sub> - dark respiration at 25°C; *J*<sub>max25</sub>:*V*<sub>cmax25</sub> – the ratio of *J*<sub>max25</sub> to *V*<sub>cmax25</sub>; *g*<sub>sw</sub> - stomatal conductance.

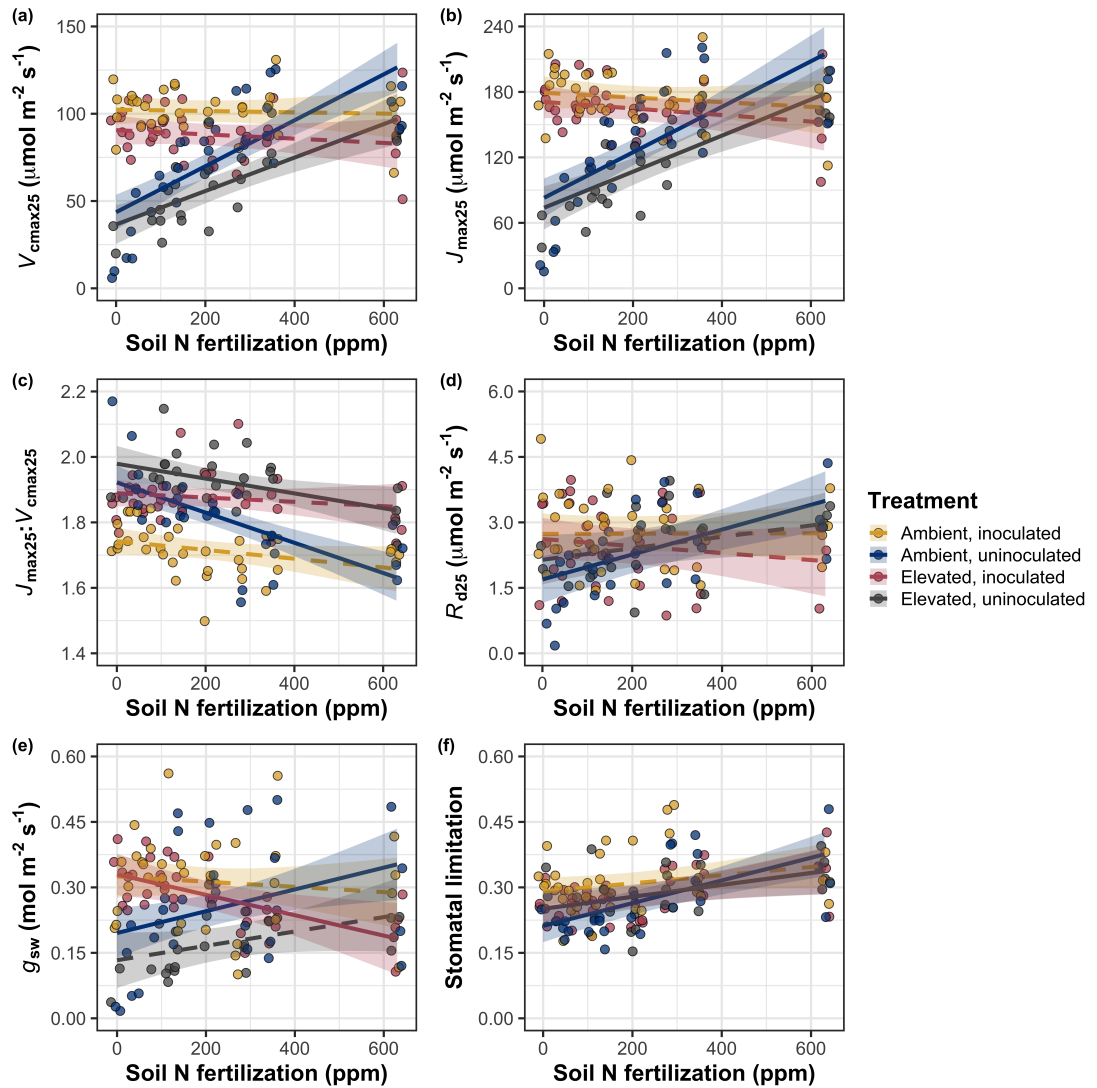


**Figure 5.2.** Effects of CO<sub>2</sub>, fertilization, and inoculation on maximum rate of Rubisco carboxylation (a), the maximum rate of RuBP regeneration (b), and the ratio of the maximum rate of RuBP regeneration to the maximum rate of Rubisco carboxylation leaf mass per unit leaf area (c), dark respiration (d), stomatal conductance (e), and stomatal limitation (f). Soil nitrogen fertilization is represented on the x-axis in all panels. Colored points and trendlines are as explained in Figure 1.

**1843** 5.3.3 *Leaf nitrogen allocation*

**1844** A relatively stronger downregulation in  $N_{\text{area}}$  than  $V_{\text{cmax25}}$  or  $J_{\text{max25}}$  resulted  
**1845** in an 20% and 29% respective stimulation in  $\rho_{\text{rubisco}}$  and  $\rho_{\text{bioe}}$  under elevated CO<sub>2</sub>  
**1846** ( $p < 0.001$  in both cases; Table 3). There was no apparent CO<sub>2</sub> effect on  $\rho_{\text{light}}$   
**1847** ( $p = 0.700$ ; Table 3), but the strong stimulation in  $\rho_{\text{rubisco}}$  and  $\rho_{\text{bioe}}$  resulted  
**1848** in a 21% stimulation of  $\rho_{\text{photo}}$  under elevated CO<sub>2</sub> ( $p < 0.001$ ; Table 3; Fig.  
**1849** 3A). The stimulation of  $\rho_{\text{rubisco}}$ ,  $\rho_{\text{bioe}}$ , and  $\rho_{\text{photo}}$  due to elevated CO<sub>2</sub> was not  
**1850** modified across the fertilization gradient (CO<sub>2</sub>-by-fertilization interaction:  $p_{\text{rubisco}}$   
**1851** = 0.269,  $p_{\text{bioe}} = 0.298$ ,  $p_{\text{photo}} = 0.281$ ; Table 3). A marginal interaction between  
**1852** inoculation and CO<sub>2</sub> on  $\rho_{\text{rubisco}}$  and  $\rho_{\text{photo}}$  (CO<sub>2</sub>-by-inoculation interaction:  $p_{\text{rubisco}}$   
**1853** = 0.057,  $p_{\text{photo}} = 0.057$ ; Table 3) indicated that the general positive effect of  
**1854** inoculation on  $\rho_{\text{rubisco}}$  and  $\rho_{\text{photo}}$  ( $p < 0.001$  in both cases; Table 3) was only  
**1855** apparent under ambient CO<sub>2</sub> (Tukey:  $p < 0.001$  in both cases), with no apparent  
**1856** effect of inoculation under elevated CO<sub>2</sub> (Tukey<sub>rubisco</sub>:  $p = 0.200$ ; Tukey<sub>photo</sub>:  $p$   
**1857** = 0.147). Inoculation did not modify the stimulation of  $\rho_{\text{bioe}}$  under elevated CO<sub>2</sub>  
**1858** (CO<sub>2</sub>-by-inoculation interaction:  $p = 0.122$ ; Table 3) or the null effect of CO<sub>2</sub> on  
**1859**  $\rho_{\text{bioe}}$  (CO<sub>2</sub>-by-inoculation interaction:  $p = 0.298$ ; Table 3). Strong interactions  
**1860** between fertilization and inoculation on  $\rho_{\text{rubisco}}$ ,  $\rho_{\text{bioe}}$ , and  $\rho_{\text{photo}}$  (fertilization-  
**1861** by-inoculation interaction:  $p < 0.001$  in all cases; Table 3) indicated that the  
**1862** general negative effect of increasing fertilization ( $p < 0.001$  in all cases; Table  
**1863** 3) was only observed in inoculated pots (Tukey:  $p < 0.001$  in all cases), with  
**1864** no apparent effect of fertilization on  $\rho_{\text{rubisco}}$  (Tukey:  $p = 0.612$ ),  $\rho_{\text{bioe}}$  (Tukey:  
**1865**  $p = 0.544$ ), or  $\rho_{\text{photo}}$  (Tukey:  $p = 0.521$ ; Fig 3B) in uninoculated pots. An  
**1866** additional interaction between fertilization and inoculation on  $\rho_{\text{light}}$  (fertilization-

1867 by-inoculation interaction:  $p < 0.001$ ; Table 3) indicated a negative effect of  
1868 increasing fertilization on  $\rho_{\text{light}}$  in inoculated pots (Tukey:  $p = 0.041$ ), but a  
1869 positive effect of increasing fertilization in uninoculated pots (Tukey:  $p < 0.001$ ).

1870 The stimulation in  $M_{\text{area}}$  resulted in an 133% stimulation of  $\rho_{\text{structure}}$  under  
1871 elevated CO<sub>2</sub> ( $p < 0.001$ ; Table 3; Fig 3C). An interaction between fertilization  
1872 and CO<sub>2</sub> (CO<sub>2</sub>-by-fertilization interaction:  $p = 0.039$ ; Table 3) indicated that the  
1873 general negative effect of increasing fertilization ( $p < 0.001$ ; Table 3) on  $\rho_{\text{structure}}$   
1874 was marginally stronger under ambient CO<sub>2</sub> (Tukey:  $p = 0.055$ ), resulting in a  
1875 stronger stimulation in  $\rho_{\text{structure}}$  under elevated CO<sub>2</sub> with increasing fertilization.  
1876 A marginal interaction between inoculation and CO<sub>2</sub> (CO<sub>2</sub>-by-inoculation inter-  
1877 action:  $p = 0.057$ ; Table 3) indicated that the general positive effect of inoculation  
1878 on  $\rho_{\text{structure}}$  ( $p < 0.001$ ; Table 3) was only observed under elevated CO<sub>2</sub> (Tukey:  
1879  $p < 0.001$ ), with no apparent inoculation effect observed under ambient CO<sub>2</sub>  
1880 (Tukey:  $p = 0.513$ ). Finally, an interaction between fertilization and inoculation  
1881 (fertilization-by-inoculation interaction:  $p < 0.001$ ; Table 3; Fig. 3D) indicated  
1882 that, while increasing fertilization generally increased  $\rho_{\text{structure}}$  ( $p < 0.001$ ; Table  
1883 3), this response was generally stronger in uninoculated pots (Tukey:  $p = 0.001$ ).

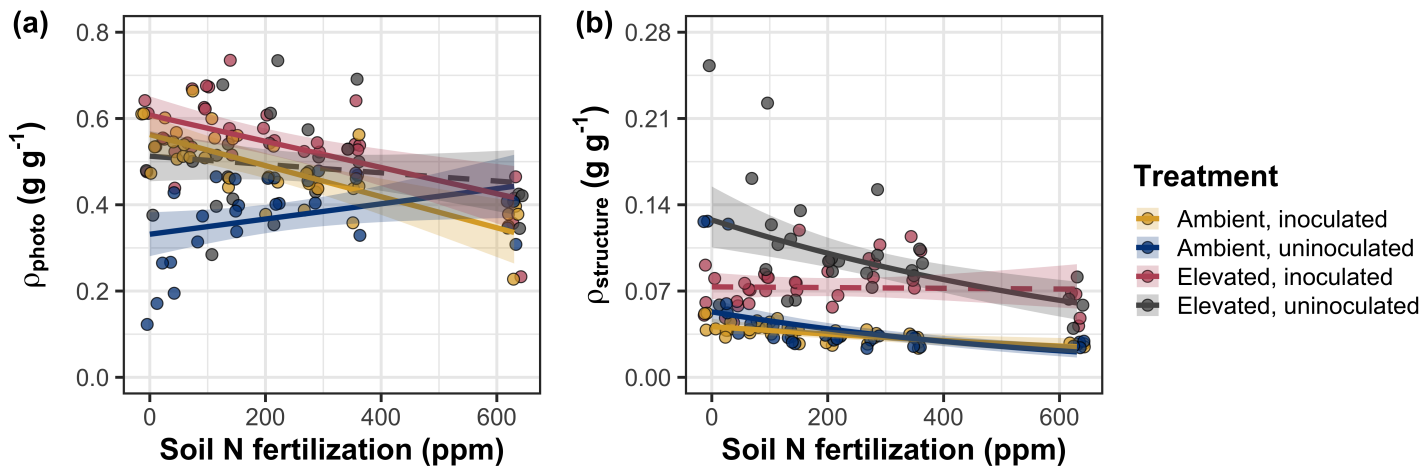
**Table 5.3.** Effects of soil N availability, soil pH, species, and  $N_{\text{area}}$  on leaf nitrogen allocation

	$\rho_{\text{rubisco}}$			$\rho_{\text{bioe}}$			$\rho_{\text{light}}$			
	df	Coefficient	$\chi^2$	p	Coefficient	$\chi^2$	p	Coefficient	$\chi^2$	p
(Intercept)	-	2.70E-01	-	-	5.26E-02	-	-	8.48E-03	-	-
CO <sub>2</sub>	1	1.42E-01	23.510	<b>&lt;0.001</b>	3.00E-02	53.899	<b>&lt;0.001</b>	2.03E-03	0.149	0.700
Inoculation (I)	1	1.83E-01	23.475	<b>&lt;0.001</b>	2.80E-02	13.860	<b>&lt;0.001</b>	2.04E-02	147.234	<b>&lt;0.001</b>
Fertilization (N)	1	1.35E-04	16.609	<b>&lt;0.001</b>	1.22E-05	26.827	<b>&lt;0.001</b>	3.22E-05	19.378	<b>&lt;0.001</b>
CO <sub>2</sub> *I	1	-1.07E-01	3.629	<i>0.057</i>	-1.67E-02	2.390	0.122	-5.33E-03	0.684	0.408
CO <sub>2</sub> *N	1	-2.16E-04	1.223	<i>0.269</i>	-3.59E-05	1.085	0.298	-7.01E-06	0.351	0.553
I*N	1	-4.26E-04	20.045	<b>&lt;0.001</b>	-6.87E-05	15.458	<b>&lt;0.001</b>	-4.37E-05	64.042	<b>&lt;0.001</b>
CO <sub>2</sub> *I*N	1	2.50E-04	3.327	<i>0.068</i>	4.08E-05	2.651	0.103	1.74E-05	3.735	<i>0.053</i>

	$\rho_{\text{photo}}$			$\rho_{\text{structure}}^a$			
	df	Coefficient	$\chi^2$	p	Coefficient	$\chi^2$	p
(Intercept)	-	3.32E-01	-	-	-2.93E+00	-	-
CO <sub>2</sub>	1	1.81E-01	27.651	<b>&lt;0.001</b>	8.77E-01	229.571	<b>&lt;0.001</b>
Inoculation (I)	1	2.31E-01	26.238	<b>&lt;0.001</b>	-2.55E-01	13.872	<b>&lt;0.001</b>
Fertilization (N)	1	1.76E-04	15.899	<b>&lt;0.001</b>	-1.51E-03	38.128	<b>&lt;0.001</b>
CO <sub>2</sub> *I	1	-1.36E-01	3.671	<i>0.055</i>	-2.99E-01	3.622	<i>0.057</i>
CO <sub>2</sub> *N	1	-2.72E-04	1.163	<i>0.281</i>	3.14E-04	4.266	<b>0.039</b>
I*N	1	-5.37E-04	21.355	<b>&lt;0.001</b>	7.00E-04	11.025	<b>0.001</b>
CO <sub>2</sub> *I*N	1	3.29E-04	4.009	<b>0.045</b>	4.52E-04	0.669	0.413

\*Significance determined using Type II Wald  $\chi^2$  tests ( $\alpha = 0.05$ ). P-values  $< 0.05$  are in bold, while p-values between 0.05 and 0.1 are italicized. A superscript “a” is included after trait labels to indicate if models were fit with natural log transformed response variables. Key: df=degrees of freedom,  $\rho_{\text{rubisco}}$  = proportion of leaf N allocated to photosynthesis,  $\rho_{\text{bioe}}$  = proportion of leaf N allocated to bioenergetics,  $\rho_{\text{light}}$ =proportion of leaf N allocated to light harvesting proteins,  $\rho_{\text{photo}}$ =proportion of leaf N allocated to photosynthesis,  $\rho_{\text{structure}}$ =proportion of leaf N allocated to cell wall structural tissue



**Figure 5.3.** Effects of  $\text{CO}_2$ , fertilization, and inoculation on the relative fraction of leaf nitrogen allocated to photosynthesis (a) and the fraction of leaf nitrogen allocated to structure (b). Soil nitrogen fertilization is represented on the x-axis in both panels. Colored points and trendlines are as explained in Figure 1.

**1884** 5.3.4 *Whole plant growth and total leaf area*

**1885** Total leaf area was 51% greater and total biomass was 102% greater un-  
**1886** der elevated CO<sub>2</sub> ( $p < 0.001$  in both cases; Table 4), a pattern that was en-  
**1887** hanced by fertilization (CO<sub>2</sub>-by-fertilization interaction:  $p < 0.001$  in both cases;  
**1888** Table 4; Fig. 4a-b) but was not modified across inoculation treatments (CO<sub>2</sub>-  
**1889** by-inoculation interaction:  $p_{total\_leaf\_area} = 0.151$ ,  $p_{total\_biomass} = 0.472$ ; Table 4).  
**1890** Specifically, the general positive effect of increasing fertilization on total leaf area  
**1891** and whole plant biomass ( $p < 0.001$  in both cases; Table 4) was stronger under  
**1892** elevated CO<sub>2</sub> (Tukey:  $p < 0.001$  in both cases). The general positive effect of  
**1893** increasing fertilization on total leaf area was modified by inoculation treatment  
**1894** (fertilization-by-inoculation interaction:  $p < 0.001$  in both cases; Table 4), in-  
**1895** dicating a stronger positive effect of increasing fertilization in uninoculated pots  
**1896** (Tukey:  $p_{total\_leaf\_area} = 0.002$ ,  $p_{total\_biomass} = 0.001$ ).

**1897** 5.3.5 *Carbon costs to acquire nitrogen*

**1898** A general 62% stimulation in  $N_{cost}$  under elevated CO<sub>2</sub> was modified thr-  
**1899** ough a strong three-way interaction between CO<sub>2</sub>, fertilization, and inoculation  
**1900** (CO<sub>2</sub>-by-inoculation-by-fertilization interaction:  $p < 0.001$ ; Table 4). This in-  
**1901** teraction revealed a general negative effect of increasing fertilization on  $N_{cost}$  ( $p$   
**1902**  $< 0.001$ ; Table 4) that was observed in all treatment combinations (Tukey:  $p <$   
**1903** 0.001 in all cases) except for inoculated pots grown under elevated CO<sub>2</sub> (Tukey:  
**1904**  $p = 0.779$ ; Fig. 5c). This response also resulted in generally stronger negative ef-  
**1905** ffects of increasing fertilization on  $N_{cost}$  in uninoculated pots grown under elevated  
**1906** CO<sub>2</sub> than uninoculated pots grown under ambient CO<sub>2</sub> (Tukey:  $p = 0.001$ ) and

1907 inoculated pots grown under either ambient CO<sub>2</sub> (Tukey:  $p < 0.001$ ) or elevated  
1908 CO<sub>2</sub> (Tukey:  $p < 0.001$ ), while uninoculated pots grown under ambient CO<sub>2</sub> had  
1909 generally stronger negative effects of increasing fertilization on  $N_{\text{cost}}$  than inocu-  
1910 lated pots grown under elevated CO<sub>2</sub> (Tukey:  $p = 0.002$ ), but not inoculated pots  
1911 grown under ambient CO<sub>2</sub> (Tukey:  $p = 0.216$ ). The general reduction in  $N_{\text{cost}}$   
1912 with increasing fertilization and in uninoculated pots were driven by a stronger  
1913 positive effect of increasing fertilization on  $N_{\text{wp}}$  (denominator of  $N_{\text{cost}}$ ) than  $C_{\text{bg}}$   
1914 (numerator of  $N_{\text{cost}}$ ), while the general stimulation in  $N_{\text{cost}}$  under elevated CO<sub>2</sub>  
1915 was driven by a stronger positive effect of elevated CO<sub>2</sub> on  $C_{\text{bg}}$  than  $N_{\text{wp}}$  (Table  
1916 4).

**Table 5.4.** Effects of soil N availability, soil pH, species, and  $N_{\text{area}}$  on total leaf area, whole plant biomass, and costs of nitrogen acquisition

	Total leaf area			Total biomass			$N_{\text{cost}}$			
	df	Coefficient	$\chi^2$	p	Coefficient	$\chi^2$	p	Coefficient	$\chi^2$	p
(Intercept)	-	8.78E+01	-	-	9.96E-01	-	-	8.67E+00	-	-
$\text{CO}_2$	1	3.36E+01	69.291	<0.001	5.07E-01	131.477	<0.001	8.75E+00	88.189	<0.001
Inoculation (I)	1	1.88E+02	35.715	<0.001	7.96E-01	34.264	<0.001	-1.68E+00	136.343	<0.001
Fertilization (N)	1	9.35E-01	274.199	<0.001	3.14E-03	269.046	<0.001	-8.50E-03	80.501	<0.001
$\text{CO}_2 * \text{I}$	1	6.44E+01	2.064	0.151	-7.69E-02	0.518	0.472	-8.38E+00	85.237	<0.001
$\text{CO}_2 * \text{N}$	1	5.05E-01	18.655	<0.001	1.61E-03	16.877	<0.001	-9.17E-03	1.050	0.306
$\text{I} * \text{N}$	1	-3.84E-01	10.804	0.001	-1.45E-03	15.779	<0.001	4.20E-03	46.489	<0.001
$\text{CO}_2 * \text{I} * \text{N}$	1	-2.97E-03	<0.001	0.990	-1.14E-04	0.023	0.880	1.32E-02	18.125	<0.001

	$C_{\text{bg}}$			$N_{\text{wp}}$			
	df	Coefficient	$\chi^2$	p	Coefficient	$\chi^2$	p
(Intercept)	-	-1.70E+00	-	-	1.24E-01	-	-
$\text{CO}_2$	1	9.21E-01	84.134	<0.001	-3.41E-03	23.890	<0.001
Inoculation (I)	1	1.18E+00	41.030	<0.001	1.68E-01	134.460	<0.001
N fertilization (N)	1	3.38E-03	152.248	<0.001	6.69E-04	529.021	<0.001
$\text{CO}_2 * \text{I}$	1	-6.18E-01	8.965	0.003	3.68E-02	1.190	0.275
$\text{CO}_2 * \text{N}$	1	-3.66E-05	1.188	0.276	1.58E-04	5.915	0.015
$\text{I} * \text{N}$	1	-2.22E-03	22.648	<0.001	-3.20E-04	55.562	<0.001
$\text{CO}_2 * \text{I} * \text{N}$	1	8.09E-04	1.109	0.292	-7.54E-05	0.620	0.431

\*Significance determined using Type II Wald  $\chi^2$  tests ( $\alpha = 0.05$ ). P-values  $< 0.05$  are in bold, while p-values between 0.05 and 0.1 are italicized. A superscript “a” after trait labels indicates if models were fit using natural log transformed response variables, while a superscript “b” indicates if models were fit using square root transformed variables. Key: df=degrees of freedom

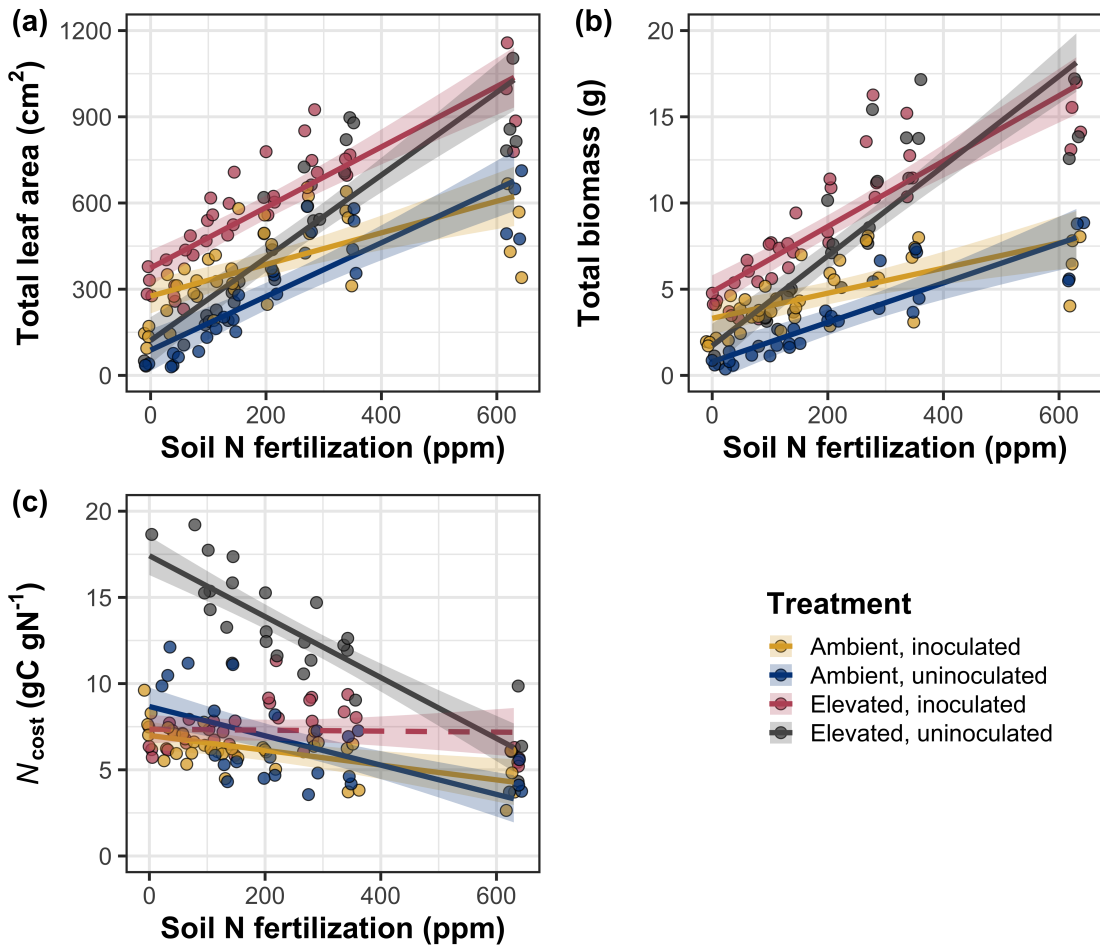


**Figure 5.4.** Effects of  $\text{CO}_2$ , fertilization, and inoculation on total leaf area (a), total biomass (b), and structural carbon costs to acquire nitrogen (c). Soil nitrogen fertilization is represented continuously on the x-axis in all panels. Colored points and trendlines are as explained in Figure 1.

**1917** 5.3.6 *Nitrogen fixation*

**1918** Nodule biomass was stimulated by 30% under elevated CO<sub>2</sub> ( $p < 0.001$ ;  
**1919** Table 5), a pattern that was modified across the fertilization gradient (CO<sub>2</sub>-by-  
**1920** fertilization interaction:  $p = 0.479$ ; Table 5), but not between inoculation treat-  
**1921** ments (CO<sub>2</sub>-by-inoculation interaction:  $p = 0.404$ ; Table 5). Specifically, the  
**1922** general negative effect of increasing fertilization on nodule biomass ( $p < 0.001$ ;  
**1923** Table 5) was stronger under elevated CO<sub>2</sub> than ambient CO<sub>2</sub> (Tukey:  $p < 0.001$ ;  
**1924** Fig. 5a), which reduced the stimulation in nodule biomass under elevated CO<sub>2</sub>  
**1925** with increasing fertilization. A strong interaction between fertilization and inocu-  
**1926** lation (fertilization-by-inoculation interaction:  $p < 0.001$ ; Table 5) was driven by  
**1927** a stronger negative effect of increasing fertilization in inoculated pots (Tukey:  $p$   
**1928**  $< 0.001$ ; Fig. 5a).

**1929** There was no effect of CO<sub>2</sub> on nodule: root biomass ( $p = 0.767$ ; Table 5),  
**1930** although an interaction between CO<sub>2</sub> and inoculation (CO<sub>2</sub>-by-inoculation inter-  
**1931** action:  $p < 0.001$ ; Table 5) indicated that the general positive effect of inoculation  
**1932** on nodule: root biomass ( $p < 0.001$ ; Table 5) was stronger under ambient CO<sub>2</sub>  
**1933** (3129% increase; Tukey:  $p < 0.001$ ) than elevated CO<sub>2</sub> (379% increase; Tukey:  
**1934**  $p < 0.001$ ; Fig. 5b). The null effect of CO<sub>2</sub> on nodule: root biomass was con-  
**1935** sistently observed across the fertilization gradient ( $p = 0.183$ ; Table 5; Fig. 5b).  
**1936** An interaction between fertilization and inoculation (fertilization-by-inoculation  
**1937** interaction:  $p < 0.001$ ; Table 5) indicated that the general negative effect of in-  
**1938** creasing fertilization on nodule: root biomass ( $p < 0.001$ ; Table 5) was stronger  
**1939** in inoculated pots (Tukey:  $p < 0.001$ ; Fig. 5b).

**1940** There was no effect of CO<sub>2</sub> on %N<sub>dfa</sub> ( $p = 0.472$ ; Table 5), a pattern

1941 that was not modified by inoculation ( $\text{CO}_2$ -by-inoculation interaction:  $p = 0.156$ ;  
1942 Table 5) or fertilization ( $\text{CO}_2$ -by-fertilization interaction:  $p = 0.099$ ; Table 5).  
1943 An interaction between fertilization and inoculation (fertilization-by-inoculation  
1944 interaction:  $p < 0.001$ ; Table 5) indicated that the general negative effect of  
1945 increasing fertilization on  $\%N_{dfa}$  ( $p < 0.001$ ; Table 5) was only observed in inoc-  
1946 ulated pots (Tukey:  $p < 0.001$ ), with no apparent effect of fertilization on  $\%N_{dfa}$   
1947 in uninoculated pots (Tukey:  $p = 0.651$ ; Table 5; Fig. 5c).

**Table 5.5.** Effects of soil N availability, soil pH, species, and  $N_{\text{area}}$  on leaf biochemistry

	df	Root nodule biomass <sup>b</sup>			Root nodule: root biomass <sup>b</sup>			% $N_{\text{dfa}}^b$		
		Coefficient	$\chi^2$	p	Coefficient	$\chi^2$	p	Coefficient	$\chi^2$	p
(Intercept)	-	9.41E-03	-	-	1.33E-02	-	-	7.48E-01	-	-
CO <sub>2</sub>	1	1.20E-01	19.258	<b>&lt;0.001</b>	9.94E-02	0.087	0.768	-1.00E-01	0.518	0.472
Inoculation (I)	1	5.74E-01	755.020	<b>&lt;0.001</b>	5.40E-01	903.691	<b>&lt;0.001</b>	9.01E+00	955.570	<b>&lt;0.001</b>
Fertilization (N)	1	7.71E-06	84.376	<b>&lt;0.001</b>	-5.99E-06	258.099	<b>&lt;0.001</b>	3.64E-04	292.938	<b>&lt;0.001</b>
CO <sub>2</sub> *I	1	-4.68E-02	0.950	0.330	-1.38E-01	20.614	<b>&lt;0.001</b>	-1.44E-01	2.010	0.156
CO <sub>2</sub> *N	1	-1.59E-04	2.106	0.147	-1.73E-04	1.773	0.183	-6.21E-05	2.716	0.099
I*N	1	-5.82E-04	44.622	<b>&lt;0.001</b>	-7.45E-04	133.918	<b>&lt;0.001</b>	-1.58E-02	231.290	<b>&lt;0.001</b>
CO <sub>2</sub> *I*N	1	7.26E-05	0.196	0.658	1.76E-04	2.359	0.125	2.77E-03	2.119	0.145

\*Significance determined using Type II Wald  $\chi^2$  tests ( $\alpha = 0.05$ ). P-values  $< 0.05$  are in bold, while p-values between 0.05 and 0.1 are italicized. Superscript letters indicate model coefficients fit to square-root (<sup>b</sup>) transformed data. Key: % $N_{\text{dfa}}$ =percent nitrogen fixed from the atmosphere.

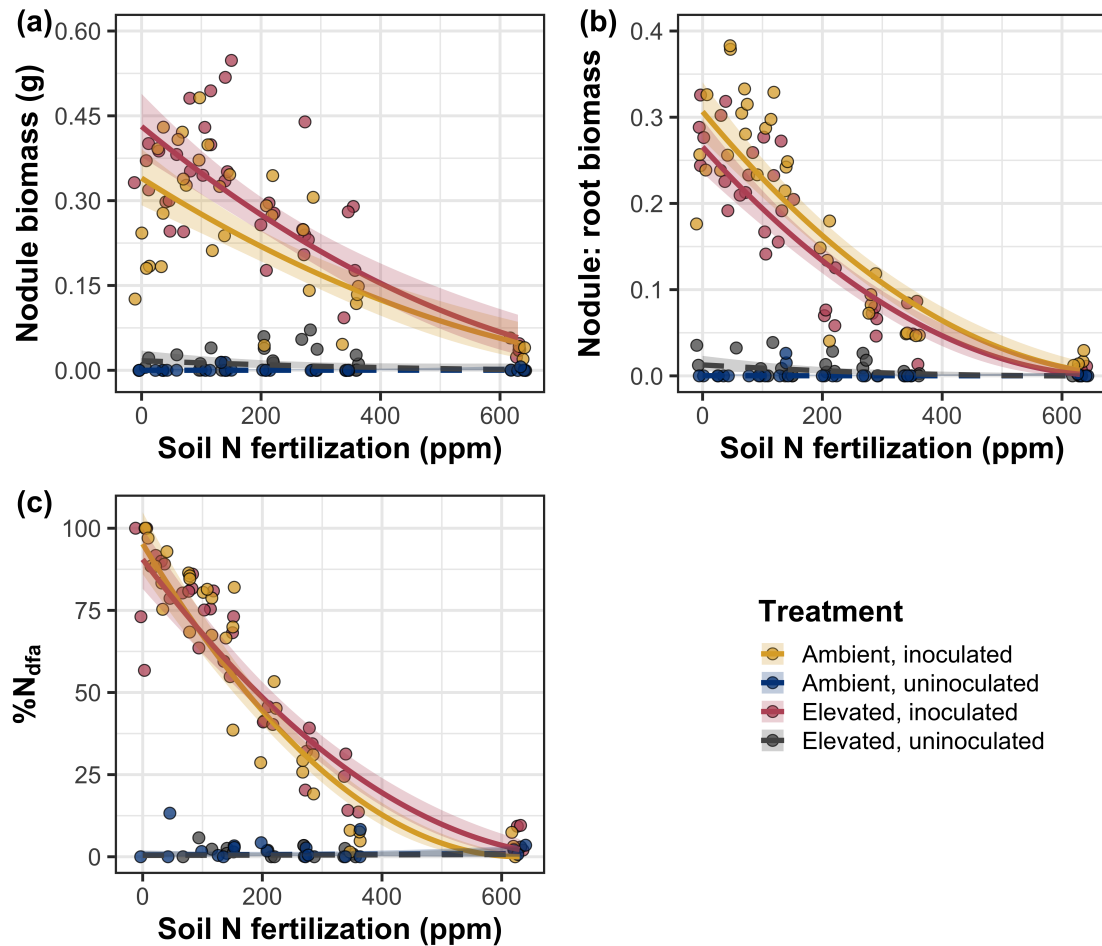


**Figure 5.5.** Effects of  $\text{CO}_2$ , fertilization, and inoculation on nodule biomass (a), nodule: root biomass (b), and percent nitrogen fixed from the atmosphere (c). Soil nitrogen fertilization is represented on the x-axis. Yellow points and trendlines indicate inoculated individuals grown under ambient  $\text{CO}_2$ , blue points and trendlines indicate uninoculated individuals grown under ambient  $\text{CO}_2$ , red points and trendlines indicate inoculated individuals grown under elevated  $\text{CO}_2$ , and grey points indicate uninoculated individuals grown under elevated  $\text{CO}_2$ . Solid trendlines indicate slopes that are different from zero ( $p < 0.05$ ), while dashed trendlines indicate slopes that are not different from zero ( $p > 0.05$ ). Curvilinear trendlines occur as a result of back-transforming models where response variables received either a natural log or square root transformation prior to fitting.

**1948** 5.4 Discussion

**1949** In this study, we determined leaf and whole plant acclimation responses of  
**1950** 7-week *G. max* seedlings grown under two CO<sub>2</sub> concentrations, two inoculation  
**1951** treatments, and nine soil nitrogen fertilization treatments in a full-factorial growth  
**1952** chamber experiment. In support of our hypotheses and patterns expected from  
**1953** theory, elevated CO<sub>2</sub> reduced  $N_{\text{area}}$ ,  $V_{\text{cmax25}}$ , and  $J_{\text{max25}}$ . The relatively stronger  
**1954** downregulation in  $V_{\text{cmax25}}$  than  $J_{\text{max25}}$  under elevated CO<sub>2</sub> resulted in a stimu-  
**1955** lation in  $J_{\text{max25}}:V_{\text{cmax25}}$  under elevated CO<sub>2</sub>. The downregulation of  $V_{\text{cmax25}}$  and  
**1956**  $J_{\text{max25}}$  under elevated CO<sub>2</sub> was similar across fertilization and inoculation treat-  
**1957** ments, indicating that the CO<sub>2</sub> responses were not due to nitrogen limitation.  
**1958** Interestingly, our results indicate that elevated CO<sub>2</sub> increased the fraction of leaf  
**1959** nitrogen allocated to photosynthesis and structure, leading to a stimulation in  
**1960** nitrogen use efficiency under elevated CO<sub>2</sub> despite the apparent downregulation  
**1961** in  $N_{\text{area}}$ ,  $V_{\text{cmax25}}$ , and  $J_{\text{max25}}$ . The downregulation in leaf photosynthetic processes  
**1962** under elevated CO<sub>2</sub> also corresponded with a strong stimulation in total leaf area  
**1963** and total biomass. Strong stimulations in whole plant growth due to elevated CO<sub>2</sub>  
**1964** were generally enhanced with increasing fertilization and were negatively related  
**1965** to structural carbon costs to acquire nitrogen. Inoculation generally did not mod-  
**1966** ify whole plant responses to elevated CO<sub>2</sub> across the fertilization gradient, likely  
**1967** due to a strong reduction in root nodulation with increasing fertilization. However,  
**1968** strong positive effects of inoculation on whole plant growth were observed under  
**1969** low fertilization, consistent with our hypothesis. Overall, observed leaf and whole  
**1970** plant acclimation responses to CO<sub>2</sub> support our hypotheses and patterns expected  
**1971** from photosynthetic least-cost theory, showing that leaf acclimation responses to

1972 CO<sub>2</sub> were decoupled from soil nitrogen availability and ability to acquire nitro-  
1973 gen via symbiotic nitrogen fixation. Instead, leaf and whole plant acclimation  
1974 responses to CO<sub>2</sub> were driven by optimal resource investment to photosynthetic  
1975 capacity, where optimal resource investment at the leaf level maximized nitrogen  
1976 allocation to structures that support whole plant growth.

1977 5.4.1 *Soil nitrogen fertilization has divergent effects on leaf and whole plant  
1978 acclimation responses to CO<sub>2</sub>*

1979 Elevated CO<sub>2</sub> reduced  $N_{\text{area}}$ ,  $V_{\text{cmax25}}$ ,  $J_{\text{max25}}$ , and stomatal conductance by  
1980 29%, 16%, 10%, and 20%, respectively (Table 5.2). The larger downregulation in  
1981  $V_{\text{cmax25}}$  than  $J_{\text{max25}}$  led to an 8% stimulation in  $J_{\text{max25}}:V_{\text{cmax25}}$  (Table 5.2), while  
1982 the larger downregulation in  $N_{\text{area}}$  than  $V_{\text{cmax25}}$  resulted in a 21% stimulation  
1983 in the fraction of leaf nitrogen allocated to photosynthesis under elevated CO<sub>2</sub>.  
1984 These acclimation responses are directionally consistent with previous studies that  
1985 have investigated or reviewed leaf acclimation responses to CO<sub>2</sub> (Drake et al.  
1986 1997; Makino et al. 1997; Ainsworth et al. 2002; Ainsworth and Long 2005;  
1987 Ainsworth and Rogers 2007; Smith and Dukes 2013; Smith and Keenan 2020;  
1988 Poorter et al. 2022), and follow patterns expected from photosynthetic least-cost  
1989 theory (Wright et al. 2003; Prentice et al. 2014; Smith et al. 2019; Smith and  
1990 Keenan 2020). Together, the stimulation in  $J_{\text{max25}}:V_{\text{cmax25}}$  and the fraction of leaf  
1991 nitrogen allocated to photosynthesis, and nitrogen use efficiency under elevated  
1992 CO<sub>2</sub> provide strong support for the idea that leaves were downregulating  $V_{\text{cmax25}}$   
1993 in response to elevated CO<sub>2</sub> in order to optimally coordinate photosynthesis such  
1994 that net photosynthesis rates approached becoming equally co-limited by Rubisco

**1995** carboxylation and RuBP regeneration (Chen et al. 1993; Maire et al. 2012).

**1996** Increasing fertilization and inoculation induced strong positive effects on

**1997**  $N_{\text{area}}$  (Fig. 1a),  $V_{\text{cmax}25}$  (Fig. 5.2a),  $J_{\text{max}25}$  (Fig. 5.2b). The general positive

**1998** response of  $N_{\text{area}}$  to increasing fertilization and in inoculated pots was enhanced

**1999** under ambient  $\text{CO}_2$ , which, paired with the general downregulation in  $N_{\text{area}}$  un-

**2000** der elevated  $\text{CO}_2$ , resulted in a stronger downregulation of  $N_{\text{area}}$  under elevated

**2001**  $\text{CO}_2$  with increasing fertilization and in inoculated pots (Fig. 5.1a). These pat-

**2002** terns suggest that  $N_{\text{area}}$  responses to  $\text{CO}_2$  were at least partially dependent on

**2003** soil nitrogen fertilization and nitrogen acquisition strategy. However, the general

**2004** stimulation in the fraction of leaf nitrogen allocated to Rubisco, bioenergetics,

**2005** or photosynthesis under elevated  $\text{CO}_2$  was not modified across the fertilization

**2006** gradient and was only marginally enhanced in inoculated pots. These patterns

**2007** suggest that the increased downregulation of  $N_{\text{area}}$  under elevated  $\text{CO}_2$  with in-

**2008** creasing fertilization was not associated with a change in relative investment to

**2009** photosynthetic tissue. Instead, a stronger downregulation in the fraction of leaf

**2010** nitrogen allocated to structure under ambient  $\text{CO}_2$  resulted in a stronger stim-

**2011** ulation in  $\rho_{\text{structure}}$  under elevated  $\text{CO}_2$  with increasing fertilization (Fig. 5.3b),

**2012** indicating that fertilization shifted relative investment in leaf structural tissue un-

**2013** der elevated  $\text{CO}_2$ . These results, combined with a stimulation in PNUE (Fig. SX)

**2014** and iWUE (Fig. SX) under elevated  $\text{CO}_2$  that was independent of fertilization

**2015** or inoculation treatment, provide additional support for the hypothesis that leaf

**2016** acclimation photosynthetic responses to  $\text{CO}_2$  were independent of fertilization;

**2017** though fertilization may contribute to changes in leaf morphology under elevated

**2018**  $\text{CO}_2$  through shifts in  $M_{\text{area}}$  (Onoda et al. 2017; Wang et al. 2017; Dong et al.

2019 2022).

2020 The downregulation in  $N_{\text{area}}$ ,  $V_{\text{cmax}25}$ , and  $J_{\text{max}25}$  under elevated CO<sub>2</sub> corresponded with a respective 62% and 100% stimulation in total leaf area (Fig. 5.4a) and total biomass (Fig. 5.4b). The stimulation in total leaf area and total biomass under elevated CO<sub>2</sub> also corresponded with generally higher structural carbon costs to acquire nitrogen (Fig. 5.4c), a pattern driven by a stimulation in belowground carbon biomass and reduction in whole plant nitrogen biomass. Alone, this result suggests that elevated CO<sub>2</sub> reduces plant nitrogen uptake efficiency, which does not explain why plants grown under elevated CO<sub>2</sub> generally had higher biomass and total leaf area. However, a strong negative effect of increasing fertilization on structural carbon costs to acquire nitrogen, which were generally similar between CO<sub>2</sub> concentrations, was driven by a stronger increase in whole plant nitrogen biomass than belowground carbon biomass. Thus, increases in the positive response of whole plant growth and total leaf area under elevated CO<sub>2</sub> with increasing fertilization were likely driven by an increase in nitrogen uptake efficiency, allowing plants to satisfy any increase in whole plant nitrogen demand associated with increased CO<sub>2</sub>.

2036 Interestingly, our results indicate that the general stimulation in total leaf area and whole plant growth under elevated CO<sub>2</sub> was not modified by inoculation despite an apparent general negative effect of inoculation on  $N_{\text{cost}}$ . This response could have been due to strong negative effect of increasing fertilization on nodulation (Fig. 5.5), which may have caused the strong increase in the positive effect of elevated CO<sub>2</sub> on whole plant growth with increasing fertilization to mask any increase in the positive effect of elevated CO<sub>2</sub> on whole plant growth due to in-

**2043** oculation. Reductions in nodulation with increasing fertilization are commonly  
**2044** observed patterns that have been inferred to be a response that allows species  
**2045** optimize nitrogen uptake efficiency as costs to acquire nitrogen via direct uptake  
**2046** become more similar (Fig. 5.4c) (Gibson and Harper 1985; Rastetter et al. 2001).  
**2047** In this study, pairwise comparisons indicated strong positive effects of inocula-  
**2048** tion on total leaf area and total biomass (158% increase in total leaf area, 119%  
**2049** increase in total biomass) under elevated CO<sub>2</sub> at 0 ppm N, but no observable  
**2050** inoculation effect on total leaf area or total biomass under elevated CO<sub>2</sub> at 350  
**2051** ppm N or 630 ppm N. While these responses did not generally differ from those  
**2052** observed under ambient CO<sub>2</sub>, they do confirm our hypothesis that positive effects  
**2053** of inoculation on whole plant growth responses to elevated CO<sub>2</sub> would decrease  
**2054** with increasing fertilization.

**2055** Combined, results reported here suggest that soil nitrogen availability has  
**2056** a divergent role in modifying leaf and whole plant acclimation responses to CO<sub>2</sub>.  
**2057** Leaf acclimation responses were generally decoupled from fertilization, while whole  
**2058** plant acclimation responses relied heavily on an increase in nitrogen uptake ef-  
**2059** ficiency and consequent reduction in costs of acquiring nitrogen associated with  
**2060** increasing fertilization. However, whole plant responses to CO<sub>2</sub> indicated that fer-  
**2061** tilization may play a more important role in determining whole plant acclimation  
**2062** responses to CO<sub>2</sub> than nitrogen acquisition strategy, although these patterns were  
**2063** likely driven by reductions in nodulation with increasing fertilization. Our results  
**2064** suggest that plants acclimate to CO<sub>2</sub> in nitrogen-limited systems by minimizing  
**2065** the number of optimally coordinated leaves, and that the downregulation in leaf  
**2066** nitrogen content under elevated CO<sub>2</sub> is not a direct response to changes in soil

**2067** nitrogen availability as previously implied.

**2068** 5.4.2 *Implications for future model development*

**2069** Many terrestrial biosphere models predict photosynthetic capacity through  
**2070** plant functional group-specific linear regressions between  $N_{\text{area}}$  and  $V_{\text{cmax}}$  (Rogers  
**2071** 2014; Rogers et al. 2017), which assumes that leaf nitrogen-photosynthesis rela-  
**2072** tionships are constant across growing environments. Our results build on previ-  
**2073** ous work suggesting that leaf nitrogen-photosynthesis relationships dynamically  
**2074** change across growing environments (Luo et al. 2021; Dong et al. 2022). Specif-  
**2075** ically, results from this experiment indicate that  $\text{CO}_2$  concentration increased  
**2076** the fraction of leaf nitrogen content allocated to photosynthesis, while a general  
**2077** negative effect of increasing fertilization on the fraction of leaf nitrogen content  
**2078** allocated to photosynthesis was dependent on inoculation treatment. Similar in-  
**2079** creases in  $N_{\text{area}}$ ,  $V_{\text{cmax}25}$ , and  $J_{\text{max}25}$  with increasing fertilization resulted in no  
**2080** change in the fraction of leaf nitrogen allocated to photosynthesis in uninoculated  
**2081** pots, while larger increases in  $N_{\text{area}}$  than  $V_{\text{cmax}25}$  and  $J_{\text{max}25}$  with increasing fertil-  
**2082** ization decreased the fraction of leaf nitrogen allocated to photosynthesis in inoc-  
**2083** ulated pots (Fig. 5.3a). As inoculated pots were able to access less finite supply of  
**2084** nitrogen across the fertilization gradient, these patterns suggest that constant leaf  
**2085** nitrogen-photosynthesis relationships may only apply in environments where ni-  
**2086** trogen is limiting and will likely change with increasing  $\text{CO}_2$  concentrations. Thus,  
**2087** terrestrial biosphere models that parameterize photosynthetic capacity through  
**2088** linear relationships between  $N_{\text{area}}$  and  $V_{\text{cmax}}$  (Rogers 2014; Rogers et al. 2017)  
**2089** may be overestimating photosynthetic capacity in systems where nitrogen is not

**2090** as limiting and may contribute to erroneous model simulations under future CO<sub>2</sub>  
**2091** concentrations.

**2092** Our results also demonstrate that optimal resource investment to photo-  
**2093** synthetic capacity defines leaf acclimation responses to elevated CO<sub>2</sub>, and that  
**2094** these responses were independent of fertilization or inoculation treatment. Cur-  
**2095** rent approaches for simulating photosynthetic responses to CO<sub>2</sub> generally invoke  
**2096** patterns expected from progressive nitrogen limitation, where the downregulation  
**2097** in  $N_{\text{area}}$ , and therefore photosynthetic capacity, due to elevated CO<sub>2</sub> are commonly  
**2098** a function of progressive reductions in soil nitrogen availability. Our results con-  
**2099** tradict this formulation, suggesting that the leaf acclimation response is driven  
**2100** by optimal resource investment to photosynthetic capacity and is independent  
**2101** of soil resource supply. Optimality models that leverage principles from optimal  
**2102** coordination and photosynthetic least-cost theories (Wang et al. 2017; Stocker  
**2103** et al. 2020; Scott and Smith 2022) are capable of capturing such acclimation re-  
**2104** sponses to CO<sub>2</sub> (Smith and Keenan 2020), suggesting that the implementation of  
**2105** these models may improve the simulation of photosynthetic processes in terrestrial  
**2106** biosphere models under increasing CO<sub>2</sub> concentrations.

**2107** 5.4.3 *Study limitations and future directions*

**2108** There are two study limitations that must be addressed to contextualize  
**2109** patterns observed in this study. First, restricting the volume of belowground  
**2110** substrate via a potted experiment does not adequately replicate belowground en-  
**2111** vironments of natural systems, and therefore may modify effects of soil resource  
**2112** availability and inoculation on plant nitrogen uptake, particularly if pot size limits

2113 whole plant growth (Poorter et al. 2012). We attempted to minimize the extent  
2114 of pot size limitation experienced in Perkowski et al. (2021) and account for the  
2115 expected stimulation in whole plant growth under elevated CO<sub>2</sub> by using 6-liter  
2116 pots. Despite attempts to minimize growth limitation imposed by pot volume, fer-  
2117 tilization and CO<sub>2</sub> treatments increased the biomass: pot volume ratio such that  
2118 all treatment combinations to exceed 1 g L<sup>-1</sup> biomass: pot volume under high  
2119 fertilization. The 1 g L<sup>-1</sup> biomass: pot volume recommendation from Poorter  
2120 et al. (2012) was designated to avoid growth limitation imposed by pot volume.  
2121 However, if pot size limitation indeed limited whole plant growth, then structural  
2122 carbon costs to acquire nitrogen, belowground carbon biomass, whole plant ni-  
2123 trogen biomass, and whole plant biomass should each exhibit strong saturation  
2124 points with increasing fertilization, which was not observed here. Additionally,  
2125 a second set of photosynthetic measurements from one week prior to the harvest  
2126 (6 weeks post-germination) revealed ... As pot limitation is expected to de-  
2127 crease net photosynthesis, and focal leaves were of similar ages between the sixth  
2128 and seventh week, one might expect growth limitation induced by constricted  
2129 pot volume to result in a dampened effect of inoculation and fertilization on net  
2130 photosynthesis,  $V_{cmax}$ , and  $J_{max25}$ . Analyses from the sixth week of development  
2131 revealed ... Additionally, analyses revealed a stronger/weaker downregulation in  
2132  $V_{cmax25}$  and  $J_{max25}$  on week 7, though disentangling the causality of this response  
2133 (i.e. whether due to pot size limitation or simply a stronger acclimation response)  
2134 would be difficult.

2135 Second, this study evaluated leaf and whole plant responses to CO<sub>2</sub> in 7-  
2136 week seedlings. Given the long-term scale of the progressive nitrogen limitation

2137 hypothesis, patterns observed here should be validated in longer-term nitrogen  
2138 manipulation experiments. Previous work in free air CO<sub>2</sub> enrichment experiments  
2139 show some support for patterns expected from the progressive nitrogen limitation  
2140 hypothesis (Reich et al. 2006; Norby et al. 2010), although results are not consis-  
2141 tent across experimental sites (Finzi et al. 2006; Moore et al. 2006; Liang et al.  
2142 2016). We found some support for patterns expected by the progressive nitrogen  
2143 limitation hypothesis, namely an increase in plant nitrogen uptake under elevated  
2144 CO<sub>2</sub> (Luo et al. 2004), though leaf acclimation responses to CO<sub>2</sub> were strongly  
2145 indicative of optimal resource investment to photosynthetic capacity as expected  
2146 from photosynthetic least-cost theory (Prentice et al. 2014; Smith et al. 2019;  
2147 Smith and Keenan 2020).

2148 5.4.4 *Conclusions*

2149 This study provides strong evidence suggesting that leaf acclimation re-  
2150 sponds to elevated CO<sub>2</sub> did not vary with soil nitrogen fertilization or ability  
2151 to acquire nitrogen through symbiotic nitrogen fixation. However, whole plant  
2152 acclimation responses to CO<sub>2</sub> were dependent on fertilization, where increasing  
2153 fertilization increased the positive effect of whole plant growth under elevated  
2154 CO<sub>2</sub>. Results also indicate that fertilization played a relatively more important  
2155 role in modifying whole plant responses to CO<sub>2</sub>, perhaps due to a reduction in  
2156 nodulation across the fertilization gradient. These patterns strongly support the  
2157 hypothesis that leaf and whole plant acclimation responses are driven by opti-  
2158 mal resource investment to photosynthetic capacity, and that leaf acclimation  
2159 responses to CO<sub>2</sub> were not modified by changes in soil nitrogen availability. Ad-

**2160** ditionally, strong interactions between fertilization and inoculation on leaf and  
**2161** whole plant traits indicated positive effects of fertilization on leaf and whole plant  
**2162** traits in uninoculated pots, but null effects of fertilization on leaf and whole plant  
**2163** traits in inoculated pots. These results build on previous work suggesting that  
**2164** constant leaf nitrogen-photosynthesis relationships are dynamic and change across  
**2165** growing environments, calling the use of constant relationships by terrestrial bio-  
**2166** sphere models into question.

**2167**

## Chapter 6

**2168**

### Conclusions

**2169** Experiments included in this dissertation leverage patterns expected from  
**2170** photosynthetic least-cost theory to investigate effects of soil resource availability  
**2171** and aboveground climate on costs of nitrogen acquisition, leaf nitrogen-water use  
**2172** tradeoffs, and plant acclimation responses to elevated CO<sub>2</sub>. Photosynthetic least-  
**2173** cost theory provides a contemporary framework for understanding impacts of  
**2174** climatic and edaphic characteristics on plant ecophysiological processes, namely  
**2175** leaf nitrogen allocation and photosynthetic capacity. When I began planning  
**2176** experiments for this dissertation in August 2018,, empirical tests of the theory  
**2177** were sparse and model development was just beginning with a goal of eventually  
**2178** implementing the theory in terrestrial biosphere models. At the time, it was  
**2179** critical that experimentation be done to test underlying assumptions of the theory  
**2180** and validate its suitability for implementing in terrestrial biosphere models.

**2181** Early iterations of model development held the unit cost of acquiring ni-  
**2182** trogen relative to water constant (Wang et al. 2017), in part because limited data  
**2183** existed to evaluate how this parameter changes across spatiotemporal scales and  
**2184** different environmental gradients. However, the Fixation and Uptake of Nitrogen  
**2185** model (Fisher et al. 2010; Brzostek et al. 2014) indicates that costs of nitro-  
**2186** gen acquisition decreased with increasing soil nitrogen availability and varies in  
**2187** species with different nitrogen acquisition strategies, suggesting that the unit cost  
**2188** of acquiring nitrogen relative to water should change across nitrogen availability  
**2189** gradients. Additionally,

**2190** All experimental chapters in this dissertation provide strong and consist-  
**2191** tent support for patterns expected from the theory across different experimental  
**2192** approaches, spatiotemporal scales, and different plant functional groups. In this  
**2193** chapter, I first summarize experimental approaches and primary findings of each  
**2194** experimental chapter. Then, I use findings from the four experimental chapters  
**2195** to synthesize recommendations for future photosynthetic least-cost theory model  
**2196** development, and propose experiments that will allow for further understanding  
**2197** of mechanisms that drive patterns expected from photosynthetic least-cost theory  
**2198** across environmental gradients.

**2199**

## References

- 2200** Abrams, M. D. and S. A. Mostoller (1995). Gas exchange, leaf structure and  
**2201** nitrogen in contrasting successional tree species growing in open and under-  
**2202** story sites during a drought. *Tree Physiology* 15(6), 361–370.
- 2203** Adams, M. A., T. L. Turnbull, J. I. Sprent, and N. Buchmann (2016). Legumes  
**2204** are different: Leaf nitrogen, photosynthesis, and water use efficiency. *Pro-  
**2205** ceedings of the National Academy of Sciences of the United States of Amer-  
**2206** ica* 113(15), 4098–4103.
- 2207** Ainsworth, E. A., P. A. Davey, C. J. Bernacchi, O. C. Dermody, E. A. Heaton,  
**2208** D. J. Moore, P. B. Morgan, S. L. Naidu, H. S. Y. Ra, X. G. Zhu, P. S. Curtis,  
**2209** and S. P. Long (2002). A meta-analysis of elevated [CO<sub>2</sub>] effects on soybean  
**2210** (*Glycine max*) physiology, growth and yield. *Global Change Biology* 8(8),  
**2211** 695–709.
- 2212** Ainsworth, E. A. and S. P. Long (2005). What have we learned from 15 years of  
**2213** free-air CO<sub>2</sub> enrichment (FACE)? A meta-analytic review of the responses  
**2214** of photosynthesis, canopy properties and plant production to rising CO<sub>2</sub>.  
**2215** *New Phytologist* 165(2), 351–372.
- 2216** Ainsworth, E. A. and A. Rogers (2007). The response of photosynthesis and  
**2217** stomatal conductance to rising [CO<sub>2</sub>]: mechanisms and environmental in-  
**2218** teractions. *Plant, Cell and Environment* 30(3), 258–270.
- 2219** Allen, K., J. B. Fisher, R. P. Phillips, J. S. Powers, and E. R. Brzostek (2020).  
**2220** Modeling the carbon cost of plant nitrogen and phosphorus uptake across  
**2221** temperate and tropical forests. *Frontiers in Forests and Global Change* 3,

- 2222 1–12.
- 2223 Allison, S. D., C. I. Czimczik, and K. K. Treseder (2008). Microbial activity
- 2224 and soil respiration under nitrogen addition in Alaskan boreal forest. *Global*
- 2225 *Change Biology* 14(5), 1156–1168.
- 2226 Andersen, M. K., H. Hauggaard-Nielsen, P. Ambus, and E. S. Jensen (2005).
- 2227 Biomass production, symbiotic nitrogen fixation and inorganic N use in dual
- 2228 and tri-component annual intercrops. *Plant and Soil* 266(1-2), 273–287.
- 2229 Andrews, M., E. K. James, J. I. Sprent, R. M. Boddey, E. Gross, and F. B. dos
- 2230 Reis (2011). Nitrogen fixation in legumes and actinorhizal plants in natural
- 2231 ecosystems: Values obtained using  $^{15}\text{N}$  natural abundance. *Plant Ecology*
- 2232 and *Diversity* 4(2-3), 117–130.
- 2233 Arndal, M. F., A. Tolver, K. S. Larsen, C. Beier, and I. K. Schmidt (2018). Fine
- 2234 root growth and vertical distribution in response to elevated CO<sub>2</sub>, warming
- 2235 and drought in a mixed heathland–grassland. *Ecosystems* 21(1), 15–30.
- 2236 Arnone, J. A. (1997). Indices of plant N availability in an alpine grassland under
- 2237 elevated atmospheric CO<sub>2</sub>. *Plant and Soil* 190(1), 61–66.
- 2238 Arora, V. K., A. Katavouta, R. G. Williams, C. D. Jones, V. Brovkin,
- 2239 P. Friedlingstein, J. Schwinger, L. Bopp, O. Boucher, P. Cadule, M. A.
- 2240 Chamberlain, J. R. Christian, C. Delire, R. A. Fisher, T. Hajima, T. Ilyina,
- 2241 E. Joetzjer, M. Kawamiya, C. D. Koven, J. P. Krasting, R. M. Law, D. M.
- 2242 Lawrence, A. Lenton, K. Lindsay, J. Pongratz, T. Raddatz, R. Séférian,
- 2243 K. Tachiiri, J. F. Tjiputra, A. Wiltshire, T. Wu, and T. Ziehn (2020).
- 2244 Carbon-concentration and carbon-climate feedbacks in CMIP6 models and
- 2245 their comparison to CMIP5 models. *Biogeosciences* 17(16), 4173–4222.

- 2246 Bae, K., T. J. Fahey, R. D. Yanai, and M. Fisk (2015). Soil nitrogen availabil-  
2247 ity affects belowground carbon allocation and soil respiration in northern  
2248 hardwood forests of New Hampshire. *Ecosystems* 18(7), 1179–1191.
- 2249 Barber, S. A. (1962). A diffusion and mass-flow concept of soil nutrient avail-  
2250 ability. *Soil Science* 93(1), 39–49.
- 2251 Barnes, J. D., L. Balaguer, E. Manrique, S. Elvira, and A. W. Davison (1992).  
2252 A reappraisal of the use of DMSO for the extraction and determination  
2253 of chlorophylls a and b in lichens and higher plants. *Environmental and*  
2254 *Experimental Botany* 32(2), 85–100.
- 2255 Bates, D., M. Mächler, B. Bolker, and S. Walker (2015). Fitting linear mixed-  
2256 effects models using lme4. *Journal of Statistical Software* 67(1), 1–48.
- 2257 Beaudette, D., J. Skovlin, S. Roeker, and A. Brown (2022). soilDB: Soil  
2258 Database Interface.
- 2259 Bengtson, P., J. Barker, and S. J. Grayston (2012). Evidence of a strong cou-  
2260 pling between root exudation, C and N availability, and stimulated SOM  
2261 decomposition caused by rhizosphere priming effects. *Ecology and Evolu-*  
2262 *tion* 93(8), 1843–1852.
- 2263 Bernacchi, C. J., E. L. Singsaas, C. Pimentel, A. R. Portis, and S. P. Long  
2264 (2001). Improved temperature response functions for models of Rubisco-  
2265 limited photosynthesis. *Plant, Cell and Environment* 24(2), 253–259.
- 2266 Bialic-Murphy, L., N. G. Smith, P. Voothuluru, R. M. McElderry, M. D.  
2267 Roche, S. T. Cassidy, S. N. Kivlin, and S. Kalisz (2021). Invasion-induced  
2268 root–fungal disruptions alter plant water and nitrogen economies. *Ecology*

- 2269** *Letters* 24(6), 1145–1156.
- 2270** Bloom, A. J., F. S. Chapin, and H. A. Mooney (1985). Resource limitation  
**2271** in plants - an economic analogy. *Annual Review of Ecology and Systemat-*  
**2272** *ics* 16(1), 363–392.
- 2273** Bloomfield, K. J., B. D. Stocker, T. F. Keenan, and I. C. Prentice (2022).  
**2274** Environmental controls on the light use efficiency of terrestrial gross primary  
**2275** production. *Global Change Biology*, 0–2.
- 2276** Bonan, G. B., M. D. Hartman, W. J. Parton, and W. R. Wieder (2013). Evaluat-  
**2277** ing litter decomposition in earth system models with long-term litterbag ex-  
**2278** periments: an example using the Community Land Model version 4 (CLM4).  
**2279** *Global Change Biology* 19(3), 957–974.
- 2280** Bonan, G. B., P. J. Lawrence, K. W. Oleson, S. Levis, M. Jung, M. Reich-  
**2281** stein, D. M. Lawrence, and S. C. Swenson (2011). Improving canopy pro-  
**2282** cesses in the Community Land Model version 4 (CLM4) using global flux  
**2283** fields empirically inferred from FLUXNET data. *Journal of Geophysical Re-*  
**2284** *search* 116(G2), G02014.
- 2285** Booth, B. B. B., C. D. Jones, M. Collins, I. J. Totterdell, P. M. Cox, S. Sitch,  
**2286** C. Huntingford, R. A. Betts, G. R. Harris, and J. Lloyd (2012). High sen-  
**2287** sitivity of future global warming to land carbon cycle processes. *Environ-*  
**2288** *mental Research Letters* 7(2), 024002.
- 2289** Borer, E. T., W. S. Harpole, P. B. Adler, E. M. Lind, J. L. Orrock, E. W.  
**2290** Seabloom, and M. D. Smith (2014). Finding generality in ecology: A model  
**2291** for globally distributed experiments. *Methods in Ecology and Evolution* 5(1),  
**2292** 65–73.

- 2293** Braghieri, R. K., J. B. Fisher, K. Allen, E. Brzostek, M. Shi, X. Yang, D. M.
- 2294** Ricciuto, R. A. Fisher, Q. Zhu, and R. P. Phillips (2022). Modeling global
- 2295** carbon costs of plant nitrogen and phosphorus acquisition. *Journal of Ad-*
- 2296** *vances in Modeling Earth Systems* 14(8), 1–23.
- 2297** Brix, H. (1971). Effects of nitrogen fertilization on photosynthesis and respi-
- 2298** ration in Douglas-fir. *Forest Science* 17(4), 407–414.
- 2299** Brzostek, E. R., J. B. Fisher, and R. P. Phillips (2014). Modeling the carbon
- 2300** cost of plant nitrogen acquisition: Mycorrhizal trade-offs and multipath
- 2301** resistance uptake improve predictions of retranslocation. *Journal of Geo-*
- 2302** *physical Research: Biogeosciences* 119, 1684–1697.
- 2303** Bubier, J. L., R. Smith, S. Juutinen, T. R. Moore, R. Minocha, S. Long, and
- 2304** S. Minocha (2011). Effects of nutrient addition on leaf chemistry, morphol-
- 2305** ogy, and photosynthetic capacity of three bog shrubs. *Oecologia* 167(2),
- 2306** 355–368.
- 2307** Cernusak, L. A., N. Ubierna, K. Winter, J. A. M. Holtum, J. D. Marshall, and
- 2308** G. D. Farquhar (2013). Environmental and physiological determinants of
- 2309** carbon isotope discrimination in terrestrial plants. *New Phytologist* 200(4),
- 2310** 950–965.
- 2311** Chen, J.-L., J. F. Reynolds, P. C. Harley, and J. D. Tenhunen (1993). Coor-
- 2312** dination theory of leaf nitrogen distribution in a canopy. *Oecologia* 93(1),
- 2313** 63–69.
- 2314** Clark, D. B., L. M. Mercado, S. Sitch, C. D. Jones, N. Gedney, M. J. Best,
- 2315** M. Pryor, G. G. Rooney, R. L. H. Essery, E. Blyth, O. Boucher, R. J.
- 2316** Harding, C. Huntingford, and P. M. Cox (2011). The Joint UK Land Envi-

- 2317 ronment Simulator (JULES), model description. Part 2: Carbon fluxes and  
2318 vegetation dynamics. *Geoscientific Model Development* 4(3), 701–722.
- 2319 Cornwell, W. K., J. H. C. Cornelissen, K. Amatangelo, E. Dorrepaal, V. T.  
2320 Eviner, O. Godoy, S. E. Hobbie, B. Hoorens, H. Kurokawa, N. Pérez-  
2321 Harguindeguy, H. M. Quested, L. S. Santiago, D. A. Wardle, I. J. Wright,  
2322 R. Aerts, S. D. Allison, P. van Bodegom, V. Brovkin, A. Chatain, T. V.  
2323 Callaghan, S. Díaz, E. Garnier, D. E. Gurvich, E. Kazakou, J. A. Klein,  
2324 J. Read, P. B. Reich, N. A. Soudzilovskaia, M. V. Vaieretti, and M. Westoby  
2325 (2008). Plant species traits are the predominant control on litter decompo-  
2326 sition rates within biomes worldwide. *Ecology Letters* 11(10), 1065–1071.
- 2327 Cornwell, W. K., I. J. Wright, J. Turner, V. Maire, M. M. Barbour, L. A.  
2328 Cernusak, T. E. Dawson, D. S. Ellsworth, G. D. Farquhar, H. Griffiths,  
2329 C. Keitel, A. Knohl, P. B. Reich, D. G. Williams, R. Bhaskar, J. H. C. Cor-  
2330 nelissen, A. Richards, S. Schmidt, F. Valladares, C. Körner, E.-D. Schulze,  
2331 N. Buchmann, and L. S. Santiago (2018). Climate and soils together regulate  
2332 photosynthetic carbon isotope discrimination within C<sub>3</sub> plants worldwide.  
2333 *Global Ecology and Biogeography* 27(9), 1056–1067.
- 2334 Cramer, W. and I. C. Prentice (1988). Simulation of regional soil moisture  
2335 deficits on a European scale. *Norsk Geografisk Tidsskrift - Norwegian Jour-*  
2336 *nal of Geography* 42(2-3), 149–151.
- 2337 Curtis, P. S. (1996). A meta-analysis of leaf gas exchange and nitrogen in trees  
2338 grown under elevated carbon dioxide. *Plant, Cell and Environment* 19(2),  
2339 127–137.
- 2340 Daly, C., M. Halbleib, J. I. Smith, W. P. Gibson, M. K. Doggett, G. H. Taylor,

- 2341 J. Curtis, and P. P. Pasteris (2008). Physiographically sensitive mapping  
2342 of climatological temperature and precipitation across the conterminous  
2343 United States. *International Journal of Climatology* 28(15), 2031–2064.
- 2344 Davies-Barnard, T., J. Meyerholt, S. Zaehle, P. Friedlingstein, V. Brovkin,  
2345 Y. Fan, R. A. Fisher, C. D. Jones, H. Lee, D. Peano, B. Smith, D. Wårlind,  
2346 and A. J. Wiltshire (2020). Nitrogen cycling in CMIP6 land surface models:  
2347 progress and limitations. *Biogeosciences* 17(20), 5129–5148.
- 2348 Davis, T. W., I. C. Prentice, B. D. Stocker, R. T. Thomas, R. J. Whitley,  
2349 H. Wang, B. J. Evans, A. V. Gallego-Sala, M. T. Sykes, and W. Cramer  
2350 (2017). Simple process-led algorithms for simulating habitats (SPLASH  
2351 v.1.0): robust indices of radiation, evapotranspiration and plant-available  
2352 moisture. *Geoscientific Model Development* 10, 689–708.
- 2353 Delaire, M., E. Frak, M. Sigogne, B. Adam, F. Beaujard, and X. Le Roux  
2354 (2005). Sudden increase in atmospheric CO<sub>2</sub> concentration reveals strong  
2355 coupling between shoot carbon uptake and root nutrient uptake in young  
2356 walnut trees. *Tree Physiology* 25(2), 229–235.
- 2357 Doane, T. A. and W. R. Horwáth (2003). Spectrophotometric determination of  
2358 nitrate with a single reagent. *Analytical Letters* 36(12), 2713–2722.
- 2359 Dong, N., I. C. Prentice, B. J. Evans, S. Caddy-Retalic, A. J. Lowe, and I. J.  
2360 Wright (2017). Leaf nitrogen from first principles: field evidence for adaptive  
2361 variation with climate. *Biogeosciences* 14(2), 481–495.
- 2362 Dong, N., I. C. Prentice, I. J. Wright, B. J. Evans, H. F. Togashi, S. Caddy-  
2363 Retalic, F. A. McInerney, B. Sparrow, E. Leitch, and A. J. Lowe (2020).  
2364 Components of leaf-trait variation along environmental gradients. *New Phy-*

- 2365** *tologist* 228(1), 82–94.
- 2366** Dong, N., I. C. Prentice, I. J. Wright, H. Wang, O. K. Atkin, K. J. Bloomfield,
- 2367** T. F. Domingues, S. M. Gleason, V. Maire, Y. Onoda, H. Poorter, and N. G.
- 2368** Smith (2022). Leaf nitrogen from the perspective of optimal plant function.
- 2369** *Journal of Ecology* 110(11), 2585–2602.
- 2370** Dong, N., I. J. Wright, J. M. Chen, X. Luo, H. Wang, T. F. Keenan, N. G.
- 2371** Smith, and I. C. Prentice (2022). Rising CO<sub>2</sub> and warming reduce global
- 2372** canopy demand for nitrogen. *New Phytologist* 235(5), 1692–1700.
- 2373** Dovrat, G., H. Bakhshian, T. Masci, and E. Sheffer (2020). The nitrogen eco-
- 2374** nomic spectrum of legume stoichiometry and fixation strategy. *New Phytol-*
- 2375** *ogist* 227(2), 365–375.
- 2376** Dovrat, G., T. Masci, H. Bakhshian, E. Mayzlish Gati, S. Golan, and E. Shef-
- 2377** fer (2018). Drought-adapted plants dramatically downregulate dinitrogen
- 2378** fixation: Evidences from Mediterranean legume shrubs. *Journal of Ecol-*
- 2379** *ogy* 106(4), 1534–1544.
- 2380** Drake, B. G., M. A. Gonzàlez-Meler, and S. P. Long (1997). More efficient
- 2381** plants: a consequence of rising atmospheric CO<sub>2</sub>? *Annual Review of Plant*
- 2382** *Biology* 48, 609–639.
- 2383** Duursma, R. A. (2015). Plantecophys - An R Package for Analysing and Mod-
- 2384** elling Leaf Gas Exchange Data. *PLOS ONE* 10(11), e0143346.
- 2385** Eastman, B. A., M. B. Adams, E. R. Brzostek, M. B. Burnham, J. E. Carrara,
- 2386** C. Kelly, B. E. McNeil, C. A. Walter, and W. T. Peterjohn (2021). Altered
- 2387** plant carbon partitioning enhanced forest ecosystem carbon storage after 25

- 2388 years of nitrogen additions. *New Phytologist* 230(4), 1435–1448.
- 2389 Ellsworth, D. S. and P. B. Reich (1996). Photosynthesis and leaf nitrogen in five  
2390 Amazonian tree species during early secondary succession. *Ecology* 77(2),  
2391 581–594.
- 2392 Espelta, J. M., P. Cortés, M. Mangirón, and J. Retana (2005). Differences in  
2393 biomass partitioning, leaf nitrogen content, and water use efficiency d13C  
2394 result in similar performance of seedlings of two Mediterranean oaks with  
2395 contrasting leaf habit. *Ecoscience* 12(4), 447–454.
- 2396 Evans, J. R. (1989). Photosynthesis and nitrogen relationships in leaves of C<sub>3</sub>  
2397 plants. *Oecologia* 78(1), 9–19.
- 2398 Evans, J. R. and V. C. Clarke (2019). The nitrogen cost of photosynthesis.  
2399 *Journal of Experimental Botany* 70(1), 7–15.
- 2400 Evans, J. R. and H. Poorter (2001). Photosynthetic acclimation of plants to  
2401 growth irradiance: the relative importance of specific leaf area and nitrogen  
2402 partitioning in maximizing carbon gain. *Plant, Cell and Environment* 24(8),  
2403 755–767.
- 2404 Evans, J. R. and J. R. Seemann (1989). The allocation of protein nitrogen in  
2405 the photosynthetic apparatus: costs, consequences, and control. *Photosyn-*  
2406 *thesis* 8, 183–205.
- 2407 Exbrayat, J.-F., A. A. Bloom, P. Falloon, A. Ito, T. L. Smallman, and  
2408 M. Williams (2018). Reliability ensemble averaging of 21<sup>st</sup> century projec-  
2409 tions of terrestrial net primary productivity reduces global and regional  
2410 uncertainties. *Earth System Dynamics* 9(1), 153–165.

- 2411** Farquhar, G. D., J. R. Ehleringer, and K. T. Hubick (1989). Carbon Isotope  
**2412** Discrimination and Photosynthesis. *Annual Review of Plant Physiology and*  
**2413** *Plant Molecular Biology* 40(1), 503–537.
- 2414** Farquhar, G. D. and T. D. Sharkey (1982). Stomatal conductance and photo-  
**2415** synthesis. *Annual Review of Plant Physiology* 33(1), 317–345.
- 2416** Farquhar, G. D., S. von Caemmerer, and J. A. Berry (1980). A biochemical  
**2417** model of photosynthetic CO<sub>2</sub> assimilation in leaves of C<sub>3</sub> species.  
**2418** *Planta* 149(1), 78–90.
- 2419** Fay, P. A., S. M. Prober, W. S. Harpole, J. M. H. Knops, J. D. Bakker, E. T.  
**2420** Borer, E. M. Lind, A. S. MacDougall, E. W. Seabloom, P. D. Wragg, P. B.  
**2421** Adler, D. M. Blumenthal, Y. M. Buckley, C. Chu, E. E. Cleland, S. L.  
**2422** Collins, K. F. Davies, G. Du, X. Feng, J. Firn, D. S. Gruner, N. Hagenah,  
**2423** Y. Hautier, R. W. Heckman, V. L. Jin, K. P. Kirkman, J. A. Klein, L. M.  
**2424** Ladwig, Q. Li, R. L. McCulley, B. A. Melbourne, C. E. Mitchell, J. L. Moore,  
**2425** J. W. Morgan, A. C. Risch, M. Schütz, C. J. Stevens, D. A. Wedin, and  
**2426** L. H. Yang (2015). Grassland productivity limited by multiple nutrients.  
**2427** *Nature Plants* 1(7), 15080.
- 2428** Feng, X. (1999). Trends in intrinsic water-use efficiency of natural trees for the  
**2429** past 100-200 years: A response to atmospheric CO<sub>2</sub> concentration. *Geochim-  
2430* *ica et Cosmochimica Acta* 63(13-14), 1891–1903.
- 2431** Field, C. B. and H. A. Mooney (1986). The photosynthesis-nitrogen relationship  
**2432** in wild plants. In T. J. Givnish (Ed.), *On the Economy of Plant Form and*  
**2433** *Function*, pp. 25–55. Cambridge: Cambridge University Press.
- 2434** Finzi, A. C., D. J. P. Moore, E. H. DeLucia, J. Lichter, K. S. Hofmockel, R. B.

- 2435 Jackson, H. S. Kim, R. Matamala, H. R. McCarthy, R. Oren, J. S. Pippen,  
2436 and W. H. Schlesinger (2006). Progressive nitrogen limitation of ecosystem  
2437 processes under elevated CO<sub>2</sub> in a warm-temperate forest. *Ecology* 87(1),  
2438 15–25.
- 2439 Firn, J., J. M. McGree, E. Harvey, H. Flores Moreno, M. Schutz, Y. M. Buckley,  
2440 E. T. Borer, E. W. Seabloom, K. J. La Pierre, A. M. MacDougall, S. M.  
2441 Prober, C. J. Stevens, L. L. Sullivan, E. Porter, E. Ladouceur, C. Allen,  
2442 K. H. Moromizato, J. W. Morgan, W. S. Harpole, Y. Hautier, N. Eisen-  
2443 hauer, J. P. Wright, P. B. Adler, C. A. Arnillas, J. D. Bakker, L. Biederman,  
2444 A. A. D. Broadbent, C. S. Brown, M. N. Bugalho, M. C. Caldeira, E. E. Cle-  
2445 land, A. Ebeling, P. A. Fay, N. Hagenah, A. R. Kleinhesselink, R. Mitchell,  
2446 J. L. Moore, C. Nogueira, P. L. Peri, C. Roscher, M. D. Smith, P. D. Wragg,  
2447 and A. C. Risch (2019). Leaf nutrients, not specific leaf area, are consistent  
2448 indicators of elevated nutrient inputs. *Nature Ecology and Evolution* 3(3),  
2449 400–406.
- 2450 Fisher, J. B., S. Sitch, Y. Malhi, R. A. Fisher, C. Huntingford, and S.-Y. Tan  
2451 (2010). Carbon cost of plant nitrogen acquisition: A mechanistic, globally  
2452 applicable model of plant nitrogen uptake, retranslocation, and fixation.  
2453 *Global Biogeochemical Cycles* 24(1), 1–17.
- 2454 Fox, J. and S. Weisberg (2019). *An R companion to applied regression* (Third  
2455 edit ed.). Thousand Oaks, California: Sage.
- 2456 Franklin, O., R. E. McMurtrie, C. M. Iversen, K. Y. Crous, A. C. Finzi, D. Tis-  
2457 sue, D. S. Ellsworth, R. Oren, and R. J. Norby (2009). Forest fine-root  
2458 production and nitrogen use under elevated CO<sub>2</sub>: contrasting responses

- 2459 in evergreen and deciduous trees explained by a common principle. *Global  
2460 Change Biology* 15(1), 132–144.
- 2461 Friedlingstein, P., M. Meinshausen, V. K. Arora, C. D. Jones, A. Anav, S. K.  
2462 Liddicoat, and R. Knutti (2014). Uncertainties in CMIP5 climate projections  
2463 due to carbon cycle feedbacks. *Journal of Climate* 27(2), 511–526.
- 2464 Friel, C. A. and M. L. Friesen (2019). Legumes modulate allocation to rhizobial  
2465 nitrogen fixation in response to factorial light and nitrogen manipulation.  
2466 *Frontiers in Plant Science* 10, 1316.
- 2467 Fujikake, H., A. Yamazaki, N. Ohtake, K. Sueoshi, S. Matsuhashi, T. Ito,  
2468 C. Mizuniwa, T. Kume, S. Hoshimoto, N.-S. Ishioka, S. Watanabe, A. Osa,  
2469 T. Sekine, H. Uchida, A. Tsuji, and T. Ohyama (2003). Quick and reversible  
2470 inhibition of soybean root nodule growth by nitrate involves a decrease in  
2471 sucrose supply to nodules. *Journal of Experimental Botany* 54(386), 1379–  
2472 1388.
- 2473 Ghimire, B., W. J. Riley, C. D. Koven, J. Kattge, A. Rogers, P. B. Reich, and  
2474 I. J. Wright (2017). A global trait-based approach to estimate leaf nitro-  
2475 gen functional allocation from observations:. *Ecological Applications* 27(5),  
2476 1421–1434.
- 2477 Giardina, C. P., M. D. Coleman, J. E. Hancock, J. S. King, E. A. Lilleskov,  
2478 W. M. Loya, K. S. Pregitzer, M. G. Ryan, and C. C. Trettin (2005). The  
2479 response of belowground carbon allocation in forests to global change. In  
2480 D. Binkley and O. Manyailo (Eds.), *Tree Species Effects on Soils: Implica-  
2481 tions for Global Change* (Volume 55 ed.), Chapter Chapter 7, pp. 119–154.  
2482 Berlin/Heidelberg: Springer-Verlag.

- 2483 Gibson, A. H. and J. E. Harper (1985). Nitrate effect on nodulation of soybean  
2484 by *Bradyrhizobium japonicum*. *Crop Science* 25(3), 497–501.
- 2485 Gill, A. L. and A. C. Finzi (2016). Belowground carbon flux links biogeochemical  
2486 cycles and resource-use efficiency at the global scale. *Ecology Letters* 19(12),  
2487 1419–1428.
- 2488 Goll, D. S., V. Brovkin, B. R. Parida, C. H. Reick, J. Kattge, P. B. Reich, P. M.  
2489 van Bodegom, and Ü. Niinemets (2012). Nutrient limitation reduces land  
2490 carbon uptake in simulations with a model of combined carbon, nitrogen  
2491 and phosphorus cycling. *Biogeosciences Discussions* 9(3), 3173–3232.
- 2492 Gregory, L. M., A. M. McClain, D. M. Kramer, J. D. Pardo, K. E. Smith, O. L.  
2493 Tessmer, B. J. Walker, L. G. Ziccardi, and T. D. Sharkey (2021, oct). The  
2494 triose phosphate utilization limitation of photosynthetic rate: Out of global  
2495 models but important for leaf models. *Plant, Cell and Environment* 44(10),  
2496 3223–3226.
- 2497 Guerrieri, R., M. Mencuccini, L. J. Sheppard, M. Saurer, M. P. Perks, P. Levy,  
2498 M. A. Sutton, M. Borghetti, and J. Grace (2011). The legacy of enhanced  
2499 N and S deposition as revealed by the combined analysis of  $\delta^{13}\text{C}$ ,  $\delta^{18}\text{O}$  and  
2500  $\delta^{15}\text{N}$  in tree rings. *Global Change Biology* 17(5), 1946–1962.
- 2501 Gulmon, S. L. and C. C. Chu (1981). The effects of light and nitrogen on pho-  
2502 tosynthesis, leaf characteristics, and dry matter allocation in the chaparral  
2503 shrub, <i>Diplacus aurantiacus</i>. *Oecologia* 49(2), 207–212.
- 2504 Gutschick, V. P. (1981). Evolved strategies in nitrogen acquisition by plants.  
2505 *The American Naturalist* 118(5), 607–637.

- 2506 Hallik, L., Ü. Niinemets, and I. J. Wright (2009). Are species shade and drought  
2507 tolerance reflected in leaf-level structural and functional differentiation in  
2508 Northern Hemisphere temperate woody flora? *New Phytologist* 184(1), 257–  
2509 274.
- 2510 Harrison, M. T., E. J. Edwards, G. D. Farquhar, A. B. Nicotra, and J. R.  
2511 Evans (2009). Nitrogen in cell walls of sclerophyllous leaves accounts for  
2512 little of the variation in photosynthetic nitrogen-use efficiency. *Plant, Cell  
2513 and Environment* 32(3), 259–270.
- 2514 Harrison, S. P., W. Cramer, O. Franklin, I. C. Prentice, H. Wang,  
2515 Å. Bränström, H. de Boer, U. Dieckmann, J. Joshi, T. F. Keenan,  
2516 A. Lavergne, S. Manzoni, G. Mengoli, C. Morfopoulos, J. Peñuelas,  
2517 S. Pietsch, K. T. Rebel, Y. Ryu, N. G. Smith, B. D. Stocker, and I. J.  
2518 Wright (2021). Eco-evolutionary optimality as a means to improve vegeta-  
2519 tion and land-surface models. *New Phytologist* 231(6), 2125–2141.
- 2520 Henneron, L., P. Kardol, D. A. Wardle, C. Cros, and S. Fontaine (2020). Rhizo-  
2521 sphere control of soil nitrogen cycling: a key component of plant economic  
2522 strategies. *New Phytologist* 228(4), 1269–1282.
- 2523 Hijmans, R. J. (2022). terra: Spatial Data Analysis.
- 2524 Hikosaka, K. and A. Shigeno (2009). The role of Rubisco and cell walls in the  
2525 interspecific variation in photosynthetic capacity. *Oecologia* 160(3), 443–  
2526 451.
- 2527 Hoagland, D. R. and D. I. Arnon (1950). The water culture method for growing  
2528 plants without soil. *California Agricultural Experiment Station: 347* 347(2),  
2529 1–32.

- 2530** Hobbie, E. A. (2006). Carbon allocation to ectomycorrhizal fungi correlates  
**2531** with belowground allocation in culture studies. *Ecology* 87(3), 563–569.
- 2532** Hobbie, E. A. and J. E. Hobbie (2008). Natural abundance of  $^{15}\text{N}$  in nitrogen-  
**2533** limited forests and tundra can estimate nitrogen cycling through mycorrhizal  
**2534** fungi: a review. *Ecosystems* 11(5), 815–830.
- 2535** Hoek, T. A., K. Axelrod, T. Biancalani, E. A. Yurtsev, J. Liu, and J. Gore  
**2536** (2016). Resource availability modulates the cooperative and competitive na-  
**2537** nature of a microbial cross-feeding mutualism. *PLOS Biology* 14(8), e1002540.
- 2538** Höglberg, M. N., M. J. I. Briones, S. G. Keel, D. B. Metcalfe, C. Campbell, A. J.  
**2539** Midwood, B. Thornton, V. Hurry, S. Linder, T. Näsholm, and P. Höglberg  
**2540** (2010). Quantification of effects of season and nitrogen supply on tree below-  
**2541** ground carbon transfer to ectomycorrhizal fungi and other soil organisms in  
**2542** a boreal pine forest. *New Phytologist* 187(2), 485–493.
- 2543** Höglberg, P., M. N. Höglberg, S. G. Göttlicher, N. R. Betson, S. G. Keel, D. B.  
**2544** Metcalfe, C. Campbell, A. Schindlbacher, V. Hurry, T. Lundmark, S. Linder,  
**2545** and T. Näsholm (2008). High temporal resolution tracing of photosynthate  
**2546** carbon from the tree canopy to forest soil microorganisms. *New Phyto-  
2547 logist* 177(1), 220–228.
- 2548** Houlton, B. Z., Y.-P. Wang, P. M. Vitousek, and C. B. Field (2008). A uni-  
**2549** fying framework for dinitrogen fixation in the terrestrial biosphere. *Nature*  
**2550** 454(7202), 327–330.
- 2551** Huber, M. L., R. A. Perkins, A. Laesecke, D. G. Friend, J. V. Sengers, M. J.  
**2552** Assael, I. N. Metaxa, E. Vogel, R. Mareš, and K. Miyagawa (2009). New  
**2553** international formulation for the viscosity of H<sub>2</sub>O. *Journal of Physical and*

- 2554      *Chemical Reference Data* 38(2), 101–125.
- 2555      Hungate, B. A., J. S. Dukes, M. R. Shaw, Y. Luo, and C. B. Field (2003).
- 2556      Nitrogen and climate change. *Science* 302(5650), 1512–1513.
- 2557      IPCC (2021). *Climate Change 2021: The Physical Science Basis. Contribution of Working Group I to the Sixth Assessment Report of the Intergovernmental Panel on Climate Change*. Cambridge University Press.
- 2559
- 2560      Johnson, N. C., J. H. Graham, and F. A. Smith (1997). Functioning of mycorrhizal associations along the mutualism-parasitism continuum. *New Phytologist* 135(4), 575–585.
- 2561
- 2562
- 2563      Kachurina, O. M., H. Zhang, W. R. Raun, and E. G. Krenzer (2000). Simultaneous determination of soil aluminum, ammonium- and nitrate- nitrogen using 1 M potassium chloride. *Communications in Soil Science and Plant Analysis* 31(7-8), 893–903.
- 2564
- 2565
- 2566
- 2567      Kaiser, C., M. R. Kilburn, P. L. Clode, L. Fuchslueger, M. Koranda, J. B. Cliff,
- 2568      Z. M. Solaiman, and D. V. Murphy (2015). Exploring the transfer of recent
- 2569      plant photosynthates to soil microbes: mycorrhizal pathway vs direct root
- 2570      exudation. *New Phytologist* 205(4), 1537–1551.
- 2571      Katabuchi, M. (2015). LeafArea: An R package for rapid digital analysis of leaf
- 2572      area. *Ecological Research* 30(6), 1073–1077.
- 2573      Kattge, J. and W. Knorr (2007). Temperature acclimation in a biochemical
- 2574      model of photosynthesis: a reanalysis of data from 36 species. *Plant, Cell*
- 2575      and Environment
- 2576      Kattge, J., W. Knorr, T. Raddatz, and C. Wirth (2009). Quantifying photosyn-

- 2577       thetic capacity and its relationship to leaf nitrogen content for global-scale  
2578       terrestrial biosphere models. *Global Change Biology* 15(4), 976–991.
- 2579       Kayler, Z., A. Gessler, and N. Buchmann (2010). What is the speed of link  
2580       between aboveground and belowground processes? *New Phytologist* 187(4),  
2581       885–888.
- 2582       Kayler, Z., C. Keitel, K. Jansen, and A. Gessler (2017). Experimental evi-  
2583       dence of two mechanisms coupling leaf-level C assimilation to rhizosphere  
2584       CO<sub>2</sub> release. *Environmental and Experimental Botany* 135,  
2585       21–26.
- 2586       Keeling, C. D., W. G. Mook, and P. P. Tans (1979, jan). Recent trends in the  
2587       <sup>13</sup>C/<sup>12</sup>C ratio of atmospheric carbon dioxide.  
2588       *Nature* 277(5692), 121–123.
- 2589       Kenward, M. G. and J. H. Roger (1997). Small sample inference for fixed effects  
2590       from restricted maximum likelihood. *Biometrics* 53(3), 983.
- 2591       Knapp, A. K., M. L. Avolio, C. Beier, C. J. W. Carroll, S. L. Collins, J. S.  
2592       Dukes, L. H. Fraser, R. J. Griffin-Nolan, D. L. Hoover, A. Jentsch, M. E.  
2593       Loik, R. P. Phillips, A. K. Post, O. E. Sala, I. J. Slette, L. Yahdjian, and  
2594       M. D. Smith (2017). Pushing precipitation to the extremes in distributed  
2595       experiments: recommendations for simulating wet and dry years. *Global  
2596       Change Biology* 23(5), 1774–1782.
- 2597       Knorr, W. (2000). Annual and interannual CO<sub>2</sub> exchanges of the  
2598       terrestrial biosphere: process-based simulations and uncertainties. *Global  
2599       Ecology and Biogeography* 9(3), 225–252.

- 2600 Knorr, W. and M. Heimann (2001). Uncertainties in global terrestrial biosphere  
2601 modeling: 1. A comprehensive sensitivity analysis with a new photosynthesis  
2602 and energy balance scheme. *Global Biogeochemical Cycles* 15(1), 207–225.
- 2603 Kulmatiski, A., P. B. Adler, J. M. Stark, and A. T. Tredennick (2017). Water  
2604 and nitrogen uptake are better associated with resource availability than  
2605 root biomass. *Ecosphere* 8(3), e01738.
- 2606 Lavergne, A., D. Sandoval, V. J. Hare, H. Graven, and I. C. Prentice (2020).  
2607 Impacts of soil water stress on the acclimated stomatal limitation of pho-  
2608 tosynthesis: Insights from stable carbon isotope data. *Global Change Biol-*  
2609 *ogy* 26(12), 7158–7172.
- 2610 Lawrence, D. M., R. A. Fisher, C. D. Koven, K. W. Oleson, S. C. Swen-  
2611 son, G. B. Bonan, N. Collier, B. Ghimire, L. Kamphout, D. Kennedy,  
2612 E. Kluzeck, P. J. Lawrence, F. Li, H. Li, D. L. Lombardozzi, W. J. Riley,  
2613 W. J. Sacks, M. Shi, M. Vertenstein, W. R. Wieder, C. Xu, A. A. Ali,  
2614 A. M. Badger, G. Bisht, M. Broeke, M. A. Brunke, S. P. Burns, J. Buzan,  
2615 M. Clark, A. Craig, K. M. Dahlin, B. Drewniak, J. B. Fisher, M. Flanner,  
2616 A. M. Fox, P. Gentine, F. M. Hoffman, G. Keppel-Aleks, R. Knox, S. Ku-  
2617 mar, J. Lenaerts, L. R. Leung, W. H. Lipscomb, Y. Lu, A. Pandey, J. D.  
2618 Pelletier, J. Perket, J. T. Randerson, D. M. Ricciuto, B. M. Sanderson,  
2619 A. Slater, Z. M. Subin, J. Tang, R. Q. Thomas, M. Val Martin, and X. Zeng  
2620 (2019). The Community Land Model Version 5: description of new features,  
2621 benchmarking, and impact of forcing uncertainty. *Journal of Advances in*  
2622 *Modeling Earth Systems* 11(12), 4245–4287.
- 2623 LeBauer, D. S. and K. K. Treseder (2008). Nitrogen limitation of net primary

- 2624** productivity. *Ecology* 89(2), 371–379.
- 2625** Lefcheck, J. S. (2016). piecewiseSEM: Piecewise structural equation modelling  
**2626** in r for ecology, evolution, and systematics. *Methods in Ecology and Evolution*  
**2627** 7(5), 573–579.
- 2628** Lenth, R. (2019). emmeans: estimated marginal means, aka least-squares  
**2629** means.
- 2630** Li, W., H. Zhang, G. Huang, R. Liu, H. Wu, C. Zhao, and N. G. McDowell  
**2631** (2020). Effects of nitrogen enrichment on tree carbon allocation: A global  
**2632** synthesis. *Global Ecology and Biogeography* 29(3), 573–589.
- 2633** Liang, J., X. Qi, L. Souza, and Y. Luo (2016). Processes regulating progressive  
**2634** nitrogen limitation under elevated carbon dioxide: a meta-analysis. *Biogeosciences*  
**2635** 13(9), 2689–2699.
- 2636** Liang, X., T. Zhang, X. Lu, D. S. Ellsworth, H. BassiriRad, C. You, D. Wang,  
**2637** P. He, Q. Deng, H. Liu, J. Mo, and Q. Ye (2020). Global response patterns of  
**2638** plant photosynthesis to nitrogen addition: A meta-analysis. *Global Change  
Biology* 26(6), 3585–3600.
- 2640** Lu, J., J. Yang, C. Keitel, L. Yin, P. Wang, W. Cheng, and F. A. Dijkstra  
**2641** (2022). Belowground Carbon Efficiency for Nitrogen and Phosphorus Ac-  
**2642** quisition Varies Between *Lolium perenne* and *Trifolium repens* and Depends  
**2643** on Phosphorus Fertilization. *Frontiers in Plant Science* 13, 1–9.
- 2644** Luo, X., T. F. Keenan, J. M. Chen, H. Croft, I. C. Prentice, N. G. Smith,  
**2645** A. P. Walker, H. Wang, R. Wang, C. Xu, and Y. Zhang (2021). Global  
**2646** variation in the fraction of leaf nitrogen allocated to photosynthesis. *Nature*

- 2647** *Communications* 12(1), 4866.
- 2648** Luo, Y., W. S. Currie, J. S. Dukes, A. C. Finzi, U. A. Hartwig, B. A. Hungate,
- 2649** R. E. McMurtrie, R. Oren, W. J. Parton, D. E. Pataki, R. M. Shaw, D. R.
- 2650** Zak, and C. B. Field (2004). Progressive nitrogen limitation of ecosystem
- 2651** responses to rising atmospheric carbon dioxide. *BioScience* 54(8), 731–739.
- 2652** Maire, V., P. Martre, J. Kattge, F. Gastal, G. Esser, S. Fontaine, and J.-F.
- 2653** Soussana (2012). The coordination of leaf photosynthesis links C and N
- 2654** fluxes in C<sub>3</sub> plant species. *PLoS ONE* 7(6), e38345.
- 2655** Makino, A. (2003). Rubisco and nitrogen relationships in rice: leaf photosyn-
- 2656** thesis and plant growth. *Soil Science and Plant Nutrition* 49(3), 319–327.
- 2657** Makino, A., M. Harada, T. Sato, H. Nakano, and T. Mae (1997). Growth and N
- 2658** Allocation in Rice Plants under CO<sub>2</sub> Enrichment. *Plant Physiology* 115(1),
- 2659** 199–203.
- 2660** Markham, J. H. and C. Zekveld (2007). Nitrogen fixation makes biomass al-
- 2661** location to roots independent of soil nitrogen supply. *Canadian Journal of*
- 2662** *Botany* (9), 787–793.
- 2663** Marschner, H. and B. Dell (1994). Nutrient uptake in mycorrhizal symbiosis.
- 2664** *Plant and Soil* 159(1), 89–102.
- 2665** Matamala, R. and W. H. Schlesinger (2000). Effects of elevated atmospheric
- 2666** CO<sub>2</sub> on fine root production and activity in an intact tem-
- 2667** perate forest ecosystem. *Global Change Biology* 6(8), 967–979.
- 2668** Medlyn, B. E., E. Dreyer, D. S. Ellsworth, M. Forstreuter, P. C. Harley,
- 2669** M. U. F. Kirschbaum, X. Le Roux, P. Montpied, J. Strassmeyer, A. Wal-

- 2670 croft, K. Wang, and D. Loustau (2002). Temperature response of parameters  
2671 of a biochemically based model of photosynthesis. II. A review of experimen-  
2672 tal data. *Plant, Cell and Environment* 25(9), 1167–1179.
- 2673 Menge, D. N. L., S. A. Levin, and L. O. Hedin (2008). Evolutionary tradeoffs can  
2674 select against nitrogen fixation and thereby maintain nitrogen limitation.  
2675 *Proceedings of the National Academy of Sciences* 105(5), 1573–1578.
- 2676 Menne, M. J., I. Durre, R. S. Vose, B. E. Gleason, and T. G. Houston (2012).  
2677 An overview of the global historical climatology network-daily database.  
2678 *Journal of Atmospheric and Oceanic Technology* 29(7), 897–910.
- 2679 Meyerholt, J., K. Sickel, and S. Zaehle (2020). Ensemble projections elucidate  
2680 effects of uncertainty in terrestrial nitrogen limitation on future carbon up-  
2681 take. *Global Change Biology* 26(7), 3978–3996.
- 2682 Meyerholt, J., S. Zaehle, and M. J. Smith (2016). Variability of pro-  
2683 jected terrestrial biosphere responses to elevated levels of atmospheric  
2684 CO<sub>2</sub> due to uncertainty in biological nitrogen fixation. *Bio-*  
2685 *geosciences* 13(5), 1491–1518.
- 2686 Minocha, R., S. Long, A. H. Magill, J. D. Aber, and W. H. McDowell (2000).  
2687 Foliar free polyamine and inorganic ion content in relation to soil and soil  
2688 solution chemistry in two fertilized forest stands at the Harvard Forest,  
2689 Massachusetts. *Plant and Soil* 222(1-2), 119–137.
- 2690 Moore, D. J., S. Aref, R. M. Ho, J. S. Pippen, J. G. Hamilton, and E. H. De  
2691 Lucia (2006). Annual basal area increment and growth duration of *Pinus*  
2692 *taeda* in response to eight years of free-air carbon dioxide enrichment. *Global*  
2693 *Change Biology* 12(8), 1367–1377.

- 2694 Morgan, J. A., D. E. Pataki, C. Körner, H. Clark, S. J. Del Grosso, J. M.  
2695 Grünzweig, A. K. Knapp, A. R. Mosier, P. C. D. Newton, P. A. Niklaus,  
2696 J. B. Nippert, R. S. Nowak, W. J. Parton, H. W. Polley, and M. R. Shaw  
2697 (2004). Water relations in grassland and desert ecosystems exposed to ele-  
2698 vated atmospheric CO<sub>2</sub>. *Oecologia* 140(1), 11–25.
- 2699 Muñoz, N., X. Qi, M. W. Li, M. Xie, Y. Gao, M. Y. Cheung, F. L. Wong, and  
2700 H.-M. Lam (2016). Improvement in nitrogen fixation capacity could be part  
2701 of the domestication process in soybean. *Heredity* 117(2), 84–93.
- 2702 Nadelhoffer, K. J. and J. W. Raich (1992). Fine root production estimates and  
2703 belowground carbon allocation in forest ecosystems. *Ecology* 73(4), 1139–  
2704 1147.
- 2705 Niinemets, Ü. and J. D. Tenhunen (1997). A model separating leaf struc-  
2706 tural and physiological effects on carbon gain along light gradients for the  
2707 shade-tolerant species <i>Acer saccharum</i>. *Plant, Cell and Environ-  
2708 ment* 20(7), 845–866.
- 2709 Norby, R. J., J. Ledford, C. D. Reilly, N. E. Miller, and E. G. O'Neill  
2710 (2004). Fine-root production dominates response of a deciduous forest to  
2711 atmospheric CO<sub>2</sub> enrichment. *Proceedings of the National Academy of Sci-  
2712 ences* 101(26), 9689–9693.
- 2713 Norby, R. J., J. M. Warren, C. M. Iversen, B. E. Medlyn, and R. E. Mc-  
2714 Murtrie (2010). CO<sub>2</sub> enhancement of forest productivity constrained by  
2715 limited nitrogen availability. *Proceedings of the National Academy of Sci-  
2716 ences* 107(45), 19368–19373.
- 2717 Novick, K. A., D. L. Ficklin, P. C. Stoy, C. A. Williams, G. Bohrer, A. C.

- 2718** Oishi, S. A. Papuga, P. D. Blanken, A. Noormets, B. N. Sulman, R. L.  
**2719** Scott, L. Wang, and R. P. Phillips (2016). The increasing importance of  
**2720** atmospheric demand for ecosystem water and carbon fluxes. *Nature Climate  
Change* 6(11), 1023–1027.
- 2722** Noyce, G. L., M. L. Kirwan, R. L. Rich, and J. P. Megonigal (2019). Asyn-  
**2723** chronous nitrogen supply and demand produce nonlinear plant allocation  
**2724** responses to warming and elevated CO<sub>2</sub>. *Proceedings of the  
2725 National Academy of Sciences* 116(43), 21623–21628.
- 2726** Onoda, Y., K. Hikosaka, and T. Hirose (2004). Allocation of nitrogen to  
**2727** cell walls decreases photosynthetic nitrogen-use efficiency. *Functional Ecol-  
ogy* 18(3), 419–425.
- 2729** Onoda, Y., I. J. Wright, J. R. Evans, K. Hikosaka, K. Kitajima, Ü. Niinemets,  
**2730** H. Poorter, T. Tosens, and M. Westoby (2017). Physiological and structural  
**2731** tradeoffs underlying the leaf economics spectrum. *New Phytologist* 214(4),  
**2732** 1447–1463.
- 2733** Oreskes, N., K. Shrader-Frechette, and K. Belitz (1994). Verification, vali-  
**2734** dation, and confirmation of numerical models in the Earth sciences. *Sci-  
ence* 263(5147), 641–646.
- 2736** Paillassa, J., I. J. Wright, I. C. Prentice, S. Pepin, N. G. Smith, G. Ethier,  
**2737** A. C. Westerband, L. J. Lamarque, H. Wang, W. K. Cornwell, and V. Maire  
**2738** (2020). When and where soil is important to modify the carbon and water  
**2739** economy of leaves. *New Phytologist* 228(1), 121–135.
- 2740** Parvin, S., S. Uddin, S. Tausz Posch, R. Armstrong, and M. Tausz (2020). Car-  
**2741** bon sink strength of nodules but not other organs modulates photosynthesis

- 2742 of faba bean (*i>Vicia faba</i> ) grown under elevated [CO<sub>2</sub>] and different  
2743 water supply. *New Phytologist* 227(1), 132–145.*
- 2744 Peng, Y., K. J. Bloomfield, L. A. Cernusak, T. F. Domingues, and I. C. Prentice (2021). Global climate and nutrient controls of photosynthetic capacity.  
2745 *Communications Biology* 4(1), 462.
- 2746 Perkowski, E. A., E. F. Waring, and N. G. Smith (2021). Root mass carbon  
2747 costs to acquire nitrogen are determined by nitrogen and light availability  
2748 in two species with different nitrogen acquisition strategies. *Journal of*  
2749 *Experimental Botany* 72(15), 5766–5776.
- 2750 Phillips, R. P., E. R. Brzostek, and M. G. Midgley (2013). The mycorrhizal-  
2751 associated nutrient economy: a new framework for predicting carbon-  
2752 nutrient couplings in temperate forests. *New Phytologist* 199(1), 41–51.
- 2753 Phillips, R. P., A. C. Finzi, and E. S. Bernhardt (2011). Enhanced root ex-  
2754 udation induces microbial feedbacks to N cycling in a pine forest under  
2755 long-term CO<sub>2</sub> fumigation. *Ecology Letters* 14(2), 187–194.
- 2756 Pinheiro, J. and D. Bates (2022). nlme: linear and nonlinear mixed effects  
2757 models.
- 2758 Poggio, L., L. M. De Sousa, N. H. Batjes, G. B. M. Heuvelink, B. Kempen,  
2759 E. Ribeiro, and D. Rossiter (2021). SoilGrids 2.0: Producing soil information  
2760 for the globe with quantified spatial uncertainty. *Soil* 7(1), 217–240.
- 2761 Pons, T. L. and R. W. Pearcy (1994). Nitrogen reallocation and photosynthetic  
2762 acclimation in response to partial shading in soybean plants. *Physiologia*  
2763 *Plantarum* 92(4), 636–644.

- 2765** Poorter, H., J. Bühler, D. Van Dusschoten, J. Climent, and J. A. Postma (2012).
- 2766** Pot size matters: A meta-analysis of the effects of rooting volume on plant growth. *Functional Plant Biology* 39(11), 839–850.
- 2768** Poorter, H., O. Knopf, I. J. Wright, A. A. Temme, S. W. Hogewoning, A. Graf,
- 2769** L. A. Cernusak, and T. L. Pons (2022). A meta-analysis of responses of C<sub>3</sub>
- 2770** plants to atmospheric CO<sub>2</sub>: dose-response curves for 85 traits ranging from
- 2771** the molecular to the whole-plant level. *New Phytologist* 233(4), 1560–1596.
- 2772** Prentice, I. C., N. Dong, S. M. Gleason, V. Maire, and I. J. Wright (2014).
- 2773** Balancing the costs of carbon gain and water transport: testing a new theo-
- 2774** retical framework for plant functional ecology. *Ecology Letters* 17(1), 82–91.
- 2775** Prentice, I. C., X. Liang, B. E. Medlyn, and Y.-P. Wang (2015). Reliable, ro-
- 2776** bust and realistic: The three R's of next-generation land-surface modelling.
- 2777** *Atmospheric Chemistry and Physics* 15, 5987–6005.
- 2778** Priestley, C. H. B. and R. J. Taylor (1972). On the Assessment of Surface
- 2779** Heat Flux and Evaporation Using Large-Scale Parameters. *Monthly Weather*
- 2780** *Review* 100(2), 81–92.
- 2781** Querejeta, J. I., I. Prieto, C. Armas, F. Casanoves, J. S. Diémé, M. Diouf,
- 2782** H. Yossi, B. Kaya, F. I. Pugnaire, and G. M. Rusch (2022). Higher leaf
- 2783** nitrogen content is linked to tighter stomatal regulation of transpiration
- 2784** and more efficient water use across dryland trees. *New Phytologist* 235(4),
- 2785** 1351–1364.
- 2786** R Core Team (2021). R: A language and environment for statistical computing.
- 2787** Raich, J. W., D. A. Clark, L. Schwendenmann, and T. E. Wood (2014). Above-

- 2788 ground tree growth varies with belowground carbon allocation in a tropical  
2789 rainforest environment. *PLoS ONE* 9(6), e100275.
- 2790 Rastetter, E. B., P. M. Vitousek, C. B. Field, G. R. Shaver, D. Herbert, and  
2791 G. I. Ågren (2001). Resource optimization and symbiotic nitrogen fixation.  
2792 *Ecosystems* 4(4), 369–388.
- 2793 Reich, P. B. (2014). The world-wide 'fast-slow' plant economics spectrum: a  
2794 traits manifesto. *Journal of Ecology* 102(2), 275–301.
- 2795 Reich, P. B., S. E. Hobbie, T. Lee, D. S. Ellsworth, J. B. West, D. Tilman,  
2796 J. M. H. Knops, S. Naeem, and J. Trost (2006). Nitrogen limitation con-  
2797 strains sustainability of ecosystem response to CO<sub>2</sub>. *Nature* 440(7086), 922–925.
- 2799 Rhine, E. D., R. L. Mulvaney, E. J. Pratt, and G. K. Sims (1998). Improving  
2800 the Berthelot reaction for determining ammonium in soil extracts and water.  
2801 *Soil Science Society of America Journal* 62(2), 473.
- 2802 Rogers, A. (2014). The use and misuse of  $V_{cmax}$  in Earth System Models. *Pho-*  
2803 *tosynthesis Research* 119(1-2), 15–29.
- 2804 Rogers, A., B. E. Medlyn, J. S. Dukes, G. B. Bonan, S. Caemmerer, M. C.  
2805 Dietze, J. Kattge, A. D. B. Leakey, L. M. Mercado, Ü. Niinemets, I. C.  
2806 Prentice, S. P. Serbin, S. Sitch, D. A. Way, and S. Zaehle (2017). A roadmap  
2807 for improving the representation of photosynthesis in Earth system models.  
2808 *New Phytologist* 213(1), 22–42.
- 2809 Saathoff, A. J. and J. Welles (2021). Gas exchange measurements in the un-  
2810 steady state. *Plant Cell and Environment* 44(11), 3509–3523.

- 2811** Saleh, A. M., M. Abdel-Mawgoud, A. R. Hassan, T. H. Habeeb, R. S. Yehia,  
**2812** and H. AbdElgawad (2020). Global metabolic changes induced by arbuscular  
**2813** mycorrhizal fungi in oregano plants grown under ambient and elevated levels  
**2814** of atmospheric CO<sub>2</sub>. *Plant Physiology and Biochemistry* 151, 255–263.
- 2815** Saxton, K. E. and W. J. Rawls (2006). Soil water characteristic estimates by  
**2816** texture and organic matter for hydrologic solutions. *Soil Science Society of  
2817 America Journal* 70(5), 1569–1578.
- 2818** Schaefer, K., C. R. Schwalm, C. Williams, M. A. Arain, A. Barr, J. M. Chen,  
**2819** K. J. Davis, D. Dimitrov, T. W. Hilton, D. Y. Hollinger, E. Humphreys,  
**2820** B. Poulter, B. M. Racza, A. D. Richardson, A. Sahoo, P. Thornton, R. Var-  
**2821** gas, H. Verbeeck, R. Anderson, I. Baker, T. A. Black, P. Bolstad, J. Chen,  
**2822** P. S. Curtis, A. R. Desai, M. C. Dietze, D. Dragoni, C. M. Gough, R. F.  
**2823** Grant, L. Gu, A. K. Jain, C. Kucharik, B. E. Law, S. Liu, E. Lokipitiya,  
**2824** H. A. Margolis, R. Matamala, J. H. McCaughey, R. Monson, J. W. Munger,  
**2825** W. Oechel, C. Peng, D. T. Price, D. Ricciuto, W. J. Riley, N. Roulet,  
**2826** H. Tian, C. Tonitto, M. Torn, E. Weng, and X. Zhou (2012). A model-  
**2827** data comparison of gross primary productivity: Results from the North  
**2828** American Carbon Program site synthesis. *Journal of Geophysical Research:*  
**2829** *Biogeosciences* 117(G3), G03010.
- 2830** Schneider, C. A., W. S. Rasband, and K. W. Eliceiri (2012). NIH Image to  
**2831** ImageJ: 25 years of image analysis. *Nature Methods* 9(7), 671–675.
- 2832** Scott, H. G. and N. G. Smith (2022). A Model of C4 Photosynthetic Acclimation  
**2833** Based on Least-Cost Optimality Theory Suitable for Earth System Model  
**2834** Incorporation. *Journal of Advances in Modeling Earth Systems* 14(3), 1–16.

- 2835 Shi, M., J. B. Fisher, E. R. Brzostek, and R. P. Phillips (2016). Carbon cost  
2836 of plant nitrogen acquisition: Global carbon cycle impact from an improved  
2837 plant nitrogen cycle in the Community Land Model. *Global Change Biology*  
2838 *22*(3), 1299–1314.
- 2839 Shi, M., J. B. Fisher, R. P. Phillips, and E. R. Brzostek (2019). Neglecting  
2840 plant–microbe symbioses leads to underestimation of modeled climate im-  
2841 pacts. *Biogeosciences* *16*(2), 457–465.
- 2842 Smith, N. G. and J. S. Dukes (2013). Plant respiration and photosynthesis in  
2843 global-scale models: incorporating acclimation to temperature and CO<sub>2</sub>.  
2844 *Global Change Biology* *19*(1), 45–63.
- 2845 Smith, N. G. and T. F. Keenan (2020). Mechanisms underlying leaf photosyn-  
2846 thetic acclimation to warming and elevated CO<sub>2</sub> as inferred from least-cost  
2847 optimality theory. *Global Change Biology* *26*(9), 5202–5216.
- 2848 Smith, N. G., T. F. Keenan, I. C. Prentice, H. Wang, I. J. Wright, Ü. Niinemets,  
2849 K. Y. Crous, T. F. Domingues, R. Guerrieri, F. oko Ishida, J. Kattge, E. L.  
2850 Kruger, V. Maire, A. Rogers, S. P. Serbin, L. Tarvainen, H. F. Togashi,  
2851 P. A. Townsend, M. Wang, L. K. Weerasinghe, and S.-X. Zhou (2019).  
2852 Global photosynthetic capacity is optimized to the environment. *Ecology*  
2853 *Letters* *22*(3), 506–517.
- 2854 Smith, N. G., D. L. Lombardozzi, A. Tawfik, G. B. Bonan, and J. S. Dukes  
2855 (2017). Biophysical consequences of photosynthetic temperature acclimation  
2856 for climate. *Journal of Advances in Modeling Earth Systems* *9*(1), 536–547.
- 2857 Smith, N. G., S. L. Malyshev, E. Shevliakova, J. Kattge, and J. S. Dukes  
2858 (2016). Foliar temperature acclimation reduces simulated carbon sensitivity

- 2859 to climate. *Nature Climate Change* 6(4), 407–411.
- 2860 Smith, S. E. and D. J. Read (2008). *Mycorrhizal Symbiosis*. Academic Press.
- 2861 Soil Survey Staff (2022). Web Soil Survey.
- 2862 Soudzilovskaia, N. A., J. C. Douma, A. A. Akhmetzhanova, P. M. van Bode-
- 2863 gom, W. K. Cornwell, E. J. Moens, K. K. Treseder, and J. H. C. Cornelissen
- 2864 (2015). Global patterns of plant root colonization intensity by mycorrhizal
- 2865 fungi explained by climate and soil chemistry. *Global Ecology and Biogeog-*
- 2866 *raphy* 24(3), 371–382.
- 2867 Stocker, B. D., H. Wang, N. G. Smith, S. P. Harrison, T. F. Keenan, D. San-
- 2868 doval, T. Davis, and I. C. Prentice (2020). P-model v1.0: An optimality-
- 2869 based light use efficiency model for simulating ecosystem gross primary pro-
- 2870 duction. *Geoscientific Model Development* 13(3), 1545–1581.
- 2871 Stocker, B. D., J. Zscheischler, T. F. Keenan, I. C. Prentice, J. Peñuelas, and
- 2872 S. I. Seneviratne (2018). Quantifying soil moisture impacts on light use
- 2873 efficiency across biomes. *New Phytologist* 218(4), 1430–1449.
- 2874 Sulman, B. N., D. T. Roman, K. Yi, L. Wang, R. P. Phillips, and K. A.
- 2875 Novick (2016). High atmospheric demand for water can limit forest car-
- 2876 bon uptake and transpiration as severely as dry soil. *Geophysical Research*
- 2877 *Letters* 43(18), 9686–9695.
- 2878 Sulman, B. N., E. Shevliakova, E. R. Brzostek, S. N. Kivlin, S. L. Malyshev,
- 2879 D. N. L. Menge, and X. Zhang (2019). Diverse mycorrhizal associations
- 2880 enhance terrestrial C storage in a global model. *Global Biogeochemical Cy-*
- 2881 *cles* 33(4), 501–523.

- 2882 Sweet, S. K., D. W. Wolfe, A. DeGaetano, and R. Benner (2017). Anatomy  
2883 of the 2016 drought in the Northeastern United States: Implications for  
2884 agriculture and water resources in humid climates. *Agricultural and Forest*  
2885 *Meteorology* 247, 571–581.
- 2886 Taylor, B. N. and D. N. L. Menge (2018). Light regulates tropical symbiotic  
2887 nitrogen fixation more strongly than soil nitrogen. *Nature Plants* 4(9), 655–  
2888 661.
- 2889 Terrer, C., S. Vicca, B. A. Hungate, R. P. Phillips, and I. C. Prentice (2016).  
2890 Mycorrhizal association as a primary control of the CO<sub>2</sub> fertilization effect.  
2891 *Science* 353(6294), 72–74.
- 2892 Terrer, C., S. Vicca, B. D. Stocker, B. A. Hungate, R. P. Phillips, P. B. Reich,  
2893 A. C. Finzi, and I. C. Prentice (2018). Ecosystem responses to elevated CO<sub>2</sub>  
2894 governed by plant–soil interactions and the cost of nitrogen acquisition. *New*  
2895 *Phytologist* 217(2), 507–522.
- 2896 Thieurmel, B. and A. Elmarhraoui (2019). suncalc: Compute sun position,  
2897 sunlight phases, moon position, and lunar phase.
- 2898 Thomas, R. Q., E. N. J. Brookshire, and S. Gerber (2015). Nitrogen limita-  
2899 tion on land: how can it occur in Earth system models? *Global Change*  
2900 *Biology* 21(5), 1777–1793.
- 2901 Thomas, R. Q., S. Zaehle, P. H. Templer, and C. L. Goodale (2013). Global pat-  
2902 terns of nitrogen limitation: confronting two global biogeochemical models  
2903 with observations. *Global Change Biology* 19(10), 2986–2998.
- 2904 Thornton, P. E., J.-F. Lamarque, N. A. Rosenbloom, and N. M. Mahowald

- 2905 (2007). Influence of carbon-nitrogen cycle coupling on land model response  
2906 to CO<sub>2</sub> fertilization and climate variability. *Global Biogeochemical Cycles* 21(4), GB4018.
- 2908 Tingey, D. T., D. L. Phillips, and M. G. Johnson (2000). Elevated CO<sub>2</sub> and  
2909 conifer roots: effects on growth, life span and turnover. *New Phytologist* 147(1), 87–103.
- 2910  
2911 Udvardi, M. and P. S. Poole (2013). Transport and metabolism in legume-  
2912 rhizobia symbioses. *Annual Review of Plant Biology* 64, 781–805.
- 2913 USDA NRCS (2022). The PLANTS Database.
- 2914 Uselman, S. M., R. G. Qualls, and R. B. Thomas (2000). Effects of increased  
2915 atmospheric CO<sub>2</sub>, temperature, and soil N availability on root exudation of  
2916 dissolved organic carbon by a N-fixing tree (*Robinia pseudoacacia* L.). *Plant  
2917 and Soil* 222, 191–202.
- 2918 van Diepen, L. T. A., E. A. Lilleskov, K. S. Pregitzer, and R. M. Miller (2007).  
2919 Decline of arbuscular mycorrhizal fungi in northern hardwood forests ex-  
2920 posed to chronic nitrogen additions. *New Phytologist* 176(1), 175–183.
- 2921 Vance, C. P. and G. H. Heichel (1991). Carbon in N<sub>2</sub> fixation: Limitation or  
2922 exquisite adaptation. *Annual Review of Plant Physiology and Plant Molec-  
2923 ular Biology* 42(1), 373–392.
- 2924 Viet, H. D., J.-H. Kwak, K.-S. Lee, S.-S. Lim, M. Matsushima, S. X. Chang,  
2925 K.-H. Lee, and W.-J. Choi (2013). Foliar chemistry and tree ring δ<sup>13</sup>C of  
2926 *Pinus densiflora* in relation to tree growth along a soil pH gradient. *Plant  
2927 and Soil* 363(1-2), 101–112.

- 2928 Vitousek, P. M., K. Cassman, C. C. Cleveland, T. Crews, C. B. Field, N. B.  
2929 Grimm, R. W. Howarth, R. Marino, L. Martinelli, E. B. Rastetter, and  
2930 J. I. Sprent (2002). Towards an ecological understanding of biological nitro-  
2931 gen fixation. In *The Nitrogen Cycle at Regional to Global Scales*, pp. 1–45.  
2932 Springer Netherlands.
- 2933 Vitousek, P. M. and R. W. Howarth (1991). Nitrogen limitation on land and in  
2934 the sea: How can it occur? *Biogeochemistry* 13(2), 87–115.
- 2935 Vitousek, P. M., S. Porder, B. Z. Houlton, and O. A. Chadwick (2010).  
2936 Terrestrial phosphorus limitation: mechanisms, implications, and nitro-  
2937 gen–phosphorus interactions. *Ecological Applications* 20(1), 5–15.
- 2938 Walker, A. P., A. P. Beckerman, L. Gu, J. Kattge, L. A. Cernusak, T. F.  
2939 Domingues, J. C. Scales, G. Wohlfahrt, S. D. Wullschleger, and F. I. Wood-  
2940 ward (2014). The relationship of leaf photosynthetic traits -  $V_{cmax}$  and  $J_{max}$   
2941 - to leaf nitrogen, leaf phosphorus, and specific leaf area: a meta-analysis  
2942 and modeling study. *Ecology and Evolution* 4(16), 3218–3235.
- 2943 Wang, H., I. C. Prentice, T. F. Keenan, T. W. Davis, I. J. Wright, W. K.  
2944 Cornwell, B. J. Evans, and C. Peng (2017). Towards a universal model for  
2945 carbon dioxide uptake by plants. *Nature Plants* 3(9), 734–741.
- 2946 Wang, W., Y. Wang, G. Hoch, Z. Wang, and J. Gu (2018). Linkage of root mor-  
2947 phology to anatomy with increasing nitrogen availability in six temperate  
2948 tree species. *Plant and Soil* 425(1-2), 189–200.
- 2949 Weatherburn, M. W. (1967). Phenol-hypochlorite reaction for determination of  
2950 ammonia. *Analytical Chemistry* 39(8), 971–974.

- 2951** Wellburn, A. R. (1994). The spectral determination of chlorophylls a and b, as  
**2952** well as total carotenoids, using various solvents with spectrophotometers of  
**2953** different resolution. *Journal of Plant Physiology* 144(3), 307–313.
- 2954** Wen, Z., P. J. White, J. Shen, and H. Lambers (2022). Linking root exuda-  
**2955** tion to belowground economic traits for resource acquisition. *New Phytolo-*  
**2956** *gist* 233(4), 1620–1635.
- 2957** Westerband, A. C., I. J. Wright, V. Maire, J. Paillassa, I. C. Prentice, O. K.  
**2958** Atkin, K. J. Bloomfield, L. A. Cernusak, N. Dong, S. M. Gleason, C. Guil-  
**2959** herme Pereira, H. Lambers, M. R. Leishman, Y. Malhi, and R. H. Nolan  
**2960** (2023). Coordination of photosynthetic traits across soil and climate gradi-  
**2961** ents. *Global Change Biology* 29(3), 1–29.
- 2962** Wieder, W. R., C. C. Cleveland, W. K. Smith, and K. Todd-Brown (2015).  
**2963** Future productivity and carbon storage limited by terrestrial nutrient avail-  
**2964** ability. *Nature Geoscience* 8(6), 441–444.
- 2965** Wieder, W. R., D. M. Lawrence, R. A. Fisher, G. B. Bonan, S. J. Cheng, C. L.  
**2966** Goodale, A. S. Grandy, C. D. Koven, D. L. Lombardozzi, K. W. Oleson,  
**2967** and R. Q. Thomas (2019). Beyond static benchmarking: using experimental  
**2968** manipulations to evaluate land model assumptions. *Global Biogeochemical*  
**2969** *Cycles* 33(10), 1289–1309.
- 2970** Wright, I. J., P. B. Reich, and M. Westoby (2003). Least-cost input mixtures  
**2971** of water and nitrogen for photosynthesis. *The American Naturalist* 161(1),  
**2972** 98–111.
- 2973** Wright, I. J., P. B. Reich, M. Westoby, D. D. Ackerly, Z. Baruch, F. Bongers,  
**2974** J. Cavender-Bares, T. Chapin, J. H. C. Cornelissen, M. Diemer, J. Flexas,

- 2975 E. Garnier, P. K. Groom, J. Gulias, K. Hikosaka, B. B. Lamont, T. Lee,  
2976 W. Lee, C. Lusk, J. J. Midgley, M.-L. Navas, Ü. Niinemets, J. Oleksyn,  
2977 N. Osada, H. Poorter, P. Poot, L. Prior, V. I. Pyankov, C. Roumet, S. C.  
2978 Thomas, M. G. Tjoelker, E. J. Veneklaas, and R. Villar (2004). The world-  
2979 wide leaf economics spectrum. *Nature* 428(6985), 821–827.
- 2980 Xu-Ri and I. C. Prentice (2017). Modelling the demand for new nitrogen fixation  
2981 by terrestrial ecosystems. *Biogeosciences* 14(7), 2003–2017.
- 2982 Zaehle, S., B. E. Medlyn, M. G. De Kauwe, A. P. Walker, M. C. Dietze, T. Hick-  
2983 ler, Y. Luo, Y. P. Wang, B. El-Masri, P. Thornton, A. Jain, S. Wang,  
2984 D. Warlind, E. Weng, W. Parton, C. M. Iversen, A. Gallet-Budynek, H. Mc-  
2985 carthy, A. C. Finzi, P. J. Hanson, I. C. Prentice, R. Oren, and R. J. Norby  
2986 (2014). Evaluation of 11 terrestrial carbon-nitrogen cycle models against  
2987 observations from two temperate Free-Air CO<sub>2</sub> Enrichment studies. *New*  
2988 *Phytologist* 202(3), 803–822.
- 2989 Zaehle, S., S. Sitch, B. Smith, and F. Hatterman (2005). Effects of parame-  
2990 ter uncertainties on the modeling of terrestrial biosphere dynamics. *Global*  
2991 *Biogeochemical Cycles* 19(3), GB3020.
- 2992 Zhu, Q., W. J. Riley, J. Tang, N. Collier, F. M. Hoffman, X. Yang, and G. Bisht  
2993 (2019). Representing nitrogen, phosphorus, and carbon interactions in the  
2994 E3SM land model: development and global benchmarking. *Journal of Ad-*  
2995 *vances in Modeling Earth Systems* 11(7), 2238–2258.
- 2996 Ziegler, C., M. E. Dusenge, B. Nyirambangutse, E. Zibera, G. Wallin, and  
2997 J. Uddling (2020). Contrasting Dependencies of Photosynthetic Capacity  
2998 on Leaf Nitrogen in Early- and Late-Successional Tropical Montane Tree

- 2999** Species. *Frontiers in Plant Science* 11, 1–12.
- 3000** Ziehn, T., J. Kattge, W. Knorr, and M. Scholze (2011). Improving the pre-  
**3001** dictability of global CO<sub>2</sub> assimilation rates under climate change. *Geophys-  
**3002** ical Research Letters* 38(10), L10404.